Synthesis, Characterization and Properties of Aromatic PDMS Multiblock Copolymers

Xu, Hongli

DOI
10.4233/uuid:df38f455-4fe0-4674-9801-f66f3628693d

Publication date
2018

Document Version
Final published version

Citation (APA)
Xu, H. (2018). *Synthesis, Characterization and Properties of Aromatic PDMS Multiblock Copolymers*. [Dissertation (TU Delft), Delft University of Technology]. https://doi.org/10.4233/uuid:df38f455-4fe0-4674-9801-f66f3628693d

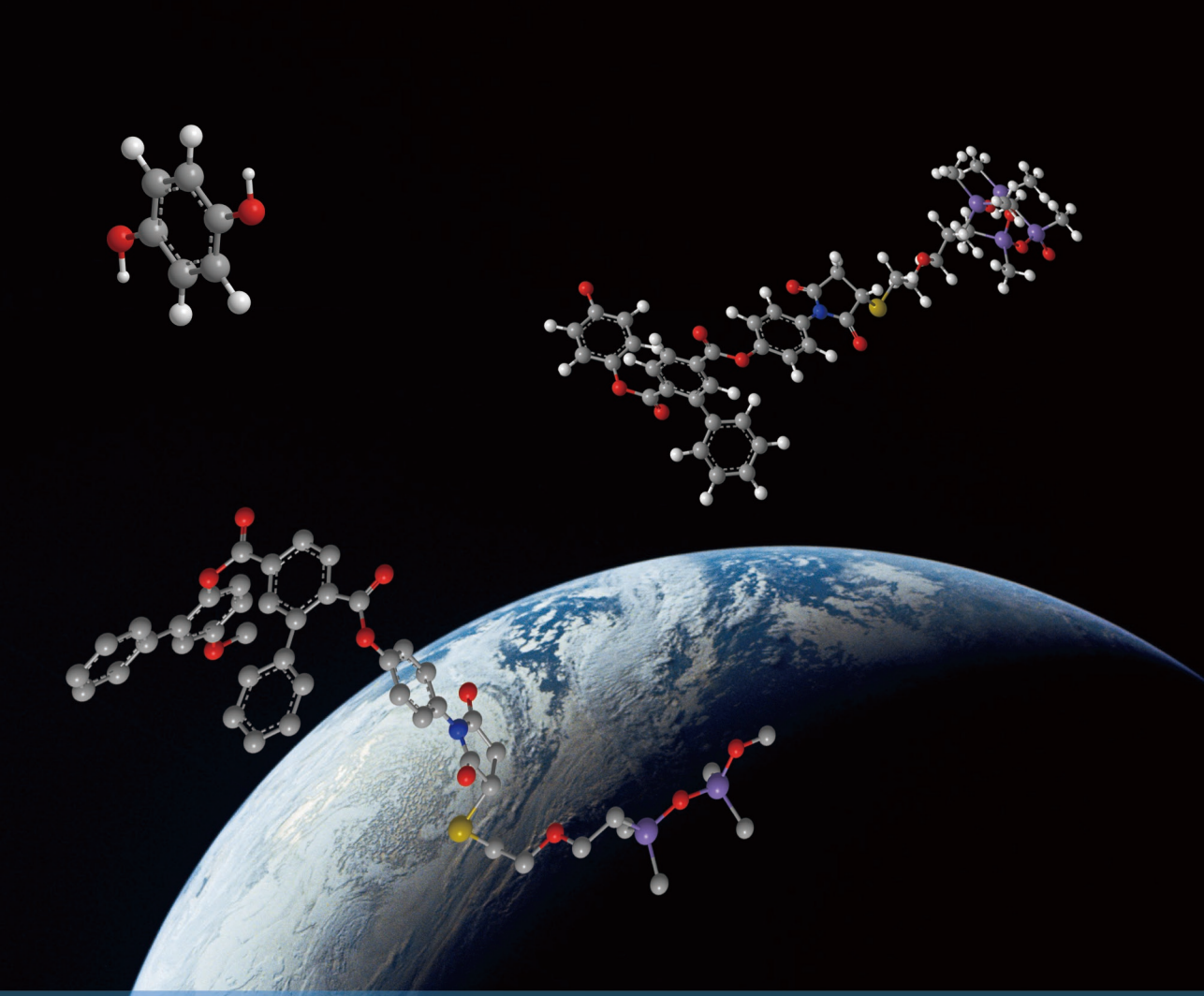

SYNTHESIS, CHARACTERIZATION AND PROPERTIES OF AROMATIC PDMS MULTIBLOCK COPOLYMERS

HONGLI XU

Synthesis, Characterization and Properties of Aromatic PDMS Multiblock Copolymers

Proefschrift

ter verkrijging van de graad van doctor
aan de Technische Universiteit Delft,
op gezag van de Rector Magnificus Prof.dr.ir. T.H.J.J. van der Hagen,
voorzitter van het College voor Promoties,
in het openbaar te verdedigen op
maandag 4 juni 2018 om 15:00 uur

door

Hongli XU

Master of Science in Polymer Chemistry and Physics
University of Science and Technology of China, Hefei, China
geboren te Huangshan, China

Dit proefschrift is goedgekeurd door de promotor:

Prof. dr. T. J. Dingemans

Samenstelling promotiecommissie:

Rector Magnificus	voorzitter
Prof. dr. T.J. Dingemans	Technische Universiteit Delft, promotor

Onafhankelijke leden:

Prof. dr. S. J. Picken	Technische Universiteit Delft
Prof. dr. E. J. R. Sudhölter	Technische Universiteit Delft
Prof. dr. A. P. H. J. Schenning	Technische Universiteit Eindhoven
Dr. S. J. Garcia Espallargas	Technische Universiteit Delft
Dr. E. Mendes	Technische Universiteit Delft

Overig lid:

Dr. J. C. Bijleveld	Technische Universiteit Delft

The research carried out in this thesis is funded by the Chinese Scholarship Council, project NO. 201206340070.

ISBN: 978-94-6186-908-1

xhl@outlook.com

Published by: Gildeprint Drukkerijen

Table of contents

Chapter 1 Introduction

1.1 High-performance Polymers

In the late 1950s, organic materials for the aerospace and electronics industry were developed in order to satisfy the increasing demands of combining lightweight materials with high mechanical properties and high thermal stability. Tremendous effort from both academia and industry was put into the field of high-performance polymers during the next 60 years, because the initial polymers were not able to withstand high temperatures and if they were, difficulties in processing were encountered.[1, 2]

The definition of high-performance polymers varies and depends on the application and the organization developing or using the material. In general, high-performance polymers are best defined by their long-term durability (> 10,000 h at elevated temperatures, typically in excess of 150 ˚C), high decomposition temperatures ($T_d^{5\%}$ > 400 ˚C), high T_g (>150 ˚C), high mechanical properties (E' of 3-120 GPa, tensile strength of 80 – 300 MPa) and/or chemical stability (stable towards fluid ingress), which surpass those of commodity polymers and engineering polymers.[1] Basic information of some representative commercial high-performance polymers are shown in table 1.1. For example, the polyimide film from DuPont, designated Kapton™ (entry 1), was invented in the late 1960s. Due to its extremely high thermal stability (>400 ˚C) and its ability to maintain its excellent physical, electrical, and mechanical properties over a wide temperature range, this material has now become the largest selling high-performance polymer in the world, and is widely used in flexible electronics, satellites, and various space instruments.[3] Another DuPont product, Kevlar™ (entry 2), was developed as a high-strength all-aromatic polyamide. The high tensile-to-weight ratio enables this material to replace steel in some applications, such as racing tires, body armor *etc*.[4] Other well developed and widely used high-performance polymers include the semi-crystalline polyetheretherketone (PEEK, Victrex™, entry 3) and the liquid crystalline polyester (Vectra-A, entry 4) and semi-crystalline polyphenylene sulfide (PPS, Fortron™, entry 5), see Table 1.1. These materials are all extensively used in the aerospace, automotive, and micro-electronics industries.[5, 6]

Table 1.1. Examples of well-known high-performance polymers.

Entry	Chemical structure	Category	T_g (℃)	T_m (℃)	Mechanical properties[b]
1	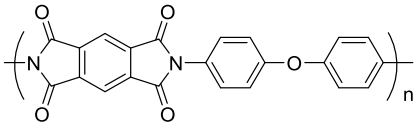	Polyetherimide, Kapton™	400	N/A[a]	E: 2.5 GPa, σ: 231 MPa ε: 72%
2	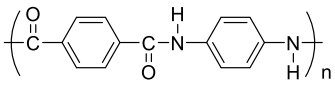	Polyamide, Kevlar™	>300	N/A[a]	E: 70.5 GPa, *Y*: 2920 MPa ε: 3.6% (Kevlar 29 yarn)
3	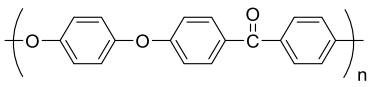	Polyetheretherketone (PEEK), Victrex™	143	334	E: 3.6 GPa, σ: 90-100 MPa ε: 50%
4	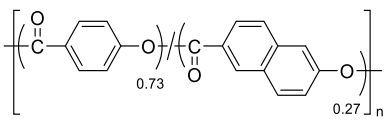	Polyester, Vectra-A™	110	280	E: 15 GPa, σ: 190 MPa ε: 2.1%
5	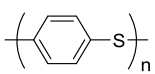	Polyphenylene sulfide (PPS), Fortron™	85	285	E: 2.2 GPa, σ: 158 MPa ε: 4.1%

[a] T_m exceeds the decomposition temperature; [b] E: elastic modulus; σ: tensile strength; ε: fracture elongation, *Y*: breaking tenacity.

As can be seen from the structures in Table 1.1, high-performance polymers are composed of aromatic and/or heterocyclic 5- or 6-membered rings and contain no aliphatic units (SP^3 carbons). As a consequence, the polymer backbones are mostly rigid or rod-like, which offer properties not found in most commodity polymers such as polyolefins, aliphatic polyesters, polystyrenes *etc*. This backbone rigidity leads to the aforementioned high mechanical properties and heat resistance. Other factors that contribute to high-performance and high temperature resistance of this class of polymers include the introduction of hetero atoms, like S, O and N. These atoms contribute to the chemical stability, due to the induced secondary bonding, like hydrogen bonds and polar interactions.[1] This enhances intermolecular interactions between the polymer chains and improves the thermo-mechanical properties such as the glass transition temperature (T_g) and Young's modulus.

The rigid or rod-like structural characteristics of high-performance polymers endow them with excellent thermo-mechanical properties, while at the same time, challenges arise with respect to processing due to the extremely poor solubility and high melting temperatures (sometimes even higher than decomposition temperature). As a consequence, these polymers have to be processed either from a soluble precursor state, or the final polymer must be processed from aggressive solvents.[7] For instance, commercial polyimide Kapton™ (entry 1 in table 1.1) films are prepared from the poly(amic acid) state and subsequently imidized to the final polyimide form.[8] The lyotropic polyamide Kevlar™ (entry 2 in table 1.1) has an extremely high melting point (>500 °C) and poor solubility in common solvents, so spinning into fibers has to be performed from a 100% sulfuric acid solution.[4]

1.2 Main-chain liquid crystal polymers

Liquid crystalline polymers (LCPs) are a unique class of aromatic polymers, since they are capable of forming highly ordered molecular arrangements in solution or in the molten state, named lyotropic or thermotropic LCPs, respectively.[9-20] The reason of LCPs to exhibit a liquid crystalline state, stems from the existence of mesogenic units, which are usually made up of a rigid core of two or more aromatic rings. Compared to other type of semi-crystalline or amorphous high-performance polymers, LCPs are capable to align spontaneously along their processing direction, thereby lowering the melt viscosity. As a consequence, LCPs can be processed into

fibers and injection molded parts with a high degree of molecular alignment. LC fibers or injected polymer parts show superior mechanical properties, such as tensile strength and storage modulus, in the processing direction.[21-23]

In terms of the position of the mesogenic cores, LCPs can be classified as main-chain[24, 25] (mesogenic units are connected together in a linear fashion), side-chain[26-28] (mesogenic units attached to a polymer backbone), combined main-chain/side-chain[29] (mesogenic units are both incorporated into and attached onto the polymer main-chain, also known as mesogen-jacketed liquid crystalline polymers) and crosslinked[30-34] (mesogenic units are cross-linked by reactive groups to form a network or thermoset). The structures of the main-chain and crosslinked LCPs are illustrated in Figure 1.1. Main-chain LCPs, for example analogues of Kevlar™, are widely used in engineering applications[35]. Crosslinked LCPs, also known as liquid crystalline thermosets, are cured networks of reactive liquid crystalline oligomers or polymers. If the crosslinking reaction takes place while in the liquid crystalline temperature range, the LC phases becomes chemically locked in, resulting in high mechanical strength. Liquid crystalline networks combine both high dimensional stability and mechanical orientability typical of polymer networks with the unique anisotropic behavior of liquid crystals.[36-38] Side-chain LCPs and combined main-chain/side-chain LCPs are mostly employed in electro-optical applications,[39, 40] and will not be discussed in this thesis.

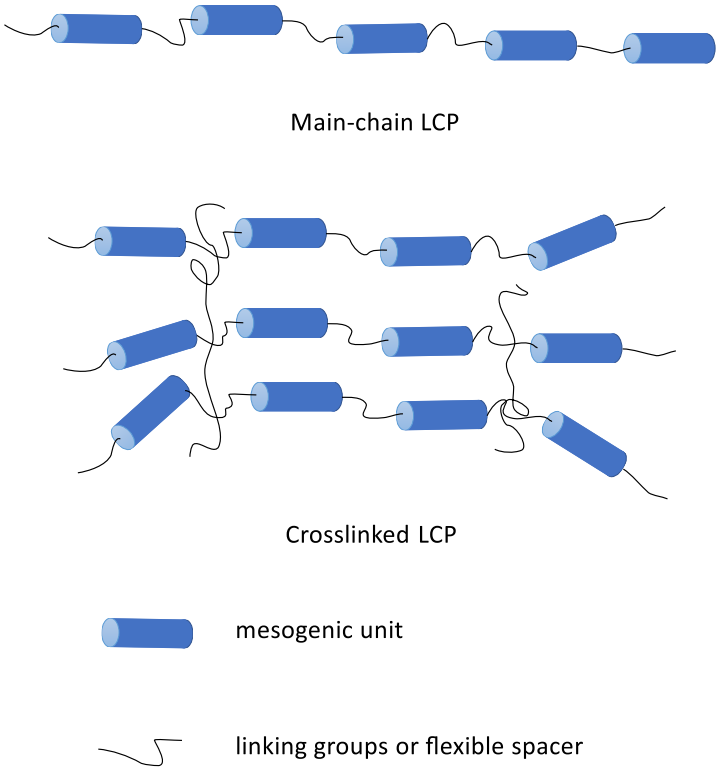

Fig. 1.1. Schematic representation of main-chain and crosslinked LCPs. Cylinders represent aromatic mesogenic groups and curved lines represent linking groups (*e.g.* imino, azo, azoxy, ester, trans-vinylene, amide or direct links between aromatic units) or flexible spacers (*e.g.* polymethylene, poly(ethylene oxide) and polysiloxane).

Typical main-chain high-performance LCPs are composed of *p*-phenylene-based rigid building units, and connected through either rigid linking groups or flexible spacers, forming rigid-rod like LCPs and semi-flexible LCPs. Widely used rigid linking groups in combination with these aromatic moieties are imino, azo, azoxy, ester, trans-vinylene, amide or direct links between aromatic units.[5, 9, 11, 41] As a result, the polymer chains are semi-rigid or completely inflexible, with respect to the conformational freedom along their polymer backbone. In contrast to all-aromatic rigid-rod LCPs, which are inherently difficult to process due to the lack of solubility and extremely high melting temperature, LCPs with flexible spacers provide the polymers with a melt-processing capability. Moreover, the liquid crystal transition

temperatures are decreased and the solubility is improved, compared to the rigid rod analogues.[42] Flexible spacers have also been extensively used to separate mesogenic units placed in the main-chain. Typical flexible spacers reported include polymethylene, poly(ethylene oxide) and polysiloxane.[5, 9, 11, 14, 19, 41, 43, 44]

Generally, semi-flexible main-chain LCPs with flexible spacers are accessible *via* two approaches.[5] The first one is chemical modification (melt transesterification) on pre-made non-liquid crystalline polymers. High temperature transesterification, however, is limited in usefulness because it often leads to polymer structures with poorly defined sequences, and is only applicable on certain types of ester-based LCPs. As an example, in the work reported by *H. F. Kuhfuss et al.* from the Eastman company[42], a liquid crystalline copolyester was prepared from poly(ethylene terephthalate) (PET) with *p*-acetoxybenzoic acid, *via* a zinc or antimony acetate catalyzed acidolysis reaction. The authors claim random polymer chain composed of ethylene, terephthalic and oxybenzoic units could be prepared. However, upon close inspection, the obtained polymer composition appears to be blocky in nature. The melt consists of isotropic PET rich domains and nematic PET/oxybenzoic acid domains. In addition, an infusible component can be observed, which is most likely pHBA.

The second method is step-growth polymerization of appropriate monomeric components. In this case, the mesogenic units can either be reactive macro-monomers, or formed *in-situ* during polymerization. Standard esterification reactions, or conventional polymerization reactions carried out in solution at low or medium temperature are suitable. A typical example is the work presented by *W. R. Krigbaum et al.*,[45] in which a liquid crystalline polyester with polymethylene flexible segments was prepared from mesogenic 4,4'-diacetoxybiphenyl and dibasic acids (5-12 methylene units). The reported polyesters show different mesophases and tunable LC transition temperatures by adjusting the number of methylene units.

Based on these two conceptual methods, varieties of main-chain liquid crystalline polymers with highly differentiating structures have been prepared. Table 1.2 shows representative structures of these combinations of mesogenic groups with flexible spacers, including liquid crystalline polyesters[45-47] (entry 1 and 5), polyethers[48, 49] (entry 2 and 3) with combinations of different spacers, such as different molecular weight poly(methylene)[45-49] (entry 1-3), polyurethanes[50-52] (entry 4) and polydimethylsiloxanes[53] (entry 5). With the incorporation of flexible alkyl spacers, the phase transition temperatures of the LCPs show an obviously decrease

comparing to the all-aromatic rigid LCPs. Especially in the case of using polydimethylsiloxanes (PDMS) as flexible spacers instead of alkyl spacers, a drastic decrease of the transition temperatures was detected. And in one case, the LCP show nematic phases over a temperature range of 311 °C.[53] However, limited information with respect to the mechanical properties of these polymers is available.

Table 1.2. Representative Liquid crystalline polymers with main-chain mesogenic groups and flexible spacers.

Entry	Mesogenic units and flexible spacers	Phase type	LC T range (°C)	Reference
1	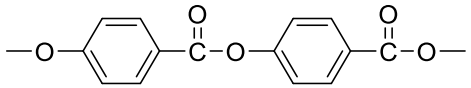 —$(CH_2)_n$— n = 5-12	Nematic	T_{LC}: 182 - 240 T_{ISO}: 208 - 281	45-47
2	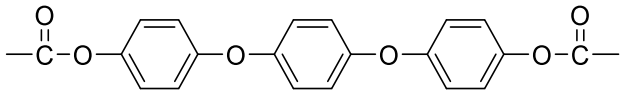 —$(CH_2)_n$— n = 2-8	N/A	T_{LC}: 144 - 205 T_{ISO}: 169 - 239	48
3	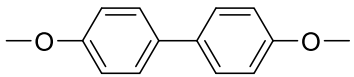 —$(CH_2)_n$— n = 1-8	Nematic or smectic	T_{LC}: 79 - 182 T_{ISO}: 97 - 206	49

Table 1.2. Continued.

Entry	Mesogenic units and flexible spacers	Phase type	LC T range (°C)	Reference
4	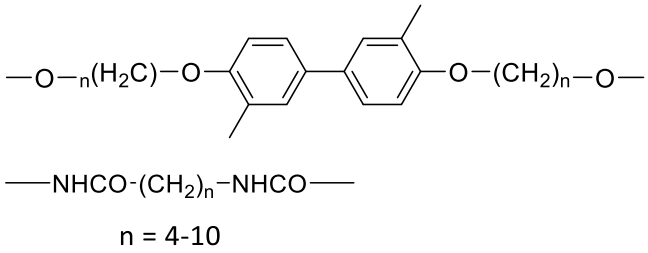	Nematic	T_{LC}: 252 - 259 T_{ISO}: 222 - 242	50-52
5	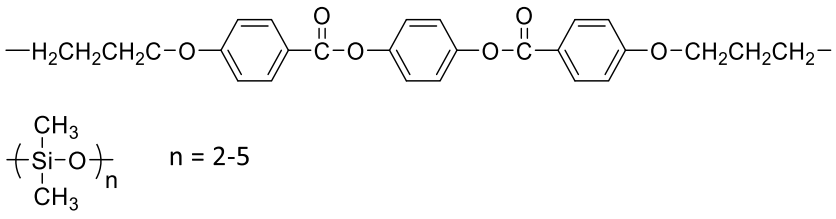	Smectic	T_{LC}: -13 - 35 T_{ISO}: 87 - 130	53

1.3 High-performance block copolymers

Block copolymers, consist of two or more chemically distinct, but covalently bound polymer fragments. Therefore, it is possible to combine the properties of two completely different polymers without macroscopic phase separation occurring. The phase separation is limited to a nanoscopic scale and is dependent on the thermodynamic interaction parameter χ, the temperature, the molecular weight and distribution and the volume fraction of the different components.[54, 55]

Commonly used block copolymers include acrylonitrile butadiene styrene (ABS), styrene\butadiene copolymer (SBR), styrene-acrylonitrile, styrene-isoprene-styrene (SIS) and ethylene-vinyl acetate.[56] These block copolymers consist of incompatible soft and rigid blocks, resulting in a nanoscale phase separation. The soft phases formed by soft blocks act as crack arrestors, and consequently increase the impact energy absorption. At the same time, the rigid blocks provide the material with high elastic modulus and high ultimate tensile stress. However, these commonly used block copolymers are not capable to be utilized in high temperature (>150 °C) applications. To meet the high temperature requirement, high-performance block copolymers were developed. With a similar structure of semi-flexible LCP with flexible spacers, high-performance block copolymers are copolymers composed of a high-performance rigid macromonomer (amorphous, semi-crystalline or liquid crystalline) and another distinctively different polymer macromonomer.

Various types of monomers and macromonomers have been used to synthesize this type of block copolymer. With respect to the synthetic method used, basically there are only two synthetic routes for the preparation of main-chain block copolymers containing high-performance polymer segments:

(**I**) polycondensation reaction of bifunctional monomers (A block) with α,ω-bifunctionalized macro-monomers (B block) or bifunctional monomers (B block), resulting in an $(AB)_n$ backbone structure;

(**II**) coupling of pre-made homopolymers (A and B blocks) with appropriate reactive mono- or di-functional end-groups, resulting in AB, ABA or $(AB)_n$ backbone structures;

The first procedure is reported frequently in literature, due to the easy synthetic approach, *i.e.,* it can be easily applied at various temperatures in the solid state or solution intermediate. However, most obtained block copolymers are

insoluble in common organic solvents, prohibiting molecular composition characterization techniques like NMR and GPC.[57] Besides, side reactions, like the formation of homopolymers from one of the monomers, are difficult to avoid, resulting in polymers with broad molecular weight distributions (PDI > 2.5) and an uncontrollable and inconsistent composition.[58] This will undoubtedly have consequences for the thermal and mechanical performance of the materials. In contrast, the second procedure is more promising, because the produced block copolymers have well-defined structures with controllable molecular weights and controllable block lengths. This is because the reactive homopolymers can be designed and prepared beforehand, to avoid side reactions (homopolymerization).

This line of research was pioneered by J. E. Mcgrath and co-workers who reported block co-polymers containing high-performance polymer segments, featuring amorphous and semi-crystalline blocks.[59] Since then, different high-performance polymer backbones and soft blocks have been used, and some representative examples are shown in Table 1.3. For instance, dihydroxyl functionalized poly(*p*-phenylene oxide)s[60, 61], dianhydride functionalized polyimide[62], dianhydride/dihydroxyl functionalized poly(arylene ether sulfone) [58, 63-66] (entry 1) and poly(arylene ether ketone)[65], reactive poly(*p*-phenyl sulfide)s[67] and polyoxytetramethylene glycols[68-71], were copolymerized to prepare high-performance block copolymers. In these reports, the block copolymers were prepared through the first method. The morphology variations were studied when block chain length and substituents in the main-chain of the blocks were changed. In particular upon the incorporation of soft blocks, processability of the high-performance block polymers was improved. Structural modification by copolymerization with more flexible oligomers such as poly(arylene ether)s yielded block copolymer with enhanced impact strength.[65]

High-performance block copolymers have also been prepared via the second synthetic route, yielding well-defined structures. In work reported by H.-W. Schmidt *et al.*[72-74] (entry 2), well-defined structured ABA triblock copolymers composed of polystyrene or poly(ethylene glycol) (as A block) with highly rigid LC polyester (as B block) were synthesized by condensation reactions of telechelic poly(2,2'-dimethyl-4,4'-biphenylene phenylterephthalate) with pre-prepared ω-hydroxy-functionalized polystyrene or poly(ethylene glycol) blocks. These polymers were found to be soluble in common organic solvents, making molecular composition characterization methods like GPC and NMR possible. Microphase separation was confirmed by TEM

measurements. The liquid crystallinity was preserved with a mesogenic content as low as 40 wt%.

Table 1.3. Representative high-performance block copolymers.

Entry	A block	B block	Remarks	reference
1	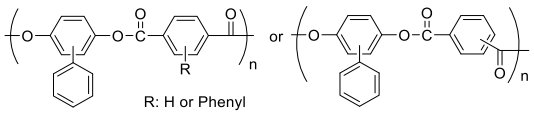	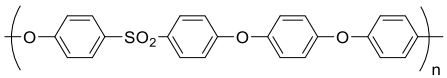	T_g: 150 – 188 ˚C T_m > 335 ˚C E’ > 2 GPa	64
2	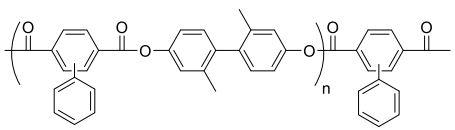	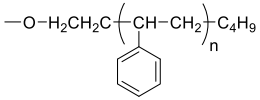	T_g: 94 – 133 ˚C	73
3	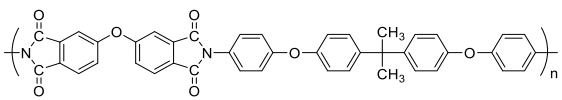	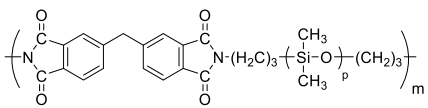	T_g: 158 – 194 ˚C	75
4	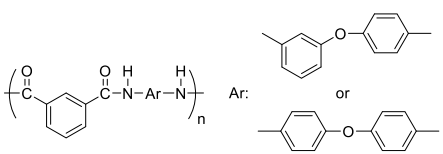	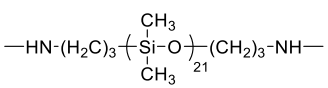	T_g *1*: ~ -120 ˚C T_g *2*: 200 - 240 ˚C σ: 3 - 56 MPa, E: 4 - 1200 MPa	76

Polydimethylsiloxane (PDMS) is a unique polymer with a low T_g *(-125 °C)*, which can be used to prepare organic/inorganic hybrid block copolymers. Although some thermal and thermo-oxidative stability typical of high-performance polymers is sacrificed by introducing a siloxane segment, a number of improvements are also observed, such as processability, toughness, flexibility, adhesion and membrane performance.[77] Jasna Djonlagic *et al.* reported thermoplastic poly(ester-siloxane) block copolymers based on PDMS and poly(butylene terephthalate) via two-step melt transesterification reactions.[78-82] Due to the improved solubility, the molecular composition of the block copolymers could be analysed by NMR. The physical properties of the block copolymers, including melting point, hardness, degree of crystallinity and glass-transition temperature, was tuned by changing the length of the polybutadiene chain length and PDMS segment. Polyimides have also been utilized to prepare high-performance block copolymers with PDMS segments (entry 3).[75, 77, 83-88] The block copolymers of poly(amide-siloxane) (entry 4) were first developed by Yoshio Imai *et al.*,[76] and since then an extensive range of properties of this set of materials, like phase behavior, tensile properties, thermo-mechanical properties, thermal stability, bio-compatibility, gel permeability, was studied.[89-101] Generally, poly(amide-siloxane)s are prepared by polycondensation reactions from amine-terminated PDMS and acid chloride-functionalized polyamides,[76, 89-100] or from dicarboxylic acid functionalized PDMS and diisocyanate-terminated polyamides,[101] through one-step or two-step reactions. Phase separation was observed due to the incompatiblility of the two blocks. Films of the block copolymer were prepared by casting from DMAc. The mechanical properties of films from the poly(amide-siloxane) multiblock copolymers depended strongly on the PDMS content. At low PDMS levels, the materials behave as rubber-toughened aramid plastics, having tensile strength and fracture elongation of 60 MPa and 9%, respectively. At higher PDMS content, the materials are analogous to thermoplastic elastomers, showing a tensile strength and fracture elongation of up to 6 MPa and 140%, respectively.[76] The synthesis and properties of block copolymers of hexafluoroisopropylidene bisphenol poly(arylene ether sulfone) and PDMS have also been reported by Richard Turner *et al.*[102] Similar to other PDMS containing block copolymers, phase separation was observed, and the thermal stability was improved by the incorporation of fluorinated methyl groups. The tensile properties of the segmented block copolymers were similar, with properties ranging from elastomeric to plastic depending on the molecular weight composition of the oligomer with the highest and lowest tensile strength of 15 and 8 MPa, respectively. Due to the high

glass transition temperatures and high melting points, block copolymers are considered to be good candidates for high temperature thermoplastic elastomer applications.[101] The best mechanical properties of the reported PDMS-based high-performance block copolymers are summarized in table 1.4. As shown in this table, with the introduction of the PDMS component, the block copolymers become more ductile. However, in all the cases reported, none of them exhibited the mechanical behavior expected of a high-performance elastomer, *i.e.* good strength (σ ~80 MPa) and elongation at break (ε >50%). It is apparent that the mechanical properties of the polymers listed are compromised by the introduction of the PDMS soft blocks.

Table 1.4. Best mechanical properties of selected PDMS-based high-performance block copolymers as reported in literature.

Block copolymers	tensile strength (MPa)	Elastic modulus (MPa)	Elongation at break (%)
PDMS-*b*-polyamide[101]	58	1400	30
PDMS-*b*-polyamide[94]	54	870	19
PDMS-*b*-poly(arylene ether sulfone) [102]	23	800	8

The aim of this thesis is to explore a novel approach towards high-performance block copolymer elastomers. As the soft block, we'll use PDMS and as the hard block we'll use either an anisotropic (liquid crystal), all-aromatic polymer or an amorphous all-aromatic polymer. Is a rigid anisotropic (LC) block preferred over a rigid amorphous block when coupled with a suitable high temperature PDMS block? How will mesophase behaviour affect the thermo-mechanical properties and stress-strain behaviour?

1.4 Scope and outline of the thesis

The focus of this thesis is to explore the design and synthesis of a new family thermoplastic high-performance elastomeric $(AB)_n$-block copolymers based on bismaleimide-functionalized all-aromatic liquid crystalline or amorphous precursors coupled with dithiol terminated PDMS oligomers. Using highly efficient thiol-ene click chemistry, we're able to access thermoplastic elastomers of high molecular weight. Our aim is to understand the structure-property relationships that govern the thermo-mechanical properties of this class of high-performance elastomeric block copolymers. The chemistry, phase behaviour, thermo-mechanical behaviour and shape-memory performance of free standing films will be described in detail.

In ***Chapter 2***, the synthetic details of the bismaleimide end-functionalized oligomers with a target number average molecular weight (Mn) of 1K, 5K and 9K will be described. Both isotropic (amorphous) and anisotropic (LC) reactive precursors were synthesized using two different synthetic methods.

The cure behaviour of the bismaleimides prepared in Chapter 2 will be discussed in ***Chapter 3***. The effect of using different morphologies on the curing behaviour and properties of the final cured thermosets will be presented. The phase behaviour and thermo-mechanical properties before and after cure were studied using TGA, DSC, DMTA, optical microscopy, XRD and tensile testing.

In ***Chapter 4***, the synthesis and molecular weight characterization of the block copolymers based on dithiol terminated PDMS (Mn of 1K, 5K and 10K) and rigid maleimide-functionalized blocks (liquid crystalline or amorphous) is described. In order to prepare the block copolymers we used well-known thiol-ene click chemistry conditions, and the molecular weights of the final products were determined by GPC and NMR.

The amorphous and liquid crystalline block copolymers as presented in Chapter 4 are characterized by TGA, DSC, DMTA, optical microscopy, XRD analysis and tensile behaviour and the results will be discussed in ***Chapter 5***. The thermal and thermo-mechanical properties of the two block copolymer series are compared. In order to understand the temperature dependent tensile behaviour of our TPEs we performed tensile experiments using the 5K PDMS samples at different temperatures.

In ***Chapter 6***, the multi-block copolymers based on all-aromatic polyester/PDMS, as discussed in chapter 4 and 5, were investigated as dual- and

triple- shape memory films, which can be used over a broad temperature range (~300 ˚C). A characterization method based on a torsion mode geometry was adopted in order to evaluate the shape fixity and recovery performance. The effect of the difference rigid blocks on the shape memory properties of the films will be discussed in detail.

1.5 References

1 P. M. Hergenrother, *High Perform. Polym.*, 2003, **15**, 3-45.
2 F. Herold and A. Schneller, *Adv. Mater.*, 1992, **4**, 143-152.
3 H.-j. Ni, J.-g. Liu, Z.-h. Wang and S.-y. Yang, *Ind. Eng. Chem. Res.*, 2015, **28**, 16-27.
4 E. G. Chatzi and J. L. Koenig, *Polym. Plast. Technol. Eng.*, 1987, **26**, 229-270.
5 D. Demus, J. W. Goodby, G. W. Gray, H. W. Spiess and V. Vill, *Handbook of Liquid Crystals, High Molecular Weight Liquid Crystals*, Wiley, 2008.
6 M. S. Abu Bakar, P. Cheang and K. A. Khor, *J. Mater. Process. Technol.*, 1999, **89–90**, 462-466.
7 T. Dingemans, in *Polymer Science: A Comprehensive Reference*, ed. M. Möller, Elsevier, Amsterdam, 2012, pp. 753-769.
8 M. Anthamatten, S. A. Letts, K. Day, R. C. Cook, A. P. Gies, T. P. Hamilton and W. K. Nonidez, *J. Polym. Sci., Part A: Polym. Chem.*, 2004, **42**, 5999-6010.
9 J. I. Jin, S. Antoun, C. Ober and R. W. Lenz, *Brit. Polym. J.*, 1980, **12**, 132-146.
10 R. W. Lenz and J. I. Jin, *Macromolecules*, 1981, **14**, 1405-1411.
11 C. K. Ober, J.-I. Jin, Q. Zhou and R. W. Lenz, in *Liquid Crystal Polymers I*, ed. N. A. Platé, Springer Berlin Heidelberg, Berlin, Heidelberg, 1984, pp. 103-146.
12 J.-I. Jin, C.-S. Kang, I.-H. Lee and Y.-K. Yun, *Macromolecules*, 1994, **27**, 2664-2670.
13 J.-I. Jin, *Mol. Cryst. Liq. Cryst. Sci. Technol., Sect. A*, 1994, **254**, 197-207.
14 M. Schmucki and A. D. Jenkins, *Makromol. Chem.*, 1989, **190**, 1303-1308.
15 M. Ebert, O. Herrmann-Schönherr, J. H. Wendorff, H. Ringsdorf and P. Tschirner, *Macromol. Rapid Commun.*, 1988, **9**, 445-451.
16 I. G. Voigt-Martin, P. Simon, S. Bauer and H. Ringsdorf, *Macromolecules*, 1995, **28**, 236-242.
17 A. Silberberg, *Makromol. Chem. M. Symp.*, 1989, **23**, 1-11.
18 W. Heitz, *Makromol. Chem. M. Symp.*, 1991, **47**, 111-125.
19 M. Rehahn, A.-D. Schlüter, G. Wegner and W. J. Feast, *Polymer*, 1989, **30**, 1054-1059.
20 M. Rehahn, A.-D. Schlüter and G. Wegner, *Makromol. Chem.*, 1990, **191**, 1991-2003.

21 E. Priestly, *Introduction to Liquid Crystals*, Springer US, 2012.
22 S. Chandrasekhar, *Liquid Crystals*, Cambridge University Press, 1992.
23 T. J. Sluckin, D. A. Dunmur and H. Stegemeyer, *Crystals That Flow: Classic Papers from the History of Liquid Crystals*, Taylor & Francis, 2004.
24 S. B. Damman and F. P. M. Mercx, *J. Polym. Sci., Part B: Polym. Phys.*, 1993, **31**, 1759-1767.
25 W. F. A. Su, *J. Polym. Sci., Part A: Polym. Chem.*, 1993, **31**, 3251-3256.
26 A. Ciferri, *Liquid crystallinity in polymers: principles and fundamental properties*, VCH Publishers, 1991.
27 D. R. Mulligan, C. T. Imrie and P. Larcey, *J. Mater. Sci.*, 1996, **31**, 1985-1989.
28 A. G. Cook, R. T. Inkster, A. Martinez-Felipe, A. Ribes-Greus, I. W. Hamley and C. T. Imrie, *Eur. Polym. J.*, 2012, **48**, 821-829.
29 A. A. Collyer, *Liquid Crystal Polymers: From Structures to Applications*, Springer Netherlands, 2012.
30 J. W. Connell, J. G. Smith and P. M. Hergenrother, *J. Macromol. Sci. Polymer. Rev.*, 2000, **40**, 207-230.
31 A. Knijnenberg, E. S. Weiser, T. L. StClair, E. Mendes and T. J. Dingemans, *Macromolecules*, 2006, **39**, 6936-6943.
32 T. J. Dingemans and M. Iqbal, *Plast. Rubber. Compos.*, 2010, **39**, 189-194.
33 T. Dingemans, A. Knijnenberg, M. Iqbal, E. Weiser and T. Stclair, *Liq. Cryst. Today*, 2006, **15**, 19-24.
34 M. Iqbal and T. J. Dingemans, *Eur. Polym. J.*, 2010, **46**, 2174-2180.
35 J.-I. Jin and C.-S. Kang, *Prog. Polym. Sci.*, 1997, **22**, 937-973.
36 A. E. Hoyt, B. C. Benicewicz and S. J. Huang, in *Liquid-Crystalline Polymers*, American Chemical Society, 1990, vol. 435, ch. 15, pp. 198-206.
37 R. Zentel, H. Kapitza, F. Kremer and S. U. Vallerien, in *Liquid-Crystalline Polymers*, American Chemical Society, 1990, vol. 435, ch. 16, pp. 207-217.
38 D. Pavel, in *Liquid Crystalline Polymers: Volume 1–Structure and Chemistry*, eds. V. K. Thakur and M. R. Kessler, Springer International Publishing, Cham, 2016, pp. 477-499.
39 T. Ganicz and W. Stańczyk, *Materials*, 2009, **2**, 95.
40 P.-P. Hou, Z.-Y. Zhang, Q. Wang, M.-Y. Zhang, Z. Shen and X.-H. Fan, *Macromolecules*, 2016, **49**, 7238-7245.
41 J. K. Fink, in *High Performance Polymers (Second Edition)*, William Andrew Publishing, 2014, pp. 381-400.
42 W. J. Jackson and H. F. Kuhfuss, *J. Polym. Sci. Pol. Chem.*, 1976, **14**, 2043-2058.
43 S. Antoun, R. W. Lenz and J. I. Jin, *J. Polym. Sci. Pol. Chem.*, 1981, **19**, 1901-1920.
44 R. W. Lenz, *J. Polym. Sci. Pol. Sym.*, 1985, **72**, 1-8.
45 J. Asrar, H. Toriumi, J. Watanabe, W. R. Krigbaum, A. Ciferri and J. Preston, *J. Polym. Sci. Pol. Phys.*, 1983, **21**, 1119-1131.
46 J. S. Moore and S. I. Stupp, *Macromolecules*, 1988, **21**, 1217-1221.

47 W. R. Krigbaum, R. Kotek, T. Ishikawa, H. Hakemi and J. Preston, *Eur. Polym. J.*, 1984, **20**, 225-235.
48 A. H. Al-Dujaili, A. D. Jenkins and D. R. M. Walton, *Macromol. Rapid Commun.*, 1984, **5**, 33-36.
49 V. Percec, T. D. Shaffer and H. Nava, *J. Polym. Sci. Pol. Lett.*, 1984, **22**, 637-647.
50 W. Mormann and B. Brahm, *Macromol. Rapid Commun.*, 1988, **9**, 175-183.
51 W. Mormann and M. Brahm, *Macromol. Chem. Phys.*, 1989, **190**, 631-642.
52 W. Mormann and M. Brahm, *Macromolecules*, 1991, **24**, 1096-1101.
53 C. Aguilera, J. Bartulin, B. Hisgen and H. Ringsdorf, *Makromol. Chem.*, 1983, **184**, 253-262.
54 M. W. Matsen and M. Schick, *Macromolecules*, 1994, **27**, 6761-6767.
55 S. L. Aggarwal, *Polymer*, 1976, **17**, 938-956.
56 Y. Li and H. Shimizu, *Eur. Polym. J.*, 2009, **45**, 738-746.
57 E. Chiellini, G. Galli, A. S. Angeloni, M. Laus, M. C. Bignozzi, Y. Yagci and E. I. Serhatli, 1994.
58 B. C. Auman and V. Percec, *Polymer*, 1988, **29**, 938-949.
59 J. M. Lambert, E. Yilgor, I. Yilgor, G. L. Wilkes and J. E. McGrath, *ACS Polym. Prepr.*, 1985, **26**, 367.
60 G. Heyde, W. Heitz, A. Karbach and R. Wehramann, *Makromol. Chem.*, 1993, **194**, 2741-2758.
61 A. Fradet and W. Heitz, *Makromol. Chem.*, 1987, **188**, 1613-1619.
62 L. Feng and J. O. Iroh, *Eur. Polym. J.*, 2013, **49**, 1811-1822.
63 T. D. Shaffer and V. Percec, *Makromol. Chem.*, 1986, **187**, 111-123.
64 S. Brenda, W. Heitz, A. Karback and R. Wehrmann, *Macromol. Chem. Phys.*, 1994, **195**, 1327-1339.
65 D. L. Wilkens, C. A. Arnold, M. J. Jurek, M. E. Rogers and J. E. McGrath, *J. Thermoplast. Compos. Mater.*, 1990, **3**, 4-12.
66 J. M. Dennis, G. B. Fahs, R. B. Moore, S. R. Turner and T. E. Long, *Macromolecules*, 2014, **47**, 8171-8177.
67 W. Heitz, *Makromol. Chem. M. Symp.*, 1989, **26**, 1-8.
68 D. Pospiech, H. Komber, D. Voigt, L. Häußler, E. Meyer, G. Schauer, D. Jehnichen and F. Böhme, *Macromol. Chem. Phys.*, 1994, **195**, 2633-2651.
69 J. Wang and R. W. Lenz, *Polym. Eng. Sci.*, 1991, **31**, 739-742.
70 M. M. Sonpatki, K. Ravindranath and S. Ponrathnam, *Polymer*, 1995, **36**, 3127-3134.
71 M. M. Sonpatki, K. Ravindranath and S. Ponrathnam, *J. Polym. Sci., Part A: Polym. Chem.*, 1994, **32**, 2999-3007.
72 U. Schulze and H.-W. Schmidt, *Polym. Bull.*, 1998, **40**, 159-166.
73 N. Reichelt, U. Schulze and H.-W. Schmidt, *Macromol. Chem. Phys.*, 1997, **198**, 3907-3930.
74 U. Schulze, N. Reichelt and H.-W. Schmidt, *Macromol. Symp.*, 1997, **117**, 131-140.

75 C. M. Mahoney, J. A. Gardella and J. C. Rosenfeld, *Macromolecules*, 2002, **35**, 5256-5266.
76 M. Kajiyama, M. Kakimoto and Y. Imai, *Macromolecules*, 1989, **22**, 4143-4147.
77 J. E. McGrath, D. L. Dunson, S. J. Mecham and J. L. Hedrick, in *Progress in Polyimide Chemistry I*, ed. H. R. Kricheldorf, Springer Berlin Heidelberg, Berlin, Heidelberg, 1999, pp. 61-105.
78 V. V. Antic, M. R. Balaban and J. Djonlagic, *Polym. Int.*, 2001, **50**, 1201-1208.
79 V. V. Antic, M. N. Govedarica and J. Djonlagic, *Polym. Int.*, 2003, **52**, 1188-1197.
80 V. V. Antic, M. N. Govedarica and J. Djonlagic, *Polym. Int.*, 2004, **53**, 1786-1794.
81 M. V. Vučković, V. V. Antić, M. N. Govedarica and J. Djonlagić, *J. Appl. Polym. Sci.*, 2010, **115**, 3205-3216.
82 M. V. Vuckovic, V. V. Antic, B. P. Dojcinovic, M. N. Govedarica and J. Djonlagic, *Polym. Int.*, 2006, **55**, 1304-1314.
83 A. Ghosh and S. Banerjee, *Polym. Adv. Technol.*, 2008, **19**, 1486-1494.
84 A. Ghosh, S. K. Sen, S. Banerjee and B. Voit, *RSC Adv.*, 2012, **2**, 5900-5926.
85 A. Ghosh and S. Banerjee, *J. Appl. Polym. Sci.*, 2008, **109**, 2329-2340.
86 C.-K. Ku and Y.-D. Lee, *Polymer*, 2007, **48**, 3565-3573.
87 S. Andre, F. Guida-Pietrasanta, A. Rousseau and B. Boutevin, *J. Polym. Sci., Part A: Polym. Chem.*, 2001, **39**, 2414-2425.
88 C. A. Arnold, D. H. Chen, Y. P. Chen, R. O. Waldbauer, M. E. Rogers and J. E. McGrath, *High Perform. Polym.*, 1990, **2**, 83-94.
89 T. Matsumoto, Y. Koinuma, K. Waki, A. Kishida, T. Furuzono, I. Maruyama and M. Akashi, *J. Appl. Polym. Sci.*, 1996, **59**, 1067-1071.
90 K. Senshu, T. Furuzono, N. Koshizaki, S. Yamashita, T. Matsumoto, A. Kishida and M. Akashi, *Macromolecules*, 1997, **30**, 4421-4428.
91 T. Furuzono, K. Seki, A. Kishida, T.-A. Ohshige, K. Waki, I. Maruyama and M. Akashi, *J. Appl. Polym. Sci.*, 1996, **59**, 1059-1065.
92 T. Furuzono, K. Senshu, A. Kishida, T. Matsumoto and M. Akashi, *Polym. J.*, 1997, **29**, 201-203.
93 T. Matsumoto, T. Uchida, A. Kishida, T. Furuzono, I. Maruyama and M. Akashi, *J. Appl. Polym. Sci.*, 1997, **64**, 1153-1159.
94 E.-C. Kang, T. Kaneko, D. Shiino and M. Akashi, *J. Polym. Sci., Part A: Polym. Chem.*, 2003, **41**, 841-852.
95 A. Kishida, T. Kanda, T. Furuzono, I. Maruyama and M. Akashi, *J. Appl. Polym. Sci.*, 2000, **78**, 2198-2205.
96 A. Korematsu, T. Furuzono and A. Kishida, *Macromol. Mater. Eng.*, 2005, **290**, 66-71.
97 E.-C. Kang and M. Akashi, *Polym. J.*, 2002, **34**, 395-399.
98 T. Furuzono, E. Yashima, A. Kishida, I. Maruyama, T. MatsumotO and M. Akashi, *J. Biomater. Sci. Polym. Ed.*, 1994, **5**, 89-98.
99 M. Akashi, T. Furuzono, T. Matsumoto, A. Kishida and I. Maruyama, in *Advanced Biomaterials in Biomedical Engineering and Drug Delivery Systems*,

eds. N. Ogata, S. W. Kim, J. Feijen and T. Okano, Springer Japan, Tokyo, 1996, pp. 183-187.

100 T. Furuzono, A. Kishida, M. Yanagi, T. Matsumoto, T. Kanda, T. Nakamura, T. Aiko, I. Maruyama and M. Akashi, *J. Biomater. Sci. Polym. Ed.*, 1996, **7**, 871-880.

101 T. Otsuki, M.-A. Kakimoto and Y. Imai, *J. Polym. Sci., Part A: Polym. Chem.*, 1991, **29**, 611-618.

102 L. T. Cureton, F. L. Beyer and S. R. Turner, *Polymer*, 2010, **51**, 1679-1686.

Chapter 2 Synthesis of soluble all-aromatic ester-based oligomers with maleimide end-groups

Abstract

Two series of all-aromatic ester-based liquid crystalline (LC) and amorphous (AM) oligomers with maleimide end-groups are presented. The oligomers are based on poly(*p*-phenylene phenyl-terephthalate) with or without a phenyl substituent on the hydroquinone moiety, resulting in polymers with liquid crystal (nematic) and isotropic phase behavior, respectively. Phenyl addition increases the solubility, which makes it possible to access all-aromatic ester-based oligomers *via* low temperature solution polycondensation techniques. The oligomers exhibit an M_n range of 1 to 9 kg·mol^{-1}. All oligomers and reference polymers were characterized with gel permeation chromatography (GPC), viscometry and nuclear magnetic resonance (NMR). Viscometry and quantitative ^{13}C NMR analysis confirm that all oligomers have molecular weights close to the targeted molecular weight, while GPC shows all of the soluble oligomers have unimodal molecular weight distributions and PDIs of ~2, which is consistent with step-growth polymerization.

2.1 Introduction

All-aromatic thermoplastic polyesters, consisting of aromatic moieties linked by ester functionalities, have been studied extensively over the past several decades.[1] Due to the rigid-rod all-aromatic main-chain, this class of polymers exhibits excellent mechanical and thermal properties, enabling them to be used as high-strength and high-modulus fibers, precision molded small components and fiber reinforced composites.[2] However, these all-aromatic main-chain polyesters show major drawbacks in terms of processing, due to their poor solubility and extremely high melting temperature (often close to or slightly above the decomposition temperature). To help overcome these problems, solubility in common organic solvents would be desirable, along with a reduction in melting temperature. Over the years, structural modifications were reported on the all-aromatic backbone resulting in polyesters with solubility in common organic solvents like chloroform, dichloromethane, tetrahydrofuran (THF), dioxane and toluene.[3-7] The introduction of substituents of variable sizes on one or more of the constituent backbone monomers disrupts the packing of the polyester chain by inter-chain separation. This results in a suppression of the crystallinity and melting point and an enhancement of the solubility. As an example, we show a prototypical all-aromatic polyester based on terephthalic acid and hydroquinone, *i.e.* poly(*p*-phenylene terephthalate), in Figure 2.1. A variety of substituents including biphenyl, phenylalkyl, phenyl, phenoxy, *tert*-butyl, trifluoromethyl and halogen either in **X** or **Y** position (Figure 2.1) were reported displaying enhanced solubility and lowered melting points, depending on the substitution pattern.[2]

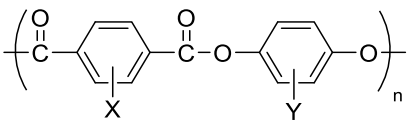

Fig. 2.1. Structure of the main-chain all-aromatic polyester. **X**, **Y** = biphenyl, phenylalkyl, phenyl, phenoxy, *tert*-butyl, trifluoromethyl and halogen.

The mono- and di-phenyl substituted poly(*p*-phenylene terephthalate), based on phenylterephthalic acid (PTPA) and hydroquinone (HQ) or phenylhydroquinone (PHQ) was first developed by Du Pont in 1980s, as shown in Figure 2.2.[8, 9] Compared

with poly(*p*-phenylene terephthalate), the phase behaviour and solubility were influenced significantly by introducing phenyl groups on the backbone.[10] For poly(*p*-phenylene terephthalate), a highly rigid polymer, the melting point is higher than 600 ˚C.[1, 11] Due to the introduction of bulky phenyl groups on the polymer chain, the phenyl substituted polymers show accessible melting temperatures. Poly(*p*-phenylene phenylterephthalate) shows a melting temperature (K-N) at 287 ˚C and an isotropization temperature (N-I) of 369 ˚C, and poly(phenyl-*p*-phenylene phenylterephthalate) was found to be completely amorphous.[10] In addition, the solubility of the polymers was substantially enhanced. Poly(*p*-phenylene phenylterephthalate) shows improved solubility in 1,1,2,2-tetrachloroethane and dichloroacetic acid. Poly(phenyl-*p*-phenylene phenylterephthalate) is soluble in most common organic solvents, such as tetrahydrofuran and chloroform. The fact that both polymer have very similar backbone structures and at the same time a distinct different phase behavior, makes them perfect candidates for studying the effect of backbone morphology in rigid-soft multiblock copolymers.

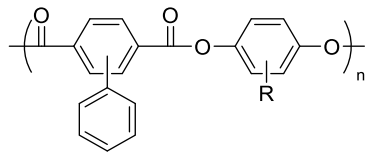

Reference polymer: R=H (LC) R=phenyl (AM)

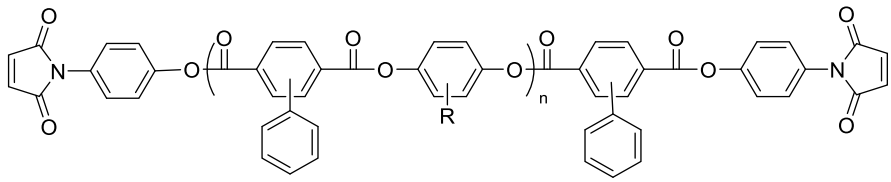

Oligomers with maleimide end-groups

in which R = H for poly(*p*-phenylene phenylterephthalate)
Phenyl for poly(phenyl-*p*-phenylene phenylterephthalate)

Fig 2.2. Chemical structures of the amorphous (AM) and liquid crystalline (LC) reference polymers and maleimide terminated oligomers based on poly(*p*-phenylene phenylterephthalate).

In order to end-functionalize the oligomers and to control the molecular weight, a maleimide functionality was selected as the polymer chain stopper, as

shown in Figure 2.2. The highly reactive maleimide end-groups enables us to work with highly effective thiol-ene click chemistry and prepare rigid-soft multiblock copolymers.[12-15] However, traditionally these polymers are prepared *via* melt polycondensation chemistry at elevated temperatures (>300 ˚C), which exceeds the crosslinking temperature of maleimides, making end-group functionalization not accessible.[16, 17] Premature crosslinking of the maleimide end-groups would prevent further functionalization of the rigid units with the soft (PDMS) segments. Thus, a solution-based synthetic method at low temperature is required for preparing this type of maleimide end-capped oligomers.

Herein, we present the solution-based synthesis and molecular weight characterization of well-defined all-aromatic ester-based oligomers (LC or AM) with maleimide end-groups having molecular weights in the range of 1 – 9 kg·mol^{-1}. The reactive oligomers were characterized by gel permeation chromatography (GPC) and nuclear magnetic resonance (NMR). Viscosity measurements were also performed to calculate and confirm the molecular weight. The presence of maleimide end-group was confirmed by NMR measurements.

2.2 Experimental

2.2.1 Materials

All chemicals were obtained from the indicated sources and used as received unless stated otherwise. 1-chloronaphthalene (85%) and 1,1,2,2-tetrachloroethane (TCE, 98%) were purchased from Acros Organics. Prior to use, both solvents were dried over CaH_2 at 120 °C for 5 h and distilled under vacuum at 125 °C. Triethylamine (NEt_3, 99%), from Sigma-Aldrich, was dried with CaH_2 at 100 °C for 5 h and distilled prior to use. Hexane (99%) was purchased from VWR and refluxed with CaH_2 under nitrogen atmosphere to remove moisture. The dried hexane was stored over CaH_2 and used only freshly distilled. Phenyl hydroquinone (PHQ, 97%) was obtained from Sigma Aldrich and recrystallized twice from chloroform under N_2 atmosphere. After performing recrystallization, PHQ was dried under vacuum at 60 °C for 24 h. The following chemicals were purchased from Sigma-Aldrich and used without further purification: maleic anhydride (99%), *p*-aminophenol (99%), sulfuric acid (98%), N,N-dimethylformamide (DMF, 99.8%), phosphorus pentoxide (P_2O_5, 99%), 2-bromo-1,4-dimethylbenzene (99%), Tetrakis(triphenylphosphine) palladium(0) ($Pd(PPh_3)_4$,

99%), Na_2CO_3 (99%), phenylboronic acid (95%), H_2O_2 (30%), pyridine (99%), potassium permanganate (99%), thionyl chloride (99%), and hydrochloric acid (30%). Ethanol, dichloromethane (DCM) and toluene were purchased from VWR. Deuterated solvents dimethyl sulfoxide (DMSO-d_6, 99.9 % D), deuterated trifluoroacetic acid (TFA-*d*, 99.5% D), and deuterated tetrachloroethane (TCE-d_2, 99.5 %D) were all purchased from Sigma Aldrich and used as received for NMR measurements.

2.2.2 Characterization

Nuclear magnetic resonance (NMR)

^{1}H and ^{13}C nuclear magnetic resonance (NMR) spectra were recorded on a 400 MHz Agilent-400 MR DD2 at room temperature. All samples were dissolved in deuterated solvents and the recorded spectra were referenced to the solvent or to TMS (DMSO-d_6: ^{1}H, 2.50 ppm and ^{13}C, 39.52 ppm. TFA-*d*: ^{1}H, 11.50 ppm).

Quantitative ^{13}C NMR spectra for end-group analysis were also recorded on a 400 MHz Agilent-400 MR DD2 spectrometer. A frequency of 100 MHz of inverse gated proton and long delays of 20 s between pulses and 1000 scans was used. All samples were dissolved in deuterated TCE and the recorded spectra were referenced to the solvent (TCE-d_2: ^{13}C, 73.78 ppm).

Gas chromatography–mass spectrometry (GC-MS)

GC-MS analyses were performed on a Shimadzu GC2010 series GC coupled to a MS detector (Shimadzu QP2010S), equipped with a BPX5 capillary column. The oven was heated from 50–300 °C at a rate of 10 °C·min^{-1} using a 1 mL·min^{-1} helium gas flow. The sample was injected using an ATAS GL Optic 3 inlet which was heated from 50–300 °C in one minute. Mass spectra were generated by electron impact and data was collected over the m/z range 45–900. Mass spectra were recorded using a Shimadzu QP2010S with direct injection port.

Gel permeation chromatography (GPC)

The molecular weights of the oligomers and polymers were determined using GPC. Samples were prepared at 1 mg·ml^{-1} in N-methyl-2-pyrrolidone (NMP) and filtered through a 0.45 µm PTFE syringe filter. Measurements were performed using a Shimadzu GPU DGU-20A3, equipped with a Shodex LF-801 column and refractive index detector. NMP containing 5 mM LiBr was used as the eluent at a flow rate of 0.5 ml·min^{-1} at 60 °C. Molecular weights were calculated using a polystyrene

standard calibration curve and data analyses were performed using labSolutions software from the refractive index detector data.

Viscometry

An Ubbelohde viscometer was used to measure the flow time of pure solvent and polymer or oligomer solutions. All viscosity measurements were carried out at 21 ± 0.01 °C in a water bath equipped with an automatic temperature controller. The flow time of pure solvent in the viscometer was first recorded. Afterwards, the flow time of an oligomer or polymer solution with known concentration (0.5 g·dL^{-1}) was measured. The ratio of flow time of polymer solution to that of pure solvent is regarded as the relative viscosity (η_{rel}). Therefore, the specific viscosity (η_{sp}) is defined as an increment of relative viscosity, and can be calculated using equation 2.1.

$$\eta_{sp} = \eta_{rel} - 1 \quad \text{(eqn. 2.1)}$$

The inherent viscosity (η_{inh}) was calculated according to equation 2.2, where *c* is the concentration of the polymer solution (g·dL^{-1}).

$$\eta_{inh} = \frac{\ln \eta_{rel}}{c} \quad \text{(eqn. 2.2)}$$

Solomon and Ciută reported the determination of intrinsic viscosity from one viscosity measurement of a polymer solution, using equation 2.3.[18, 19]

$$[\eta] = \frac{\sqrt{2}}{c} \times \sqrt{\eta_{sp} - \ln \eta_r} \quad \text{(eqn. 2.3)}$$

The Mark-Houwink-Sakurada equation relates the intrinsic viscosity ($[\eta]$) to the number average molecular weight (M).

$$[\eta] = K \times M^{\alpha} \quad \text{(eqn. 2.4)}$$

For poly(*p*-phenylene phenyl terephthalate) (*i.e.* LC-ref), the values of K and α were reported to be 1.06×10^{-2} and 1.0, respectively.[20] The K and α values at a low molecular weight range ($25 \leq [\eta] \leq 257$ cm^3·g^{-1}) for poly(phenyl-*p*-phenylene phenyl terephthalate) (*i.e.* AM-ref) were calculated to be 4.00×10^{-3} and 1.11, respectively.[21]

2.2.3 Synthesis of N-(4-hydroxyphenyl) maleimide

The synthesis of *N*-(4-hydroxyphenyl) maleimide (HPM) was based on literature procedures [22-25] and is depicted in scheme 2.1.

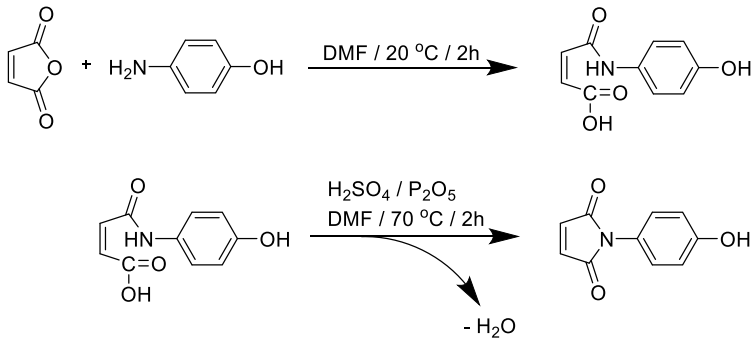

Scheme 2.1. Synthetic approach towards *N*-(4-hydroxyphenyl) maleimide (HPM).

A 250 mL round-bottom flask with magnetic stirring was charged with 16.37 g (0.15 mol) of *p*-aminophenol and 50 mL of DMF. A solution of 14.71 g (0.15 mol) maleic anhydride in 50 mL DMF was added dropwise. The solution was stirred at room temperature for 2 h, followed by the addition of 12.00 g P_2O_5 in 10 mL H_2SO_4 and 70 mL DMF. The mixture was allowed to stir for additional 2 h at 70 °C to complete the reaction. The mixture was then cooled in an ice bath and subsequently poured into 1 L cold water. The yellow precipitate was filtered, washed with water and recrystallized twice from isopropanol. This reaction yielded yellow needle-like crystals, which were dried under vacuum at 60 °C overnight. Yield: 20.20 g (71%). m. p.: 182 °C (lit: 182 - 184 °C); ^{1}H NMR (DMSO-d_6, 400 MHz) δ: 9.69 (s, OH); 7.13 (s, 2H); 7.07 (d, *J* = 8.7 Hz, 2H); 6.84 (d, *J* = 8.7 Hz, 2H). ^{13}C NMR (DMSO-d_6, 100 MHz) δ: 170.74, 157.45, 134.94, 128.84, 122.94, 115.85 ppm. MS *m/z* (relative intensity): 189.00 (100%, M+), 52.10 (73), 119.05 (65), 54.10 (64), 53.10 (35), 79.10 (24), 107.10 (24), 133.10 (23), 51.15 (22), 120.10 (21).

2.2.4 Synthesis of phenylterephthaloyl chloride

Phenylterephthaloyl chloride (PTPC) was synthesized according to a modified literature procedure[26], as shown in scheme 2.2.

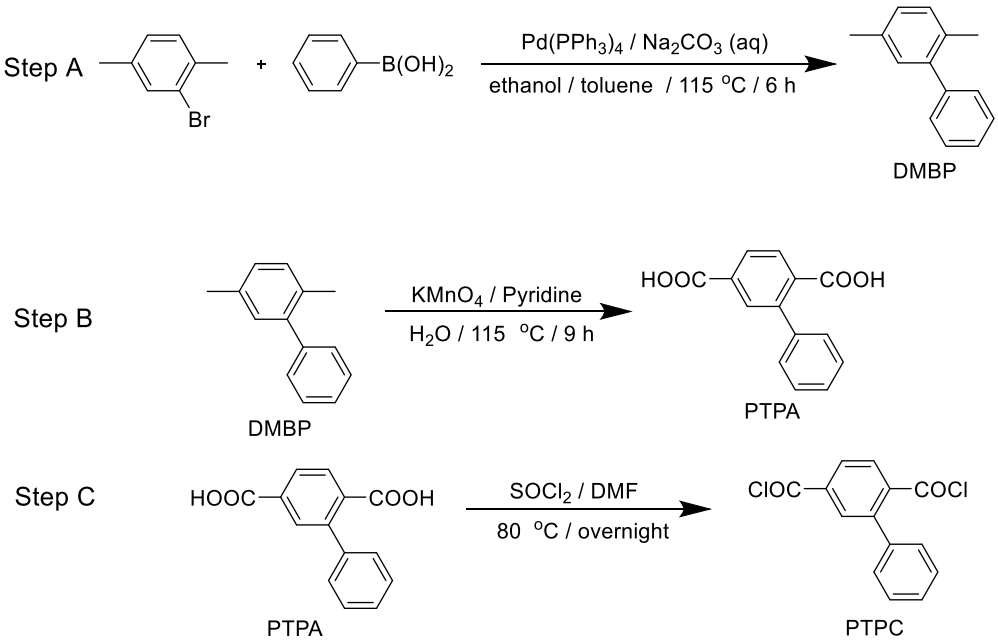

Scheme 2.2. Synthetic approach towards phenylterephthaloyl chloride (PTPC).

Synthesis of 2,5-dimethyl-biphenyl (DMBP)

A 2-L three-necked flask equipped with an overhead mechanical stirrer and reflux condenser was charged with 46.27 g (250 mmol) of 2-bromo-1,4-dimethylbenzene, 500 mL of toluene and 250 mL of an aqueous solution of 2 mol·L^{-1} Na_2CO_3 under an argon atmosphere. A solution of 32.00 g (262.50 mmol) of phenylboronic acid in 125 mL of ethanol was added, followed by 1.5 g (1.3 mmol) of $Pd(PPh_3)_4$ as catalyst. After degassing and backfilling with argon for 3 times, the yellow, dual-phase mixture was refluxed at 115 °C under vigorous stirring. The reaction was monitored using TLC with hexane as the mobile phase. After the reaction was completed (6 h), the residual phenylboronic acid was oxidized by 20 mL H_2O_2 (30 %) at room temperature for 1 h. The reaction mixture was extracted with ether, washed with brine, and subjected to a short silica gel filtration step with hexane as eluent to remove traces of catalyst. The product (DMBP) was obtained as a colorless oil, which was dried under vacuum at room temperature overnight. Crude yield: 45.40 g (249.1 mmol), 99.6 %. ^{1}H NMR (DMSO-d_6, 400 MHz): δ 2.17 (s, 3H), 2.29 (s, 3H), 7.00 (s, 1H), 7.08 (d, *J* = 7.7 Hz, 1H), 7.16 (d, *J* = 7.7 Hz, 1H), 7.27 – 7.47 (m, 5H). ^{13}C NMR (DMSO, 100 MHz): δ 141.85, 141.55, 135.18, 131.85, 130.64,

130.54, 129.30, 128.57, 128.28, 127.20, 20.94, 20.10. GC-MS *m/z* (relative intensity): t_r = 9.1 min. 182 (100%, M+), 165 (58), 181 (36), 166 (33), 152 (28), 89 (22), 77 (16).

Synthesis of phenylterephthalic acid (PTPA)

In a 2-L three-necked flask equipped with overhead mechanical stirrer and reflux condenser, 45.40 g (249 mmol) of DMBP was dissolved in a mixture of 750 mL of pyridine and 75 mL of H_2O. After an addition of 92 g $KMnO_4$, the mixture was allowed to reflux at 115 °C for 1 h. Over the next 8 hours, a total of 220 g of $KMnO_4$ in 500 mL of water was added in 8 portions, to the refluxing mixture. After cooling to room temperature, the phase separated mixture was filtered and the solid residual manganese dioxide was extracted twice with boiling water. The majority of pyridine from the water layer was removed by distillation under vacuum, after which dilute hydrochloric acid (10%) was added until the water layer was acidic. The precipitated white powder was filtered and washed several times with distilled water until the filtrate was neutral. After drying under vacuum at 80 °C, the crude product was recrystallized twice from glacial acetic acid. A white solid was obtained. Yield: 48.87 g (81 %). m. p.: 280 °C (lit: 278 -280 °C). ^{1}H NMR (DMSO-d_6, 400 MHz): δ 7.29 – 7.49 (m, 5H), 7.81 (d, *J* = 8.0 Hz, 1H), 7.88 (s, *J* = 8.0 Hz, 1H), 7.99 (d, 1H), 13.19 (s, COOH); ^{13}C NMR (DMSO-d_6, 100 MHz): δ 169.62, 166.94, 141.22, 140.35, 136.73, 133.05, 131.42, 129.69, 128.75, 128.65, 128.46, 128.03; MS *m/z* (relative intensity): 242 (100%, M+), 152 (87), 225 (72), 241 (50), 151 (43), 153 (39), 115 (32), 51 (31), 76 (30).

Synthesis of phenylterephthaloyl chloride (PTPC)

A 100-mL round-bottom flask, equipped with a reflux condenser, 6.00 g (0.0248 mol) of PTPA, 30 mL of thionyl chloride and 2 drops of DMF catalyst was added under a nitrogen atmosphere and refluxed at 80 °C overnight. The slightly yellow reaction solution was cooled to 60 °C and the residual thionyl chloride was distilled off under light vacuum. The remaining crude yellowish product was recrystallized from freshly distilled dry hexane, resulting in white flakes. Yield: 6.47 g (94%). m. p.: 58 °C (lit: 54 - 55 °C); ^{1}H NMR (DMSO-d_6, 400 MHz): δ 7.31 – 7.51 (m, 5H), 7.82 (d, *J* = 7.8 Hz, 1H), 7.88 (s, 1H), 7.98 (d, *J* = 7.8 Hz, 1H); MS *m/z* (relative intensity): 243 (100%, [M-Cl]+), 152(73), 76 (39), 151 (37), 245 (35), 180 (21).

2.2.5 Synthesis of reference polymers

The reference polymers were synthesized using standard solution polycondensation techniques with 1-chloronaphthalene as solvent, as shown in scheme 2.3.[27, 28] The reference polymer based on PTPC and HQ was reported to be liquid crystalline[10] and therefore labelled as "LC-ref", where LC refers to the liquid crystalline polymer backbone. The reference polymer from PTPC and PHQ has been reported as amorphous[10], and is therefore labelled as "AM-ref", referring to the amorphous polymer main-chain.

LC-ref: 2.79 g of PTPC (10.00 mmol), 1.10 g of HQ (10.00 mmol) and 60 mL of freshly distilled, dry 1-chloronaphthalene were charged to a 100 mL three-neck round-bottom flask, equipped with an argon gas inlet and outlet. After degassing and backfilling with argon three times, the clear solution was stirred at 180 °C for 24 h under a steady argon gas flow, removing the HCl by-product. After 24 hours, the reaction flask was allowed to cool down to room temperature, and the turbid mixture was quenched into 200 mL of ethanol. The obtained white solid was washed with hot DCM and ethanol for 3 times and dried in a vacuum oven at 60 °C overnight. A white solid was obtained in 98% yield (3.46 g). ^{1}H NMR (TFA-*d*, 400 MHz): δ 8.10 – 8.40 (m), 6.84 – 7.52 (m).

AM-ref: The same procedure as for LC-ref was used, except that 2.79 g of PTPC (10.00 mmol) and 1.86 g of PHQ (10.00 mmol) were added to 60 mL of dry freshly distilled 1-chloronaphthalene. A white solid was obtained after work-up in 97% yield (4.16 g). ^{1}H NMR (TFA-*d*, 400 MHz): δ 7.66 – 8.39 (m), 6.81 – 7.42 (m).

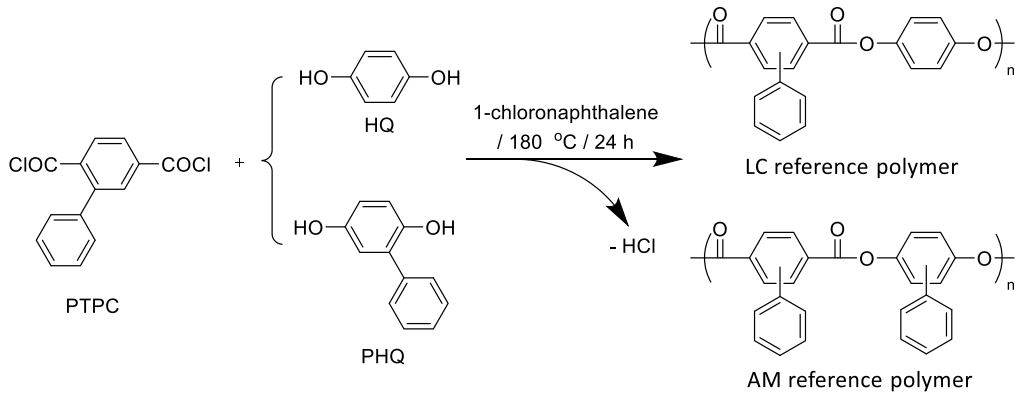

Scheme 2.3. Synthesis and backbone composition of the all-aromatic LC and AM reference polymers.

2.2.6 Synthesis of the maleimide terminated oligomers (small scale)

The reactive oligomers were synthesized using standard solution polycondensation techniques with 1-chloronaphthalene as solvent, as shown in scheme 2.4.[27, 28]

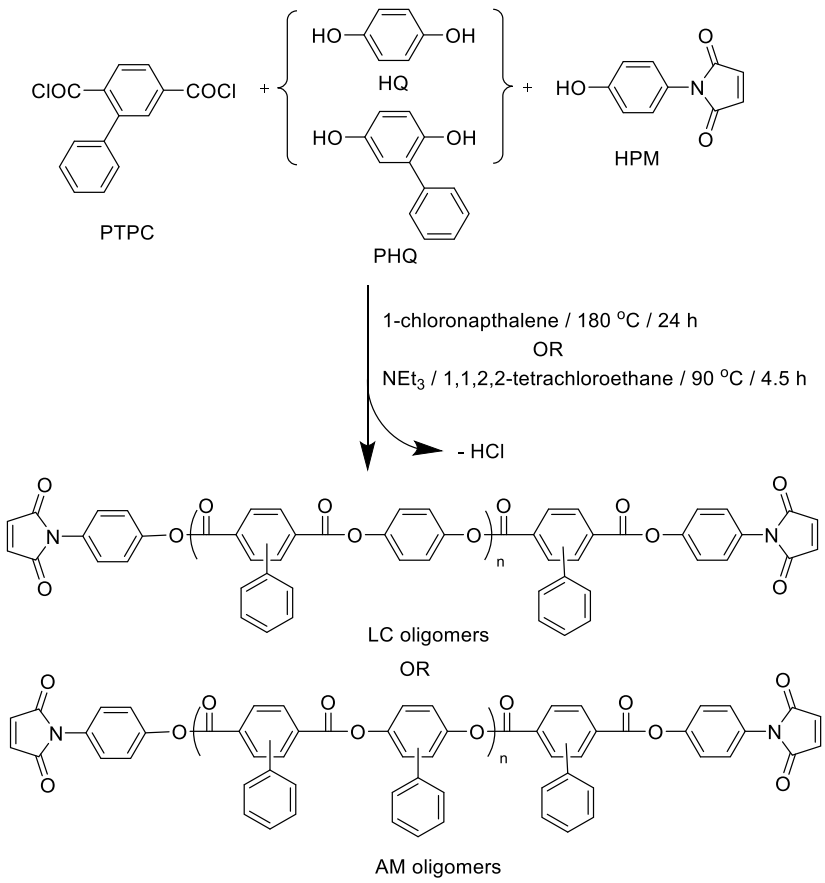

Scheme 2.4. Synthesis and backbone composition of the all-aromatic LC and AM oligomers (target $\overline{M}_n$ = 1, 5 and 9 kg·mol^{-1}) with maleimide end-groups.

In the first series, three reactive oligomers based on PTPC and HQ were prepared with a target $\overline{M}_n$ of 1, 5, and 9 kg·mol^{-1}. The samples were labelled, LC-1K, LC-5K, and LC-9K respectively, where LC refers to the liquid crystalline phase behavior and the integers reflect the polymer molecular weight (*i.e.* 5K = 5 kg·mol^{-1}). Similarly, another series of reactive oligomers were prepared from PTPC and PHQ *via* an identical procedure. These oligomers were labeled in the same fashion. For example, AM-1K, AM-5K and AM-9K refers to oligomers with an amorphous phase behavior with $\overline{M}_n$ of 1, 5, and 9 kg·mol^{-1}, respectively.

Molecular weight control

The classic Carothers[29] and Flory[30] theory for step polymerizations was utilized to calculate the ratios between the various monomers and the reactive end-groups, which is required to prepare the oligomers with a pre-specified molecular weight. The general Carothers equation for a polycondensation of *AA-BB* type is used to control the anticipated number average degree of polymerization ($\overline{x}_n$), as given by equation 2.5.

$$\overline{x}_n = \frac{1+r}{1+r-2rp} \quad \text{(eqn. 2.5)}$$

In this equation, p is the extent of the reaction, which is assumed to approach 1 upon complete polymerization, while r is the reactant ratio defining the ratio of various functionalities initially present in the reaction mixture.

The number average molecular weight ($\overline{M}_n$) can be calculated from the number average degree of polymerization $\overline{x}_n$ and the average molecular weight of the respective monomers ($\overline{M}_0$) *via* equation 2.6.

$$\overline{M}_n = \overline{M}_0 \, \overline{x}_n \quad \text{(eqn. 2.6)}$$

As can be concluded from equations 2.5 and 2.6, the conversion has to reach 100% (p approaches 1) and perfect stoichiometry ($r = 1$) is necessary in order to achieve high molecular weight polymer.

When an oligomeric species is desired, an offset in the monomer feed is used, and this is can be achieved by adding a mono-functional end-group. From equation 2.5 and 2.6, the number average degree of polymerization $\overline{x}_n$ and the reactant ratio r can be calculated. The reactant ratio r, is defined in equation 2.7.

$$r = \frac{N_{AA}}{N_{BB}} \quad (r \leq 1) \quad \text{(eqn. 2.7)}$$

The number of functional groups of AA monomer (diacid chloride) is defined as N_{AA}, while N_{BB} is the molar number of functional groups of BB monomer (bisphenol). In order to fully end-cap the A functionality excess oligomer with reactive mono-functional B end-groups, the molar amount of the two reacting functionalities must be equal, as expressed in equation 2.8, where N_B, represents the number of mono-functional B end-group (HPM).

$$2N_{AA} = 2N_{BB} + N_B, \quad \text{(eqn. 2.8)}$$

As an example, the stoichiometric ratio for the synthesis of a 5 kg·mol^{-1} (LC-5K) oligomer is calculated. The average molecular mass ($\overline{M}_0$) of a monomer unit in this ester-based oligomer is 158 g·mol^{-1}. For an anticipated oligomer with a number average molecular weight ($\overline{M}_n$) equal to 5 kg·mol^{-1}, the average degree of polymerization ($\overline{x}_n$) is 31.65. Assuming complete polymerization, the extent of the reaction will approach 1, therefore the reactant ratio r is calculated to be 0.94. By using equations 2.7 and 2.8, the stoichiometric offset can now be calculated. To prepare a 5 kg·mol^{-1} oligomer from 1 mol of diacid chloride (N_{AA}) and 0.94 mol of bisphenol (N_{BB}), 0.12 mol of HPM (N_B,) will be needed. The same approach was used to calculate the values for all other oligomers.

Synthesis of reactive oligomers in 1-chloronapthalene

LC-1K: PTPC (1.40 g, 5.00 mmol), HQ (0.39 g, 3.57 mmol), HPM (0.54 g, 2.86 mmol) and 30 mL freshly distilled dry 1-chloronaphthalene were charged to a 100 mL three-necked round-bottom flask, which was equipped with argon gas inlet and outlet. After degassing and backfilling with argon three times, the clear solution was allowed to stir at 180 °C for 24 h under a steady argon gas flow, removing the HCl by-product. Subsequently, the reaction flask was allowed to cool to room temperature and the turbid mixture was quenched with 200 mL ethanol. The obtained white solid was dissolved in hot DCM and precipitated in ethanol three times and dried under vacuum at 60 °C overnight. A white solid was obtained. Yield: 2.04 g, 96%. ^{1}H NMR (TFA-*d*, 400 MHz): δ 8.10 – 8.40 (m), 6.84 – 7.52 (m).

LC-5K: Following a procedure identical to *LC-1K*, except that 1.40 g of PTPC (5.00 mmol), HQ (0.52 g, 4.69 mmol), HPM (0.12 g, 0.69 mmol) were used as starting materials, yielding: 1.73 g of white solid, 95%. ^{1}H NMR (TFA-*d*, 400 MHz): δ 8.10 – 8.40 (m), 6.84 – 7.52 (m).

LC-9K: Following a procedure identical to *LC-1K*, except that PTPC (1.40 g, 5.00 mmol), HQ (0.53 g, 4.83 mmol), HPM (0.065 g, 0.35 mmol) were used as starting materials, yield: 1.75 g of white solid, 97%. ^{1}H NMR (TFA-*d*, 400 MHz): δ 8.10 – 8.40 (m), 6.84 – 7.52 (m).

AM-1K: Following a procedure identical to *LC-1K*, except that PTPC (1.40 g, 5.00 mmol), PHQ (0.62 g, 3.34 mmol), HPM (0.63 g, 3.31 mmol) were used as starting materials, yield: 2.31 g of white solid, 94%. ^{1}H NMR (TFA-*d*, 400 MHz): δ 8.01 – 8.38 (m), 6.81 – 7.77 (m).

AM-5K: Following a procedure identical to *LC-1K*, except that PTPC (1.40 g, 5.00 mmol), PHQ (0.86 g, 4.62 mmol), HPM (0.29 g, 0.015 mol) were used as starting materials, yield: 2.24 g of white solid, 95%. ^{1}H NMR (TFA-*d*, 400 MHz): δ 8.01 – 8.38 (m), 6.81 – 7.77 (m).

AM-9K: Following a procedure identical to *LC-1K*, except that PTPC (1.40 g, 5.00 mmol), PHQ (0.89 g, 4.79 mmol), HPM (0.081 g, 0.43 mmol) were used as starting materials, yield: 2.10 g of white solid, 96%. ^{1}H NMR (TFA-*d*, 400 MHz): δ 8.01 – 8.38 (m), 6.81 – 7.77 (m).

2.2.7 Scale-up synthesis of LC-1K-large, -5K-large and AM-1K-large, -5K-large oligomers

The scale-up synthesis of 1K and 5K oligomers of both LC and AM series were conducted in TCE with NEt_3 as an acid scavenger. The feed ratios of monomers and end-groups are discussed above, following the Carothers theory.

LC-1K-large: In a 500 mL three-necked round bottom flask equipped with overhead mechanical stirrer, 13.96 g (50.00 mmol) of PTPC, 3.93 g (35.71 mmol) of HQ and 5.41 g (28.57 mmol) of HPM were charged together with 140 mL freshly distilled, dry TCE at room temperature. After degassing and backfilling with argon, 14.0 mL (100.00 mmol) of dry triethylamine was added dropwise, while the temperature was gradually increased to 90 ° over 7 h. The turbid mixture was allowed to react at 90 °C for another 4.5 h. After the reaction was completed, the mixture was cooled to room temperature and precipitated in 500 mL of ethanol. The product was washed with hot DCM and ethanol for 3 times. A white solid was obtained after drying under vacuum at 60 °C overnight. Yield: 19.05 g, 97%. ^{1}H NMR (TFA-*d*, 400 MHz): δ 8.10 – 8.40 (m), 6.84 – 7.52 (m).

LC-5K-large: Following the procedure mentioned above for the synthesis of *LC-1K-large*: 9.77 g (35.00 mmol) of PTPC, 3.62 g (32.83 mmol) of HQ and 0.82 g (4.33 mmol) of HPM were added to 100 mL of freshly distilled, dry TCE with the addition of 10.0 mL (70 mmol) of dry triethylamine as an acid scavenger. A white solid was obtained after work up. Yield: 12.67 g, 98%. ^{1}H NMR (TFA-*d*, 400 MHz): δ 8.10 – 8.40 (m), 6.84 – 7.52 (m).

AM-1K-large: Following the procedure mentioned above for the synthesis of *LC-1K-large*: 12.84 g (46.00 mmol) of PTPC, 5.73 g (30.77 mmol) of PHQ and 5.76 g (30.46 mmol) of HPM were added to 130 mL of freshly distilled, dry TCE with the

addition of 13.0 mL (92.00 mmol) of dry triethylamine as an acid scavenger. A white solid was obtained after work up. Yield: 20.43 g, 96%. ^{1}H NMR (TFA-*d*, 400 MHz): δ 8.01 – 8.38 (m), 6.81 – 7.77 (m).

AM-5K-large: Following the procedure mentioned above for the synthesis of *LC-1K-large*: 9.77 g (35.00 mmol) of PTPC, 6.02 g (32.35 mmol) of PHQ and 1.00 g (5.30 mmol) of HPM were added to 100 mL of freshly distilled, dry TCE with the addition of 19.5 mL (140 mmol) of dry triethylamine as an acid scavenger. A white solid was obtained after work up. Yield: 15.01 g, 97%. ^{1}H NMR (TFA-*d*, 400 MHz): δ 8.01 – 8.38 (m), 6.81 – 7.77 (m).

2.3 Results and Discussion

2.3.1 Synthesis of HPM and PTPC

The reactive end-group HPM was synthesized following literature procedures.[22-25] Structural characterizations, including NMR and MS, confirmed the molecular structure and are comparable to the reported data.

The synthesis of phenylterephthaloyl chloride has been reported in literature by Tore *et al.* with an overall yield of less than 46%.[26] The synthesis consists of three steps: first, 2,5-dimethylbiphenyl was synthesized; next, the methyl groups were oxidized with $KMnO_4$; and finally, the dicarboxylic acid was converted to the diacid chloride by reacting with thionyl chloride, catalysed by DMF. The authors tried three different starting materials for synthesizing 2,5-dimethylbiphenyl: dibenzoyl peroxide, benzene diazonium tetrafluoroborate and the Ni-promoted reaction of Grignard compounds with iodobenzene to introduce a phenyl substituent. All three attempts suffered from either low yields or the formation of significant amounts of side products.

To increase the yield and decrease the formation of side products, a modified procedure was developed. Here, 2,5-dimethylbiphenyl was prepared by phenylation of 2-bromo-1,4-dimethylbenzene using the highly efficient Suzuki coupling reaction with a commercially available palladium catalyst, $Pd(PPh_3)_4$. The yield was found to be nearly quantitative, comparable to similar reports in the literature.[31] The palladium catalyst was conveniently removed by filtering the reaction mixture over

a short silica gel column. The purity of the product was confirmed by GC-MS and ^{1}H NMR.

The obtained 2,5-dimethylbiphenyl was oxidized with $KMnO_4$, in moderate yields according to the literature procedure, with pyridine as a phase transfer agent. The resulting diacid was converted to the diacid chloride under reflux with thionyl chloride. The target product phenylterephthaloyl chloride was purified by recrystallization in dry hexane to give white crystal flakes. The overall yield was 76%, which is significantly higher than the 46% yield reported by Tore *et al*.[26] Structural characterization using NMR and MS confirmed the successful synthesis of PTPC.

2.3.2 Synthesis of maleimide terminated oligomers and reference polymers

The maleimide functionalized oligomers were synthesized *via* solution polycondensation in 1-chloronaphthalene, according to literature procedures.[27, 28] The small-scale polymerizations were straightforward and no evidence for premature cross-linking of the maleimide end-group, such as gelation or precipitation, was observed under the reaction conditions used. The obtained oligomers were analysed by ^{1}H NMR and the assignment of protons of the LC oligomers and reference polymers are shown in Figure 2.3, as representative examples. The proton signal of the maleimide end-group in Figure 2.3 increases from the oligomer samples LC-9K to 1K, which can be considered as qualitative evidence for the successful synthesis of the maleimide end-capped oligomers. The spectra obtained for the AM-series gave similar results.

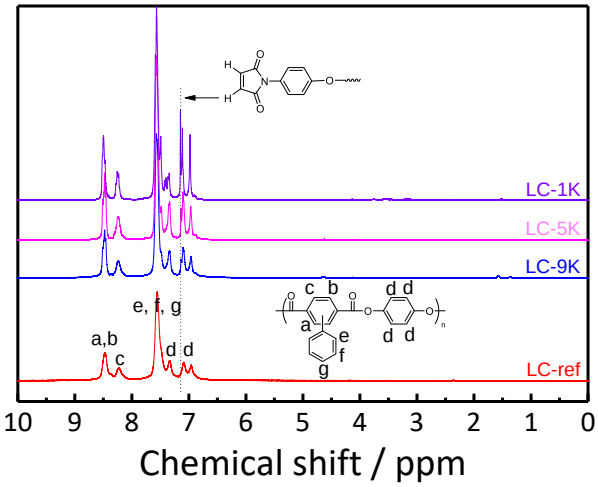

Fig. 2.3. ^{1}H NMR spectra of the LC oligomers ($\overline{M}_n$ = 1, 5 and 9 kg·mol^{-1}) and reference polymer were recorded in TFA-*d*. The spectra were offset for clarity. The assignment of protons of the LC oligomers and reference polymers are shown in the inset. The intensity of maleimide peak (δ = 7.14 ppm) varies depending on the end-group contents.

2.3.3 Molecular weight characterization and end-group analysis

GPC and viscometry

Soluble samples were characterized by GPC and viscometry. Table 2.1 summarizes the molecular weights of the oligomers and reference polymers as determined with GPC and the traces are shown in Figure 2.4. All the soluble samples showed unimodal molecular weight distributions and PDIs of ~2, which is consistent with step-growth polymerization. The LC-5K sample showed a lower molecular weight than AM-5K measured by GPC. However, LC-5K exhibited higher inherent viscosity than AM-5K. This can be explained considering that the higher molecular weight portion of LC-5K was filtered off before the GPC experiment due to the limited solubility of this oligomer in NMP. This claim is supported by the slightly lower PDI value of LC-5K. The GPC data confirms the trend, an increase in molecular weight going from 1 to 9 kg·mol^{-1}, but the $\overline{M}_n$ values deviate from the calculated values. This can be understood when one considers the fact that polystyrene, a random coil polymer, was used as the internal standard for the GPC measurements.

The molecular weights calculated using the Mark-Houwink-Sakurada equation of eqn. 2.3 and 2.4 from intrinsic viscosity ($[\eta]$), as well as the inherent viscosity of all the oligomers and reference polymers are presented in Table 2.1. Generally, the experimental molecular weight vlaues from viscometry measurements show a trend that is in line with the calculated $\overline{M}_n$ values.

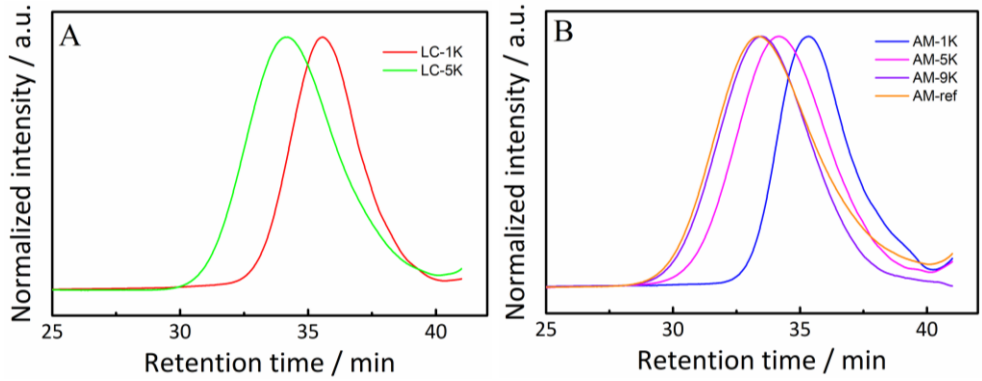

Fig. 2.4. GPC curves of reactive oligomers and the reference polymer. The curves are normalized to the maximum intensity. **A**- The liquid crystal reactive oligomers; **B**- The amorphous reactive oligomers and reference polymers.

Calculation of $\overline{M}_n$ using quantitative ^{13}C NMR

Determination the end-group concentration is of great importance, as it will provide information about the molecular weight and is critical for future block copolymer synthesis or thermal curing. Characterization using ^{1}H NMR spectroscopy is generally the most valuable technique, as spectra obtained give reliable integrations that are directly related to specific proton ratios.[32] However, this technique is limited by spectral congestion of closely grouped proton peaks. In literature, polymers have alternatively been analyzed by quantitative solution ^{13}C NMR spectroscopy, to determine the degree of polymerization ($\overline{DP}$)[33, 34]. In our case, since proton peaks assigned to maleimide end-groups overlap with those of aromatic protons in the main-chain, as shown in Figure 2.3, quantitative ^{13}C NMR was performed on the oligomers to quantify the maleimide end-groups. This information can then be used to determine the molecular weight of the oligomers.[34-37] To achieve sufficient signal-to-noise ratios, long relaxation delays are required. Integration of

carbon resonances of two different groups of carbon atoms can only be compared if the same number of hydrogen atoms are present in each group. This is to minimize differences in nuclear Overhauser effect.[38]

In order to calculate the number average molecular weight ($\overline{M}_n$) of our oligomers from quantitative ^{13}C NMR data, the degree of polymerization ($\overline{DP}$) of the oligomers was determined using equation 2.9. For a dual end-capped ester-based oligomer, the number of carbonyl groups within the main-chain (N_{CO}) corresponds to two carbonyl group in one repeating unit, while the number of maleimide end-groups (N_{end}), corresponds to 4 carbonyl groups. Combined with $\overline{DP}$ a relationship is formed where I_{end} and I_{CO} represent the integrals of the peaks of the terminal end-group and the carbonyl groups within the polymer chain, respectively.

$$\frac{N_{end}}{N_{CO}} = \frac{I_{end}}{I_{CO}} = \frac{4}{2\times\overline{DP}} \quad \text{(eqn. 2.9)}$$

Therefore $\overline{M}_n$s of the oligomers can be calculated by equation 2.10,

$$\overline{M}_n = \overline{DP} \times M_0 + 2 \times M_{end} \quad \text{(eqn. 2.10)}$$

Where M_0 and M_{end} are molecular weights of the repeat units (316 and 392 g·mol^{-1} for LC and AM oligomers, respectively) and maleimide end-groups (188 g·mol^{-1}).

In Figure 2.5 the quantitative ^{13}C NMR spectra of both LC-5K and AM-5K are shown with the assignment of oligomer carbonyl groups. The carbonyl carbons of the polymer gave rise to 2 (for LC oligomers) or 3 (for AM oligomers) distinct resonances covering a total chemical shift range of 4 ppm (ranging from 163 to 167 ppm). This is due to the random arrangements of the bulky phenyl groups at the backbone in consecutive repeating units along the polyester chain.[7, 39] The resonance at 169 ppm is assigned to the carbonyl carbon of maleimide end-groups. As an example, the calculation of $\overline{M}_n$ for the LC-5K sample is further explained. Using equation 2.9, $\overline{DP}$ is calculated to be 17.06 using the integrals of carbonyl peaks from both maleimide and main-chain (peaks a and b at 169 ppm and 164/166 ppm in Figure 2.5, respectively). Using equation 2.10, $\overline{M}_n$ is calculated to be 5.7 kg·mol^{-1}. The calculated $\overline{M}_n$ and experimental data is summarized in Table 2.1. The calculated $\overline{M}_n$s of the oligomers are in close proximity of the targeted molecular weights and similar to those obtained by viscometry analysis. The calculation based on the integrals in ^{13}C NMR was performed on all maleimide-functionalized samples except

LC-9K and AM-9K oligomers, due to the low signal-to-noise ratios, which is the result of the low solubility of the 9K samples in deuterated TCE.

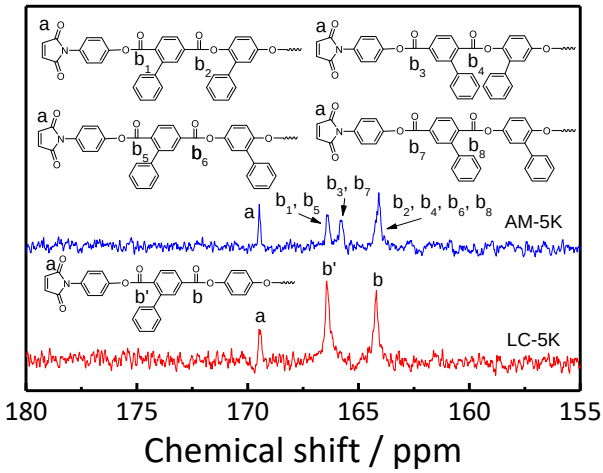

Fig. 2.5. Quantitative ^{13}C NMR spectra of carbonyl groups of LC-5K and AM-5K. The integration can be used to calculate the molecular weight ($\overline{M}_n$) of the oligomers.

Table 2.1. Molecular weight results of the reactive oligomers and their reference polymers.

Sample	*GPC results*[1]			$\overline{M}_v$ (kg·mol^{-1})	η_{inh} (*dL·g^{-1}*)[5]	$\overline{M}_n$ (kg·mol^{-1}, *NMR*)
	$\overline{M}_n$ (kg·mol^{-1})	$\overline{M}_w$ (kg·mol^{-1})	*PDI*			
LC-1K	5.2	10	1.9	1.8[3]	0.19	1.5
LC-5K	8.0	15	1.8	5.6[3]	0.57	5.7
LC-9K	N/A[2]	N/A[2]	N/A[2]	9.6[3]	0.94	N/A[6]
LC-ref	N/A[2]	N/A[2]	N/A[2]	13[3]	1.22	N/A[7]
AM-1K	5.3	10	1.9	1.5[4]	0.16	1.7
AM-5K	9.3	17	1.9	4.6[4]	0.47	6.7
AM-9K	12	23	2.1	7.6[4]	0.63	N/A[6]
AM-ref	12	25	2.0	11[4]	0.85	N/A[7]

[1] GPC characterization was performed using NMP as eluent and polystyrene as internal standard.

[2] Could not be determined due to limited solubility in NMP at room temperature.

[3] Viscometry measurements in TCE of LC oligomers and reference polymer was at a concentration of 0.5 g·dL^{-1}.

[4] Viscometry measurements of AM oligomers and reference polymer in 1,4-dioxane at a concentration of 0.5 g·dL^{-1}.

[5] Viscometry measurements of the LC and AM oligomers and reference polymers in TCE at a concentration of 0.5 g·dL^{-1}.

[6] Could not be determined due to low signal-to-noise ratio.

[7] Not applicable because of no detectable end-groups on ^{13}C NMR spectra.

2.3.4 Scale-up synthesis of LC-1K-large, -5K-ref and AM-1K-large, -5K-ref

After synthesis of the LC and AM oligomers with various molecular weights, oligomers with molecular weights of 1 and 5 kg·mol^{-1} were selected for scale-up syntheses. This is because preliminary polymerization experiments showed that oligomers with an $\overline{M}_n$ of 9 kg·mol^{-1} did not result in high molecular weight block copolymers. However, large scale production of the desired oligomers proved to be unsuccessful if the batch scale was larger than 5 g. In the ^{1}H NMR spectrum of the obtained product (the bottom curve shown in Figure 2.6), two extra resonances at 1.47 (triplet) and 4.53 (quartet) ppm emerged. These peaks can be assigned to the resonances of an ethyl ester formed during the precipitation after the reaction and is most likely caused by the incomplete reaction of acid chloride and phenol under the reaction conditions. GPC measurements showed substantially lower molecular weights for these LC-5K oligomers ($\overline{M}_n$, $\overline{M}_w$ and PDI for LC-5K are 4.0, 6.0 kg·mol^{-1} and 1.5, respectively) than that was measured for the small-scale reaction products.

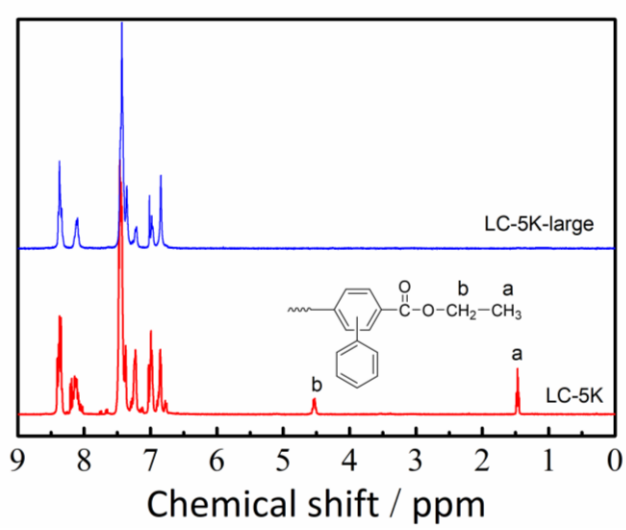

Fig. 2.6. Side reaction of alkyl ester in the LC-5K oligomer as confirmed by NMR. The peaks located at 1.47 (triplet) and 4.53 (quartet) ppm are assigned to the resonances of an ethyl ester formed by reaction between the unreacted acid chloride and ethanol in work-up of the polymers. The ester is not present in the LC-5K-large batch.

The reason for the lower molecular weight and incomplete reaction of the acid chloride is the incomplete removal of the HCl by-product. During synthesis of the oligomers in 1-chloronaphthalene, the by-product HCl is removed by a steady argon gas flow, which proved to be too slow or inefficient even though the equilibrium constant for acid chloride-phenol polyarylate synthesis is large (K = 4700).[40] The efficiency of HCl removal is highly depending on relative surface area, reaction time and temperature, etc. If the reaction time was extended (≥36 h) at 180 °C, an insoluble white solid precipitated from the solution, due to premature crosslinking of the maleimide end-groups. The LC main-chain has limited solubility at lower temperatures, therefore adjusting the reaction temperature (<170 °C) results in precipitation and substantially lower yields and molecular weights.

In order to synthesize the oligomers on a larger scale, a TCE-based polycondensation route was developed. Here, TCE was used as the solvent, while NEt_3 was added as a hydrochloric acid acceptor to help push the equilibrium towards the formation of oligomer. Pyridine was proved to be inappropriate as the acid scavenger, because gelation was observed at ~80 °C, resulting in an insoluble

product. This can be explained by the observation that maleimide functionalities can undergo catalyzed polymerization in the presence of pyridine.[41]

The GPC and viscometry characterization of both oligomers are summarized in Table 2.2. The LC-1K-large and AM-1K-large show similar molecular weights to those of the LC-1K and AM-1K oligomers synthesized in 1-chloronaphthalene. Both of the LC-5K-large and AM-5K-large samples show slightly higher molecular weights and inherent viscosity, proving the assumption of incomplete reaction and low molecular weight caused by the low efficiency of HCl removal problem discussed earlier. It is also worth noting that the molecular weights of LC-5K-large and AM-5K-large calculated by quantitative ^{13}C NMR data are slightly lower than those of LC-5K and AM-5K oligomers, even though the scaled-up samples show slightly higher inherent viscosity. This is because the calculation is based on an assumption that every chain-end is end-capped with maleimide groups, but under the harsh reaction conditions at 180 °C in 1-chloronaphtalene a loss of end-group functionality (e.g. premature crosslinking reaction of maleimide end-groups) might occur. The higher concentration of end-groups of LC-5K-large and AM-5K-large might be an indication that the TCE based route is more compatible with the reactive maleimide end-groups.

Table 2.2. Molecular weight characterization of the scale-up reactive oligomers.

Sample	***GPC results*[1]**			$\overline{M}_v$ (kg·mol^{-1})	η_{inh} (dL·g^{-1})	$\overline{M}_n$ (kg·mol^{-1}, NMR)
	$\overline{M}_n$ (kg·mol^{-1})	$\overline{M}_w$ (kg·mol^{-1})	***PDI***			
LC-1K-large	5.2	10	1.9	1.7	0.20	1.4
AM-1K-large	5.5	11	1.9	1.6	0.18	1.8
LC-5K-large	N/A[2]	N/A[2]	N/A[2]	7.1	0.70	5.3
AM-5K-large	11	20	2.0	5.5	0.52	4.9

[1] GPC characterization was performed using NMP as eluent and polystyrene as internal standard.

[2] Could not be measured due to limited solubility in NMP at room temperature.

2.4 Conclusion

We have successfully demonstrated the synthesis of maleimide terminated oligomers from PTPC and HQ (LC) or PHQ (AM) with various molecular weights of 1, 5 and 9 kg·mol^{-1}, as well as their high molecular weight reference polymers, by solution-based polycondensation. The molecular weight of the oligomers was controlled using the Carothers equation. GPC, viscometry and quantitative ^{13}C NMR were used to characterize the molecular weight of the oligomers and polymers. The molecular weights of the oligomers determined experimentally by ^{13}C NMR and viscometry are very close to the calculated theoretical values, *i.e.* 1, 5 and 9 kg·mol^{-1}. The GPC data confirms the trend, an increase in molecular weight going from 1 to 9 kg·mol^{-1}, but the $\overline{M}_n$ values deviate from the calculated values. This can be understood when one considers the fact that polystyrene, a random coil polymer, was used as the internal standard. All soluble samples showed unimodal molecular weight distributions and PDIs of ~2, which is consistent with step-growth polymerization. ^{1}H NMR shows that the maleimide end-groups remain intact during synthesis, enabling further functionalisation of these oligomers towards block copolymers.

2.5 References

1 W. J. Jackson, *Brit. Polym. J.*, 1980, **12**, 154-162.

2 H. Han and P. K. Bhowmik, *Prog. Polym. Sci.*, 1997, **22**, 1431-1502.

3 C. Noël, C. Friedrich, F. Lauprêtre, J. Billard, L. Bosio and C. Strazielle, *Polymer*, 1984, **25**, 263-273.

4 R. Sinta, R. A. Gaudiana, R. A. Minns and H. G. Rogers, *Macromolecules*, 1987, **20**, 2374-2382.

5 W. Heitz and H.-W. Schmidt, *Makromol. Chem. M. Symp.*, 1990, **38**, 149-160.

6 F. Navarro and J. L. Serrano, *J. Polym. Sci., Part A: Polym. Chem.*, 1992, **30**, 1789-1798.

7 P. K. Bhowmik and H. Han, *Macromolecules*, 1993, **26**, 5287-5294.

8 *J. F. Harris, US Pat.,* US4294955 A, 1981.

9 *C. R. Payet, US Pat.,* US4159365 A, 1979.

10 W. R. Krigbaum, H. Hakemi and R. Kotek, *Macromolecules*, 1985, **18**, 965-973.

11 N. P. Cheremisinoff, *Handbook of Polymer Science and Technology*, Taylor & Francis, 1989.

12 C. E. Hoyle and C. N. Bowman, *Angew. Chem. Int. Ed.*, 2010, **49**, 1540-1573.
13 M. J. Kade, D. J. Burke and C. J. Hawker, *J. Polym. Sci., Part A: Polym. Chem.*, 2010, **48**, 743-750.
14 H. Li, S. Thanneeru, L. Jin, C. J. Guild and J. He, *Polym. Chem.*, 2016, **7**, 4824-4832.
15 A. B. Lowe, *Polym. Chem.*, 2010, **1**, 17-36.
16 G. D. Lyle, J. S. Senger, D. H. Chen, S. Kilic, S. D. Wu, D. K. Mohanty and J. E. McGrath, *Polymer*, 1989, **30**, 978-985.
17 P. Mison and B. Sillion, in *Progress in Polyimide Chemistry I*, ed. H. R. Kricheldorf, Springer Berlin Heidelberg, Berlin, Heidelberg, 1999, DOI: 10.1007/3-540-49815-x_5, pp. 137-179.
18 O. F. Solomon and I. Z. Ciută, *J. Appl. Polym. Sci.*, 1962, **6**, 683-686.
19 V. O. F. Solomon and B. S. Gotesman, *Makromol. Chem.*, 1967, **104**, 177-184.
20 V. N. Tsvetkov, S. V. Bushin, L. N. Andreeva, C. P. Smirnov, E. V. Belyaeva, A. Y. Bilibin and A. R. Stepanova, *Eur. Polym. J.*, 1992, **28**, 91-96.
21 S. V. Bushin, K. P. Smirnov, L. N. Andreeva, Y. V. Belyaeva, A. Y. Bilibin, A. R. Stepanova and V. N. Tsvetkov, *Polym. Sci. (USSR) (Engl. Transl.)*, 1990, **32**, 1015-1021.
22 I. A. Mohammed and A. Mustapha, *Molecules*, 2010, **15**, 7498.
23 P. S. G. Krishnan, C. He and C. T. S. Shang, *J. Polym. Sci., Part A: Polym. Chem.*, 2004, **42**, 4036-4046.
24 J. O. Park and S. H. Jang, *J. Polym. Sci., Part A: Polym. Chem.*, 1992, **30**, 723-729.
25 G. Pitchaimari and C. T. Vijayakumar, *J. Appl. Polym. Sci.*, 2014, **131**, 39935.
26 H. T. Land, W. Hatke, A. Greiner, H.-W. Schmidt and W. Heitz, *Makromol. Chem.*, 1990, **191**, 2005-2016.
27 N. Reichelt, U. Schulze and H.-W. Schmidt, *Macromol. Chem. Phys.*, 1997, **198**, 3907-3930.
28 U. Schulze and H.-W. Schmidt, *Polym. Bull.*, 1998, **40**, 159-166.
29 W. H. Carothers, *Chem. Rev.*, 1931, **8**, 353-426.
30 P. J. Flory, *Chem. Rev.*, 1946, **39**, 137-197.
31 N. Miyaura, T. Yanagi and A. Suzuki, *Synth. Commun.*, 1981, **11**, 513-519.
32 F. Malz and H. Jancke, *J. Pharm. Biomed. Anal.*, 2005, **38**, 813-823.
33 M. R. Seger and G. E. Maciel, *Anal. Chem.*, 2004, **76**, 5734-5747.
34 J. N. Shoolery, *Prog. Nucl. Magn. Reson. Spectrosc.*, 1977, **11**, 79-93.
35 T. H. Mareci and K. N. Scott, *Anal. Chem.*, 1977, **49**, 2130-2136.
36 D. J. Cookson and B. E. Smith, *J. Magn. Reson.*, 1984, **57**, 355-368.
37 E. Caytan, G. S. Remaud, E. Tenailleau and S. Akoka, *Talanta*, 2007, **71**, 1016-1021.
38 D. A. L. Otte, D. E. Borchmann, C. Lin, M. Weck and K. A. Woerpel, *Org. Lett.*, 2014, **16**, 1566-1569.

39 P. K. Bhowmik, E. D. T. Atkins, R. W. Lenz and H. Han, *Macromolecules*, 1996, **29**, 3778-3786.
40 A. Fradet and M. Tessier, in *Synthetic Methods in Step-Growth Polymers*, John Wiley & Sons, Inc., 2003, pp. 17-134.
41 D. Decker, *Makromol. Chem.*, 1973, **168**, 51-58.

Chapter 3 Characterization and properties of soluble all-aromatic ester-based oligomers with maleimide end-groups

Abstract

In this chapter, we will describe the thermal stability, thermo-mechanical properties and phase behavior of the maleimide terminated LC and AM oligomers and their reference polymers. With the introduction of phenyl groups onto the backbone, all oligomers and reference polymers show improved solubility and excellent thermal stabilities, with $T_d^{5\%}$ >390 °C. T_gs of the uncured LC oligomers and reference polymer are in the range of 136–157 °C, whereas the AM series show T_gs ~130 °C. After crosslinking, an increase in T_g was found for all oligomers. Marbled nematic textures were observed for the LC polymer and oligomers, and the nematic phase became fixed after cure. The AM series, on the other hand, is completely amorphous before and after cure. The phase behavior for both the LC and AM series was confirmed by WAXD. All oligomers with a Mn of 1 and 5 kg·mol^{-1} became highly crosslinked after cure, whereas the oligomers with a Mn of 9 kg·mol^{-1} appeared to be partly crosslinked. All thermoset films are mechanically stable up to ~300 °C as confirmed by DMTA, which is the result of network formation. In tensile test, all cured AM oligomers show superior mechanical properties over their LC analogs at 25 °C, with tensile strengths of ~90 MPa, elongation at break ~ 10% and toughness of ~8 MJ·m^{-3}.

3.1 Introduction

High-performance polymers are macromolecules that typically exhibit high glass transition temperatures, high decomposition temperatures, and excellent mechanical properties. Ever since the introduction of high-performance polymers, enormous efforts from both academia and industry have been put into the field. Well-known high-performance polymers include polyimides (*e.g.*, Kapton™ and Upilex™), main-chain all-aromatic liquid crystal (LC) polymers such as *para*-aramid (*e.g.*, Twaron™ and Kevlar™), polybenzoxazoles (*e.g.*, Zylon™), and polybenzimidazoles (PBIs; *e.g.*, Celazole™). These polymers exhibit excellent mechanical properties and high thermal stability, attributed to their rigid all-aromatic backbones. However, they are inherently difficult to process due to poor solubility and extremely high melting temperatures.[1] Rigid-rod aromatic polyesters, for example poly(*p*-phenylene terephthalate) (PPTT), as shown in Figure 3.1, has a melting point (T_m) at 600 °C at a heating rate of 80 °C·min^{-1}, which is higher than the decomposition temperature.[2, 3] Research has shown that the introduction of substituents on the aromatic rings is an effective way of lowering the melting temperature of high-performance polymers and to prepare melt processable materials.[2, 4]

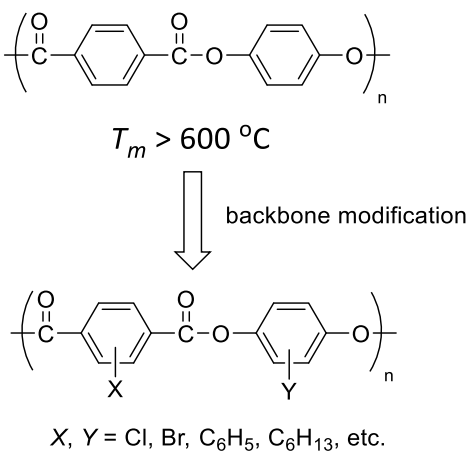

Fig. 3.1. Chemical structure of the parent aromatic polyester poly(*p*-phenylene terephthalate) (PPTT) and a few examples of substituted analogs. PPTT melts at temperatures above 600 °C, whereas main-chain modifications (**X-** and **Y-** substituents) can lower the melt temperature to well below 300 °C.

W. R. Krigbaum and colleagues studied the effect of –Cl, –Br, $–C_6H_5$ and $–C_6H_{13}$ substituents upon the transition temperatures of poly(*p*-phenylene terephthalate)s.[4] Compared to the extremely high melting point ($T_{K\text{-}N}$) of PPTT of 600 °C, the melting point of the phenyl-substituted poly(*p*-phenylene terephthalate) (**X-** and **Y-** substituted, as shown in Figure 3.1), was lowered to 287 and 346 °C, respectively. The melt viscosity was also lowered substantially, making melt processing possible.

Another effective means to avoid difficulties in processing of high-performance polymers is to prepare low molecular weight oligomers (Mn ~500–9000 g/mol) with curable chain-end functionalities, and cure the oligomers at a certain processing temperature.[1] The low melt viscosities and low after-cure coefficients of thermal expansion (CTE) of the high-performance thermosets enables one to prepare complex final products in, for instance microelectronic and fiber-reinforced composite applications.

Bis-maleimides (BMIs), including small molecules and oligomers, are one of the most extensively studied high-performance thermosets, benefitting from the low costs, high after-cure T_g, excellent processability, low curing temperatures and void-free curing. However, the cured small molecular bis-maleimide thermosets tend to be brittle ($\varepsilon < 1\%$), where bis-maleimide end-capped oligomers have shown to overcome this by incorporating properties from other backbone structures. A large variety of backbones have been used to prepare oligomers with bis-maleimide end-groups, such as polysulfones[5], poly(etherketoneketone)s[6, 7], poly(ether ketones)[8], poly(diethyleneglycol terephthalate)[9], poly(oxyethylene)[10], and polymethylene[11]. Compared to cured small BMI molecules, the oligomers show lower crosslinking densities and higher toughness.[12]

In Chapter 2, the synthesis and molecular weight characterization of the bis-maleimide functionalized oligomeric phenyl-substituted poly(*p*-phenylene terephthalate) AM- and LC-series was presented. With the ultimate aim of preparing high-performance block copolymers based on rigid all-aromatic ester-based blocks and flexible PDMS blocks, it is critical to understand the morphology, phase behavior and the (thermo)mechanical properties of the constituent rigid blocks. In this Chapter, we will report on the temperature dependent properties and cure behavior of the LC- and AM-maleimide terminated rigid blocks.

3.2 Experimental

3.2.1 Materials

The maleimide end-capped liquid crystalline (LC, PTPC-HQ) and amorphous (AM, PTPC-PHQ) oligomers and their reference polymers used here were prepared as described in Chapter 2. All other chemicals were obtained from the indicated sources and used as received. 1,1,2,2-tetrachloroethane (98.5%, TCE), tetrahydrofuran (99%, THF), dimethyl sulfoxide (99%, DMSO), anhydrous N-Methyl-2-pyrrolidone (99.5%, NMP) were all purchased from Acros Organics. Chloroform (95%, $CHCl_3$) was obtained from VWR international BV.

3.2.2 Characterization

Solubility test

Solubility test was performed by dissolving ~10 mg samples in 1 mL of solvent, either at room temperature or elevated temperature. The elevated temperatures used here were 60 °C ($CHCl_3$), 65 °C (THF), 140 °C (TCE), 150 °C (DMF) and 200 °C (NMP), close to their boiling point.

Thermogravimetric analysis (TGA) and Differential scanning calorimetry (DSC)

A Perkin Elmer Pyris Diamond TG/DTA was used to study the dynamic thermal stability. The samples were analyzed using a heating rate of 10 °C·min^{-1} under a nitrogen atmosphere. The melt behavior of the polymers was determined by DSC using a Perkin Elmer Sapphire DSC with a heating rate of 20 °C·min^{-1}. All DSC measurements were also conducted under a nitrogen atmosphere.

Polarizing Optical microscopy (POM)

A Leica DMLM optical microscope equipped with a Linkham hot stage was used to investigate the melt behavior as a function of time and temperature. The samples were investigated between glass slides upon heating using a heating rate of 20 °C·min^{-1}.

Dynamic mechanical thermal analyses (DMTA)

DMTA was performed using a Perkin Elmer Diamond DMTA in tension mode, using thin films of the following approximate dimensions: 20 × 4 × 0.1 mm^3. All experiments were performed under a nitrogen atmosphere and at a heating rate of 2 °C·min^{-1} at a frequency of 1 Hz.

Density

The density of the cured oligomers was measured using a METTLER TOLEDO hydrostatic balance applying the Archimedes principle. Cured film samples were weighed in air and distilled water at room temperature to yield the polymer density based on the following equation:

$$\rho = \frac{A}{A-B}(\rho_0 - \rho_l) + \rho_l \qquad \text{(eqn. 3.1)}$$

Where ρ, ρ_0 and ρ_l represent the densities of the polymer, water and air at the test temperature and A and B stand for the measured weight of the polymer in air and under water, respectively.

Rheology

The complex melting and cure behavior of the oligomers was investigated using a Rheometric MARS III rheometer equipped with a force-rebalanced transducer in a parallel plate geometry. Parallel plates of 20 mm diameter were used and samples were prepared by compression molding (20 mm in diameter and ~0.2 mm thick). The samples were investigated under a nitrogen atmosphere with temperature ramping (5 °C·min^{-1}) from 50 °C to a predetermined temperature (250 or 300 °C) followed by an isothermal hold at that temperature for 1 h. All experiments were performed at a frequency of 1.0 Hz and a strain amplitude of 0.1%, which is within the linear viscoelastic range (frequency of 0.1–10 Hz and a strain amplitude of 0.001–1.0%). The *in-situ* FTIR measurements of the curing behavior of the oligomers during the rheological experiments were carried out with a Rheonaut module.

XRD

Wide angle X-ray scattering measurements were performed on the custom-made MINA X-ray instrument built on a Cu rotation anode (λ=1.5413Å). The measurement was performed using a sample-to-detector distance of 9.3 cm with a scanning time of 10 min and the 2D patterns were collected using a Vantec500 detector (1024× 1024 pixels array with pixel size 136× 136 microns). The beam center position on the detector and the sample-to-detector distance were calibrated using the diffraction rings from a standard Silver Behenate powder. Stretch ratios for the tested samples: AM-9K: 220%, LC-9K: 150%. The degree of crystallinity (%) was calculated from the ratio of the integrated intensity of the crystal peaks to the total integrated area using equation 3.2.

$$\text{Crystallinity } (\%) = \frac{crystalline\ area}{(crystalline + amorphous)area} \qquad \text{(Eqn. 3.2.)}$$

Tensile testing

An Instron 3365 universal tensile machine with a 1 kN force cell was used to investigate the stress-strain behavior of the thin polymer films. Tensile tests were performed by fixing the films with an adhesive onto a rectangular paper frame with the side arms cut. The specimens have dimensions of approximately 30 mm × 3 mm × 0.1 mm. All experiments were performed at room temperature at a strain rate of 1 mm/mm·min^{-1}. The data were reported as an average of 5 samples. The elastic modulus was measured by calculating the slope of the stress-strain curve between 0.1% and 0.3% strain. Toughness was calculated as the area under the stress-strain curve.

3.2.3 Preparation of cured thin films

All amorphous thin films (PTPC-PHQ), were prepared by casting a 10 % w/v NMP solution of reference polymer or oligomer, filtered through a PTFE syringe filter (pore size: 5 µm), in a level 8 cm diameter petri dish. The solvent was allowed to evaporate slowly at 60 ˚C under vacuum in a vacuum oven. After 2 h, when most of the solvent was removed, thermal curing of the oligomers was conducted in 3 steps: 100 ˚C for 1 h, 180 ˚C for 1 h and 250 ˚C for 1 h, respectively. Subsequently, the oven was turned off and the films were allowed to reach room temperature overnight under vacuum. Freestanding films were obtained after soaking the petri dish in lukewarm water. Figure 3.2 shows a representative freestanding film of cured AM-1K.

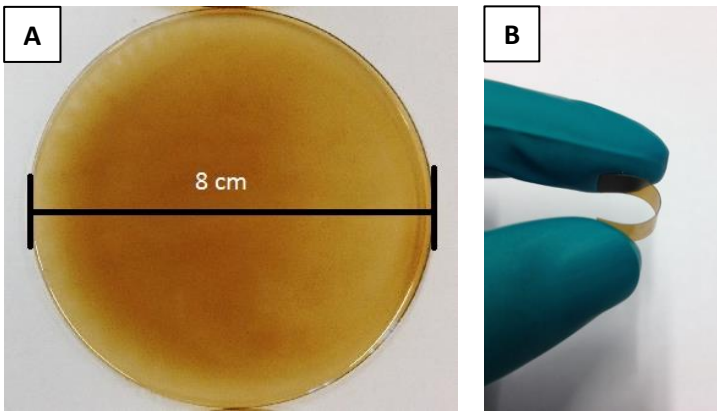

Fig. 3.2. ***A***- Representative freestanding film of cured AM-1K. Thermoset films prepared by casting and curing at 250 °C in a petri dish. ***B***- Cut films are flexible and easy to handle.

Due to the limited solubility, LC thin films from PTPC-HQ analogues were prepared using a mould in a hot press using standard melt compression techniques. The reference polymer and oligomers were ground into a fine powder, placed between two Kapton™ films and consolidated in a Joos hot press using a constant force of 5 kN. The temperature was increased to 300 °C with a heating rate of 5 °C·min^{-1}, holding for 60 min, and cooling to 50 °C at 20 °C·min^{-1}.

3.3 Results and Discussion

3.3.1 Solubility test

The solubility of the oligomers and the reference polymers (thin films of ~ 10 mg in 1 mL solvent) was tested in various common organic solvents, and the results are listed in Table 3.1.

Table 3.1. Solubility of the oligomers and reference polymers in several common solvents.

Samples	$CHCl_3$	THF	TCE	DMF	NMP
LC-1K	+-	+-	++	+-	++
LC-5K	--	--	+-	--	+-
LC-9K	--	--	+-	--	--
LC-ref	--	--	+-	--	--
All AM samples	++	++	++	++	++

(++): soluble at room temperature.
(+-): soluble or partially soluble at elevated temperature.
(--): insoluble even upon heating.

The elevated temperatures used here were 60 °C ($CHCl_3$), 65 °C (THF), 140 °C (TCE), 150 °C (DMF) and 200 °C (NMP), close to their boiling point.

In general, substituents reduce the interaction between polymer chains, resulting in improved solubility and a decrease in crystallization tendency.[13] Improved solubility in common organic solvents can also be achieved by decreasing the molecular weights of the polymer.[13-16] With phenyl substituents on the backbone and the oligomer approach, the LC-1K, -5K and -9K oligomers and reference polymer show enhanced solubility depending on molecular weights, compared to PPTT. Due to the lower molecular weight, around 3 repeating units, LC-1K exhibits good solubility in TCE and NMP at room temperature and in chloroform and DMF with increased temperatures, above 60 and 150 °C, respectively. Other LC oligomers are only soluble in TCE when heated to 140 °C, where LC-5K also showed partial solubility in NMP at high temperature (> 100 °C).

In sharp contrast to the LC oligomers, the AM (amorphous) analogs exhibit excellent solubility in all of the selected solvents. The solubility differences between the LC polymer/oligomers and the AM analogs is due to the presence of an additional phenyl substituent on the hydroquinone unit, which lowers the degree of crystallinity, and at the same time this increases the entropy of the (more soluble) polymer chains.[13]

After curing the oligomers at a temperature in excess of 250 °C, none of the 1K and 5K oligomers were found soluble in any of the 5 solvents tested, while the reference polymers retained their solubility, which is considered as proof that the maleimide terminated oligomers have indeed crosslinked.

3.3.2 Dynamic thermogravimetric analysis (TGA)

The thermal stability of the oligomers and the reference polymers was evaluated by TGA under nitrogen atmosphere and the results are summarized in Table 3.2. Figure 3.3A and 3.3B show the TGA curves of the LC series and AM series, respectively.

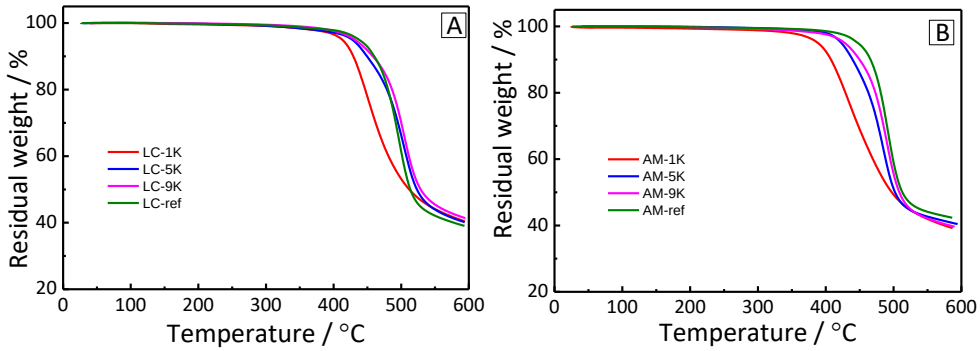

Fig. 3.3. Dynamic TGA thermograms of the oligomers and their reference polymers (***A***- LC series; ***B***- AM series) recorded under a nitrogen atmosphere using a heating rate of 10 °C·min^{-1}.

The decomposition temperature was defined as the temperature of 5% weight loss ($T_d^{5\%}$). Compared to the high $T_d^{5\%}$ of higher molecular weights oligomers, LC-1K and AM-1K oligomers show lower $T_d^{5\%}$s of 389 and 413 °C, respectively, due to lower molecular weight and higher content of end-groups. The $T_d^{5\%}$ of all the 5K and 9K oligomers is comparable to the reference polymers, since they possess very similar chemical composition. The $T_d^{5\%}$s and char yields at 600 °C in nitrogen atmosphere are representative for conventional bismaleimide thermosets.[5, 17] The typical curing temperature of the maleimides (< 250 °C)[8], is considerably lower than the decomposition temperatures of all oligomers, suggesting the oligomers are highly thermal stable and the cure temperature is safe to operate for all oligomers.

Table 3.2. Thermomechanical properties of the LC and AM oligomers and their reference polymers

Sample	TGA[1]		DSC					DMTA		
	$T_d^{5\%}$ (°C)	Char yield (wt%)[2]	T_g (°C)[3]	T_g (°C)[4]	$T_{K\text{-}K'}$ (°C)	$T_{K\text{-}N}$ (°C)	T_{iso} (°C)	E' (GPa) at 25 °C	E' (GPa) at 100 °C	T_g (°C)[5]
LC-1K	413	40	136	-	-	188	-	4.5	3.4	176
LC-5K	428	40	-	-	237, 270	295	-	5.6	4.1	165
LC-9K	432	41	-	-	244, 271	299	385	6.0	4.8	157
LC-ref	438	39	157	-	275	295	380	6.1	5.0	143
AM-1K	395	40	130	151	-	-	-	5.1	4.0	190
AM-5K	423	40	131	145	-	-	-	7.2	6.2	157
AM-9K	428	40	134	139	-	-	-	7.1	5.9	143
AM-ref	448	42	134	131	-	-	-	7.2	5.9	141

1. TGA measured at 10 °C·min^{-1} under a nitrogen atmosphere.

2. Char yield at 600 °C under nitrogen atmosphere.

3. T_g data of uncured oligomers were obtained from the first heating scan of DSC experiments. Heating rate 20 °C·min^{-1}.

4. T_g data of cured thermosets were obtained from the second heating scan of DSC experiments.

5. T_g data of cured thermosets were obtained from DMTA experiments. T_g is defined by the maximum of the loss modulus (E") peak. Heating rate of 2 °C·min^{-1} in nitrogen atmosphere and a frequency of 1 Hz.

3.3.3 Differential scanning calorimetry analysis

The thermal transitions of the oligomers and reference polymers were determined using differential scanning calorimetry (DSC). Figure 3.4 shows the first and second heating scans of the LC oligomers and the reference polymer obtained with a scanning rate of 20 °C·min^{-1}. The data is summarized in Table 3.2.

In the thermograms of LC-1K and LC-ref a glass transition temperature (T_g) is observed at 136 °C and 157 °C, respectively. The shift to higher T_g for LC-ref is due to a higher molecular weight. As reported in literature[4], the multiple endothermic peaks around 240 and 270 °C upon the first heat (Figure 3.4A) originate from a crystal to crystal transition ($T_{K\text{-}K'}$). In contrast to the low $T_{K\text{-}N}$ of LC-1K (at 180 °C), the higher molecular weight oligomers and reference polymer all show the $T_{K\text{-}N}$ around 295 °C. The LC-ref has a $T_{N\text{-}I}$ at 380 °C (369 °C as reported by Krigbaum *et al.*)[4], which was not observed in the oligomers due to crosslinking of end-groups during the DSC experiment. An exothermic peak, indicating the curing of the end-groups, was not detected during the first heating, probably due to the broad temperature range of this reaction.

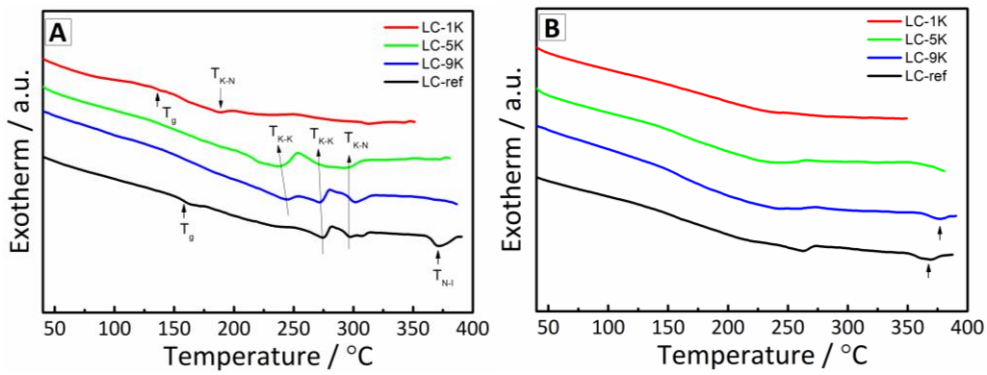

Fig. 3.4. ***A-*** First DSC heating trace of the LC-1K, -5K, -9K and the reference polymer and ***B-*** second heating trace of the same series. Heating rate of 20 °C·min^{-1} in nitrogen atmosphere.

After curing the samples in the first heating step, the samples were cooled from to 20 °C at a cooling rate of 20 °C·min^{-1}. Since the curing temperature for maleimide end-groups is lower than the maximum temperature of the first heating

cycle, the second heating scan reflects the thermal behavior of cured thermosets. The second heating scan shows a broad endothermic peak attributed to $T_{K\text{-}K'}$ only, instead of the multiple endothermic peaks. The cured LC oligomers have a $T_{K\text{-}K'}$ at around 240 °C, whereas the LC-ref polymer exhibits a $T_{K\text{-}K'}$ of 262 °C. No detectable $T_{N\text{-}I}$ below 400 °C was observed for LC-1K and LC-5K. This is most likely due to the higher crosslinking density of the smaller molecular weight oligomers, the nematic phase is fixed before decomposition. In contrast, The LC-9K and LC-ref show a $T_{N\text{-}I}$ at 385 and 380 °C, respectively. This is due to the low crosslinking density or no crosslinking (chain extension only).

All AM oligomers and reference polymer show a T_g only, as shown in Figure 3.5***A*** and ***B***. The absence of a melting point is again indicative of the amorphous nature of these compounds. The cured AM thermosets (second heat cycle) show higher T_gs compared to the uncured oligomers (first heat cycle), due to crosslinking of the oligomers and the subsequent reduction of the mobility of the chain segments.

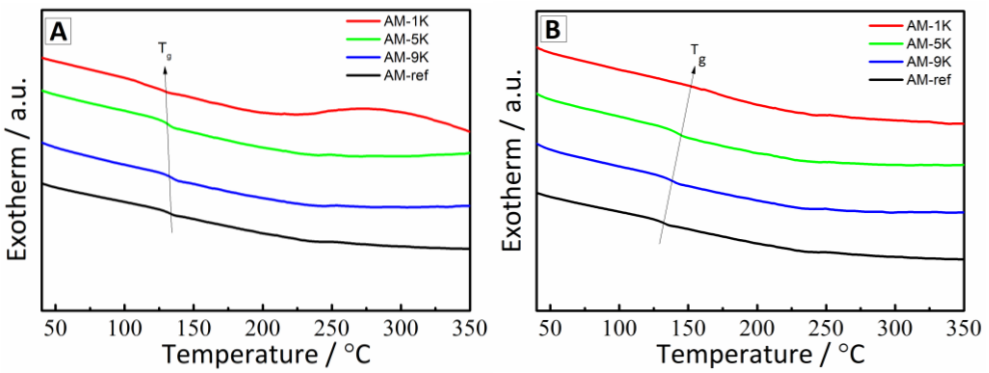

Fig. 3.5. *A*- First DSC heating trace of the AM-1K, -5K, -9K and the reference polymer and ***B*-** second DSC heating trace of the same series. Heating rate 20 °C·min^{-1} in nitrogen atmosphere.

3.3.4 Polarized optical microscopy

The melt behavior of the soluble all-aromatic oligomers and the reference polymers was evaluated by optical microscopy. The microscope was equipped with crossed polarizers and a hot stage.

All LC oligomers and reference polymers display typical marbled nematic textures with broad mesophase range of 180 to ~400 °C, depending on the molecular weights. No indication for a smectic or higher ordered liquid crystal textures was found. As reported by Krigbaum[4], LC-ref, shows a crystal to nematic transition ($T_{K\text{-}N}$) at approximately 295 °C. After the formation of this highly viscous nematic phase, the viscosity of the polymer drops and the polymer becomes mobile upon further heating. The nematic texture was preserved until the nematic to isotropic transiton ($T_{N\text{-}I}$) at ~380 °C. As was determined from DSC experiments, LC-5K and -9K have a $T_{K\text{-}N}$ at ~295 °C and LC-1K exhibited a lower $T_{K\text{-}N}$ of ~185 °C, again in close proximity of the value from the DSC experiment. All three LC oligomers form stable nematic phases before decomposition. Upon rapid heating at 20 °C·min^{-1}, all maleimide end-capped LC oligomers solidify and their nematic textures are fixed due to the crosslinking reaction of the maleimide end-groups. Upon cooling to room temperature at a cooling rate of 20 °C·min^{-1}, the LC textures appear to be fixed. No shearing is possible, indicating a nematic network was obtained. When the temperature reaches values in excess of 400 °C, the samples start to decompose, resulting in a nematic to isotropic transition.

In case of the AM oligomers and the corresponding reference polymer, no liquid crystal phases could be observed upon heating. The AM-1K oligomer shows a flow temperature of ~170 °C, while AM-5K, -9K and -ref all showed similar flow temperatures of approximately 210 °C. Upon further heating all AM oligomers solidified.

Typically, all the LC oligomers were cured at 300 °C and the melt viscosity increases rapidly and the samples solidify after a 1 h isothermal hold, while maintaining their nematic order. The amorphous analogous were cured at 250 °C to solidify into insoluble cured thermosets. Representative nematic textures (for LC oligomers) and the amorphous state (for AM oligomers) of our oligomers before and after crosslinking are shown in Figure 3.6. None of the investigated oligomers and reference polymers showed lyotropic liquid crystalline behavior in good solvents, e.g. TCE, at all concentrations.

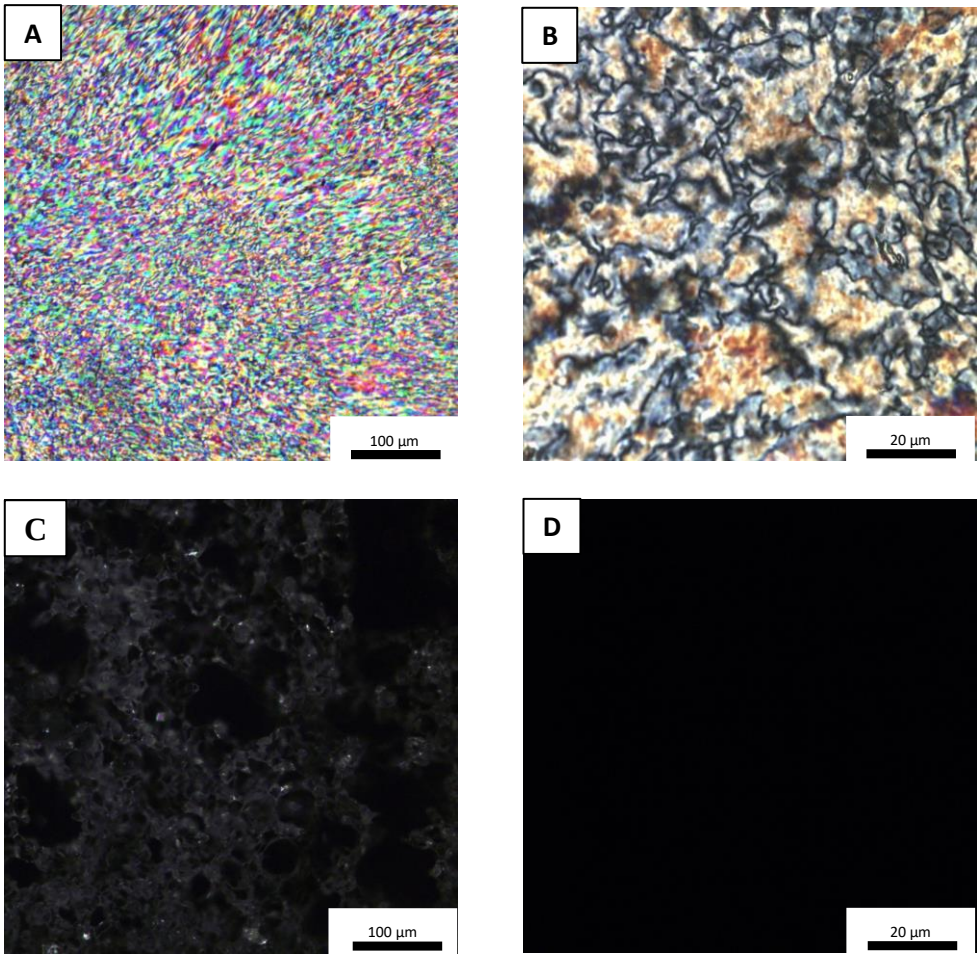

Fig. 3.6. Microphotographs of LC-1K and AM-1K. ***A-*** Low viscous nematic texture at 200 °C of LC-1K. ***B-*** Vitrified nematic thermoset at room temperature of LC-1K after isothermal hold at 250 °C for 1 h. ***C-*** Amorphous melt of AM-1K at 200 °C. ***D-*** Solidified amorphous thermoset at room temperature after 1 h isothermal hold at 250 °C.

3.3.5 Rheology

Measuring the melting and curing behavior of the oligomers is crucial to define the processing window. The complex melt viscosity (|η*|) of the reference polymer and oligomers as function of temperature and time was measured using a rheometer. Due to the high melting point of the LC oligomers and reference polymer,

the LC series were cured at 300 °C. The AM analogues are cured at 250 °C, which is high enough for the cure reaction of maleimides[8] and the slightly lower temperature prevents any unwanted side reactions.

The LC-ref shows a typical melting behavior of a high molecular weight polymer with a small decrease in |η*| at the T_g (~150 °C) and a large decrease in |η*| at ~295 °C, due to the K-N transition where the polymer chains become mobile (Figure 3.7***A***). During the 1 h isothermal at 300 °C, no obvious increase in viscosity of the LC-ref polymer was observed. LC-9K and LC-5K, with $T_{K\text{-}N}$ of 297 °C and 299 °C, respectively, have slightly higher minimum melt viscosities, due to the maleimide end-groups, which start reacting at ~250 °C, before the minimum melt viscosity is reached. LC-1K, with a $T_{K\text{-}N}$ of 180 °C, starts flowing before the end-group starts reacting and hence reaches the lowest melt viscosity of 10 Pa·s at ~200 °C. After reaching the minimum value, the viscosity of all oligomers starts increasing to higher values reflecting crosslinking density. The viscosity of LC-9K does not exceed that of the reference polymer, probably due to the low concentration of crosslinkable end-groups resulting in chain-extension only. This assumption is confirmed by the observation that cured LC-1K and -5K are insoluble in TCE at elevated temperature, whereas the cured LC-9K samples are still partly soluble.

The AM-ref polymer sample shows a sharp drop in viscosity at 130 °C due to the glass transition event, and a further decrease at ~210 °C, where the polymer starts to flow. During the 1 h isothermal at 250 °C, no obvious increase in viscosity of the AM-ref was observed (Figure 3.7***B***). The curable oligomer of AM-9K shows a gradually increase in viscosity upon heating. Cured AM-1K and -5K are insoluble in NMP, indicating crosslinked thermosets have formed during the 250 °C isothermal hold. AM-9K is partly soluble at high temperature, again indicating only chain-extension of the highest molecular weight oligomer. The initial increase in viscosity before 20 min., is due to contact issues between the disks and the sample pellet.

All scaled-up oligomers (*i.e.,* LC-1K-large, LC-5K-large, AM-1K-large and AM-5K-large) show similar melt and cure behavior.

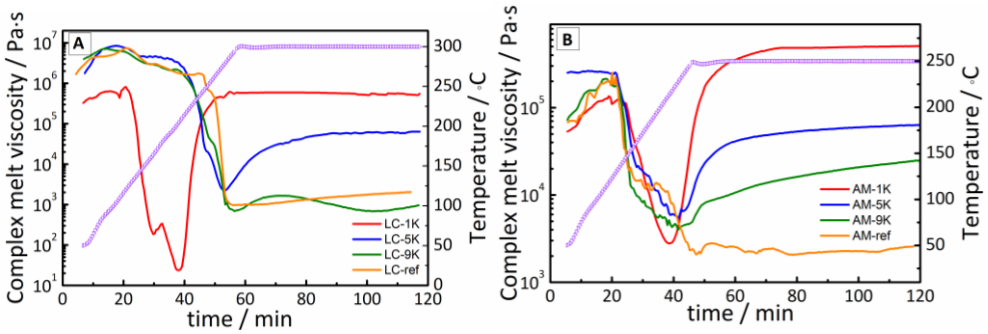

Fig. 3.7. Rheology behavior of the LC and AM oligomers and their reference polymers. **A-** |η*| of the LC oligomers and LC-ref reference polymer as a function of temperature. **B-** |η*| of the AM oligomers and AM-ref reference polymer as a function of temperature. Experiments were performed using a frequency of 1 Hz and heating rate of 5 °C·min^{-1} in N_2 atmosphere.

In order to understand the network formation and to determine the crosslink density, the classical rubber elasticity theory[18] was used to characterize the polymer networks prepared from the maleimide terminated oligomers with molecular weights of 1 and 5 kg·mol^{-1}, as shown by equation 3.3

$$M_c = \frac{\emptyset \rho(T) RT}{G_e(T)} \qquad \text{(eqn. 3.3)}$$

where $G_e$is the equilibrium shear modulus as determined by a temperature sweep in a rheology test, $\rho(T)$ is the density of the crosslinked material at the testing temperature, R is the universal gas constant and T is the absolute temperature. $\emptyset$ is termed as the "front factor", which is given as the ratio of the size of the bridging chain between crosslinking points in the cured polymer to that of the bridge in free space. For the sake of simplicity, the density of the samples at room temperature was used, and $\emptyset$ was estimated to be unity.[19] M_c is the molecular weight between chemical crosslinks, which reflects the degree of crosslinking. A lower M_c value implies that the cured thermosets have a higher crosslinking density. Here, G_e is taken from the rheology experiments at *t* = 120 min and *T* = 250 or 300 °C (523 or 573 K), as the oligomers are fully crosslinked and the modulus |G*| has reached a stable plateau value. The results calculated by the rubber elasticity theory are summarized in table 3.3.

Table 3.3. Calculated molecular weight values between crosslinks (M_c).

Samples	M_n (kg·mol^{-1})[1]	G_e (MPa)[2]	ρ (kg·m^{-3})[3]	T (K)[4]	M_c (kg·mol^{-1})[5]
LC-1K	1.5	3.47	1.30×10^3	573	1.8
LC-5K	5.7	0.58	1.30×10^3	573	10.7
AM-1K	1.7	3.18	1.25×10^3	523	1.7
AM-5K	6.7	0.38	1.25×10^3	523	14.3

1. M_n was calculated from NMR experiments (Table 2.2).
2. G_e was taken as the $|G^*|$ at the plateau region, as obtained by rheology.
3. ρ is the density of the cured thermoset films as obtained by density measurements.
4. T is the absolute temperature.
5. M_c was calculated based on the classical rubber elasticity theory.

The results from the M_c calculations show that the cured LC-1K and AM-1K oligomers are highly crosslinked, since the estimation of M_cs for both of the cured thermosets are close to the M_n values as calculated by NMR. In the case of the cured 5K thermosets, the M_c values for LC-5K and AM-5K oligomers are estimated to be 10.7 and 14.3 kg·mol^{-1} respectively, which are values exceeding the initial M_n of the unreacted oligomers (5.7 and 6.7 kg·mol^{-1} as determined by NMR, respectively). In this sense, one can say that the maleimide end-groups of oligomers with molecular weight of 5 kg·mol^{-1} undergo both chain extension and crosslinking. However, the crosslinking chemistry of maleimides is more complicated than can be explained by a simplified model of rubber elasticity. In real life, trapped entanglements may contribute to G_e and act as physical crosslinks.[20] Also polymer chain scission may be a side reaction during cure in the case of incomplete maleimide conversion. As a result, more accurate M_c values can only be established if one considers all of the above-mentioned factors.

3.3.6 Curing behavior by *in-situ* Rheo-FTIR

Conventional experimental techniques such as DSC[21-25], FTIR[26] and UV-reflection spectroscopy[27] can be used to characterize the cure of maleimides, with isothermal and non-isothermal techniques. Studies have shown that curing of maleimide is a first order kinetic reaction with an activation energy of ~100 kJ·mol^{-1}.[28, 29] Coupling the rheometer to a FTIR spectrometer allows one to monitoring the cure behavior of the maleimide functionalized oligomers during the curing reaction, and follow the conversion of the maleimide functionalities. Depletion of the end-groups in a sample can be monitored simultaneously with the evolution of the viscosity, provided that the absorption peaks are distinguishable from the non-reacting and product peaks. The FTIR absorbance spectrum of the LC-1K oligomer is shown in Figure 3.8. The peak corresponding to the out-of-plane bending of H-C=C-H in maleimide groups appear at 828 cm^{-1}, The peaks at 1711 and 1735 cm^{-1} are attributed to C=O stretching of both the backbone and the maleimides, but since they show large overlap, this peak is not suitable to follow the reaction.

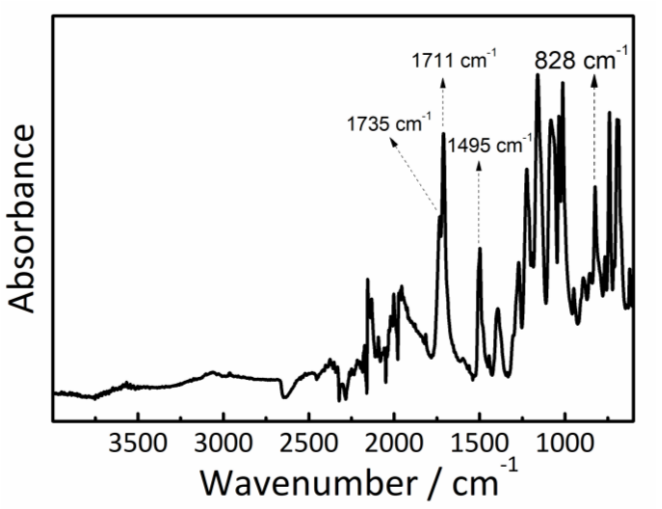

Fig. 3.8. *In-situ* FTIR spectra of LC-1K, collected from the Rheonaut module of the HAAke Mars III rheometer at 180 °C.

Figure 3.9 shows the changes of *in-situ* absorbance of the peak at 828 cm^{-1} for the LC-1K oligomer during cure at 250 ˚C using the Rheo-FTIR technique, as a representative example. The absorption was monitored independently during cure to follow the reaction kinetics. The Beer-Lambert law was applied for quantitative

analysis of the reaction.[30] It should be mentioned that the variation in the integration intensities can result not only from reaction of the maleimide double bond but also from physical changes, such as changes in the thickness of the sample pellet.[31] Therefore, the absorption intensities corresponding to the out-of-plane bending mode of the aromatic carbon-hydrogen bonds in the backbone of the polymer at 1495 cm^{-1} were used as internal thickness bands to correct for the effects associated with dimensional changes.

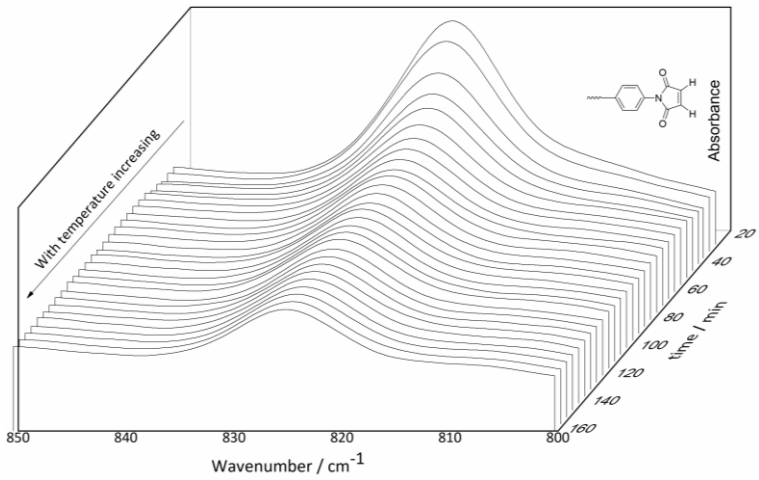

Fig. 3.9. Close up of the *In-situ* FTIR spectra of LC-1K at 828 cm^{-1} collected using the Rheonaut module of the HAAke Mars III rheometer. The data was collected using a temperature ramp (5 °C·min^{-1}) from 50 °C to 250 °C, followed by an isothermal hold at 250 °C for 2 h under nitrogen atmosphere.

Equation 3.4 was used to calculate the normalized fractional conversion from the obtained FTIR absorption data.

$$\alpha = 1 - \frac{A_t}{A_0} \quad \text{(eqn. 3.4)}$$

Where α is the fractional conversion of double bonds at time t. A_t and A_0 are the integrated area of the peak at time *t* and *t= 0*. Plotting the conversion as a function of time and temperature, curves as shown in Figure 3.10 are obtained. In the case of LC-1K, the conversion shows an increase from 200 °C, and reaches a quasi-steady state at 250 °C, where the conversion does not increase substantially. The conversion

of the maleimide double bonds reaches 72 % after two hours isothermal hold at 250 °C, leaving less than 30% of the double bonds unreacted. This is most likely due to the reduced mobility of the molecules and maleimide end-groups once the majority of the double bonds have reacted and a network has formed. The conversion of double bonds after two hours at 300 °C is 91 %, leaving less than 10% of the maleimide groups unreacted. The higher conversion of end-groups is due to the higher reaction temperature induced enhanced reactivity and higher mobility of the oligomers. The conversion of maleimide double bonds of AM-1K shows a very similar trend, but with a much steeper increase at 200 °C and reaches a quasi-steady state at 250 °C. However, the final conversions after 2 h cure at 250 and 300 °C (82% and 99%, respectively) are obviously higher than those of LC-1K. This is most likely due to the amorphous nature and higher free volume, lowering the chain motion barrier. When comparing the conversion of the AM-1K double bond with that of LC-1K (Figure 3.10), the AM-1K oligomer cures significantly faster, *i.e.*, AM-1K reaches a quasi-plateau within ~45 min, while LC-1K takes ~70 min. This is mostly likely because AM-1K shows a lower mobile temperature (~170 °C) than the melting point (~185 °C) of LC-1K. Beyond the mobile temperature, the oligomer chain mobility increases dramatically, resulting a rapid increase in cure dynamics. Besides, the amorphous nature and higher free volume may also contribute in the faster cure of AM-1K. This test, together with the solubility after the rheology tests, clearly shows that curing at 250 and 300 °C both yields thermoset materials. However, the crosslinking density is significantly different, depending on the phase behavior of the start materials and curing temperatures, which can have an effect on the final (thermo)mechanical properties of the final cured materials.

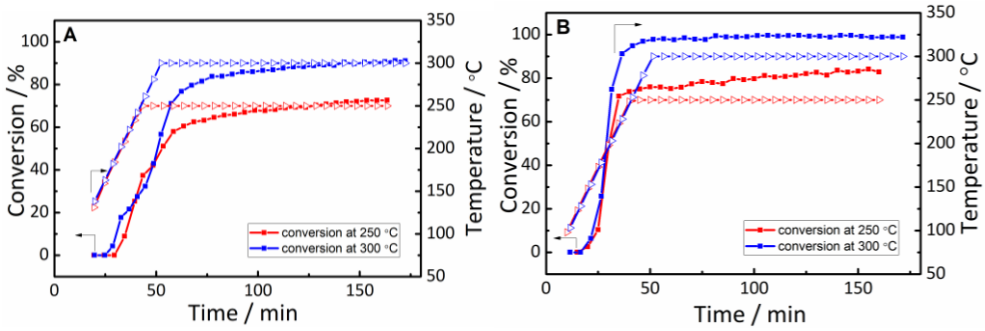

Fig. 3.10. Conversion of the maleimide double bond as a function of time and temperature of LC-1K (***A***) and AM-1K (***B***) during heating to 250 °C (red curves) and

300 °C (blue curves), collected using the Rheonaut module of the HAAke Mars III rheometer.

3.3.7 Dynamic mechanical thermal analysis (DMTA)

To explore the thermo-mechanical properties of the cured oligomer films and reference polymer films, the storage modulus (E') and loss modulus (E") as function of temperature were measured using DMTA at a constant heating rate of 2 °C·min^{-1} under a nitrogen atmosphere with a frequency of 1 Hz. The results are summarized in Table 3.2 and the DMTA curves are shown in Figure 3.11.

As shown in Figure 3.11***A***, with increasing amount of bis-maleimide end-groups, the cured LC films show a lower E' before T_g. This is most likely due to the higher crystallinity of the cured high molecular weight thermosets (section 3.3.8). The T_gs, as determined from the max of the E" peak, increases with the increase in bis-maleimide content, *i.e.,* LC-1K, -5K and -9K show T_g*s* of 176, 165 and 157 °C, respectively, while the LC-ref exhibits the lowest T_g of 143 °C. This is logical because the maleimide end-groups crosslink during cure and form a crosslinked network, which typically reduces the chain mobility and results in an increase in T_g.

The storage moduli (E') and loss moduli (E") as function of temperature for the amorphous oligomers and reference polymer films are shown in Figure 3.11***B***. The T_gs collected from the peak of E" also show an increase with an increase in maleimide end-group content.

Even though the LC-ref and AM-ref polymers show very similar T_gs (143 and 141 °C), the cured LC-5K and -9K oligomers show higher T_gs compared to their AM analogues. This is likely due to higher crystallinity of the LC oligomer films, as observed by XRD analysis (section 3.3.8). In contrast, cured AM-1K films exhibit a higher T_g compared to the LC-1K film, due to the higher crosslink density of the film. In general, the AM thermosets show a higher E', possibly as a result of the higher crosslink density, which is supported by our rheology experiments (see Figure 3.7). The network plateau, after the T_g event, is reflecting the concentration of crosslinks, as expected. The E' of the LC-ref and AM-ref polymers drop dramatically above the T_g, again confirming the thermoplastic nature of the reference polymer.

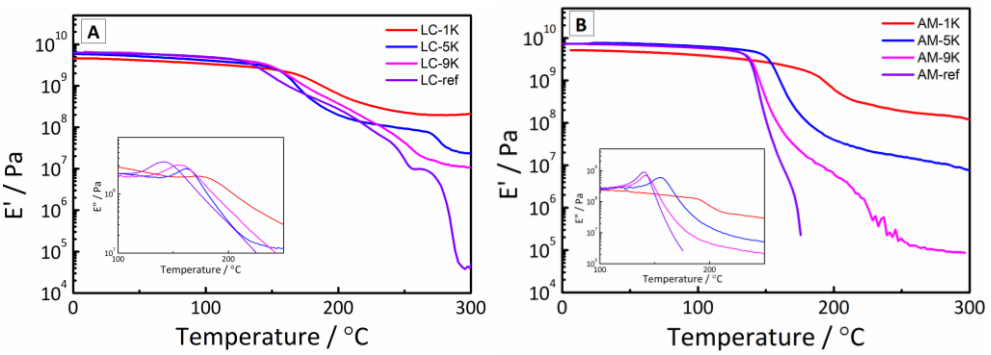

Fig. 3.11. DMTA curves of the cured oligomers and their reference polymers. ***A***- Storage moduli (E') as function of temperature for the LC series. ***B***- Storage moduli (E') as function of temperature for the AM series. The insets show the loss modulus (E") near the glass transition. Heating rate of 2 °C·min^{-1} in nitrogen atmosphere with a frequency of 1 Hz.

3.3.8 X-ray diffraction (XRD) analysis

During the DMTA experiments we noticed that the cured 9K oligomers and their reference polymer films showed high stretch ratios (> 150%) when heated above their T_g. The cured 1K and 5K films are hardly stretchable above their T_g, which is due to a high degree of crosslinking that prohibits stretching and subsequent alignment of these films. To study the effect of curing on the orientation of the liquid crystals and their networks, the cured AM-9K and LC-9K film samples from DMTA experiments were subjected to an X-ray diffraction study. The thermally stretched films of cured AM-9K and LC-9K were obtained directly after the DMTA test, with stretch ratios of 220% and 150%, respectively. The 2D diffraction patterns of both AM-9K and LC-9K cured films, recorded at room temperature, are displayed in Figure 3.12***A*** and 3.12***B***. The stretched AM-9K film shows a broad halo only, indicating a very typical amorphous diffraction pattern, even when subjected to a high stretch ratio. In contrast, the LC-9K film shows a typical nematic diffraction pattern, as shown in Figure 3.12***B***, confirming that this nematogenic polymer is indeed aligned upon stretching.

After converting the 2D diffraction patterns (Figure 3.12***A*** and 3.12***B***) to an intensity vs 2Θ plot (Figure 3.12***C***), the stretched AM-9K film shows a broad interchain diffraction peak only at 2Θ of 20.5˚ (*d*-spacing of 4.5 Å), confirming the

amorphous nature. The stretched LC-9K film also shows an interchain diffraction peak at 2Θ of 20˚. Besides, the reflection at around 7.8˚ (11.32 Å) is associated with the projection length of the repeating unit in the crystalline unit cell. The reflection at around 27° is ascribed to d_{310}, as reported in literature.[32] By calculating the ratio of the integrated intensities of the crystal peaks to the total integrated intensity, the degree of crystallinity of cured LC-9K is 37%. The scattering data on a ring along the 2Θ direction containing the scattering peaks (Figure 3.12***A*** and ***B***) were integrated to get the scattering intensity, as a function of the Azimuthal angle, χ. The intensity profiles of Figure 3.12***D*** were fitted using a Maier-Saupe-type function to calculate the order parameter $\langle P_2 \rangle$.[33, 34] The order parameter of the stretched LC-9K sample was calculated to be 0.15, while that of the stretched AM-9K show no alignment.

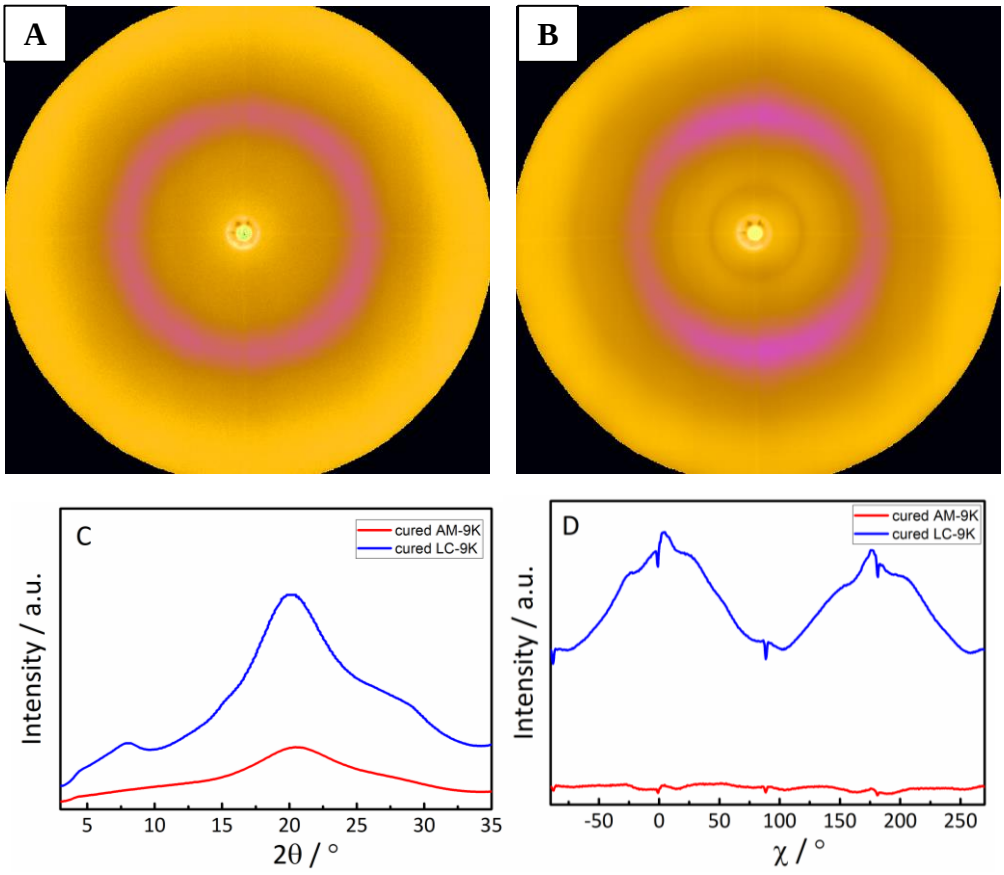

Fig. 3.12. Diffraction patterns recorded using a two-dimensional detector at 25 °C. ***A*-** AM-9K film stretched to 220% (amorphous); ***B*-** LC-9K film stretched to 150%

(aligned nematic); ***C-*** XRD patterns for the LC-9K film (semi-crystalline) and the AM-9K film (amorphous); ***D-*** Scattering intensity as a function of the azimuthal angle (χ) using the data of the stretched LC-9K and AM-9K films as grouped around the scattering peaks.

3.3.9 Tensile properties

The room temperature tensile properties of the thin films are shown in Figure 3.13 and 3.14. In order to remove any possible insoluble particles, which may cause irregularities in the resulting films, filtration of the casting solution over a 5 µm syringe filter was performed prior to preparing the films. The AM oligomers and the reference polymers were cast and cured at 250 °C for 1h, whereas the LC analogs were prepared using a hot press at 300 °C for 1h, due to the poor solubility of the LC oligomers. The best tensile properties of the cured films out of 5 experiments are shown in Figure 3.13.

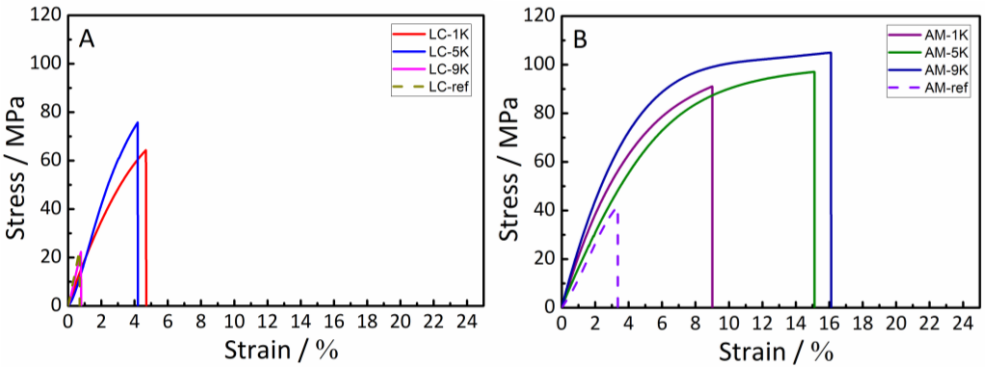

Fig. 3.13. Room temperature stress-strain curves of cured LC and AM oligomers, as well as their reference polymers. ***A***- cured LC oligomers and reference polymer and ***B***- cured AM oligomers and reference polymer. Shown are the best results out of 5 stress-strain experiments.

Overall, the stress-strain behavior of the thermally cured AM thermoset films is much better than the LC-based films. This is most likely due to the higher crystallinity of the LC thermosets, as observed from XRD analysis, making the LC

samples more brittle. The cured oligomers showed higher tensile properties than the reference polymers in both systems, possibly caused by the crosslinking and chain extension inducing higher molecular weight.

Figure 3.14 shows the average data of the tensile strength (***A***), elastic modulus (***B***), elongation at break (***C***) and toughness (***D***) of the as-prepared LC and AM films of 5 experiments.

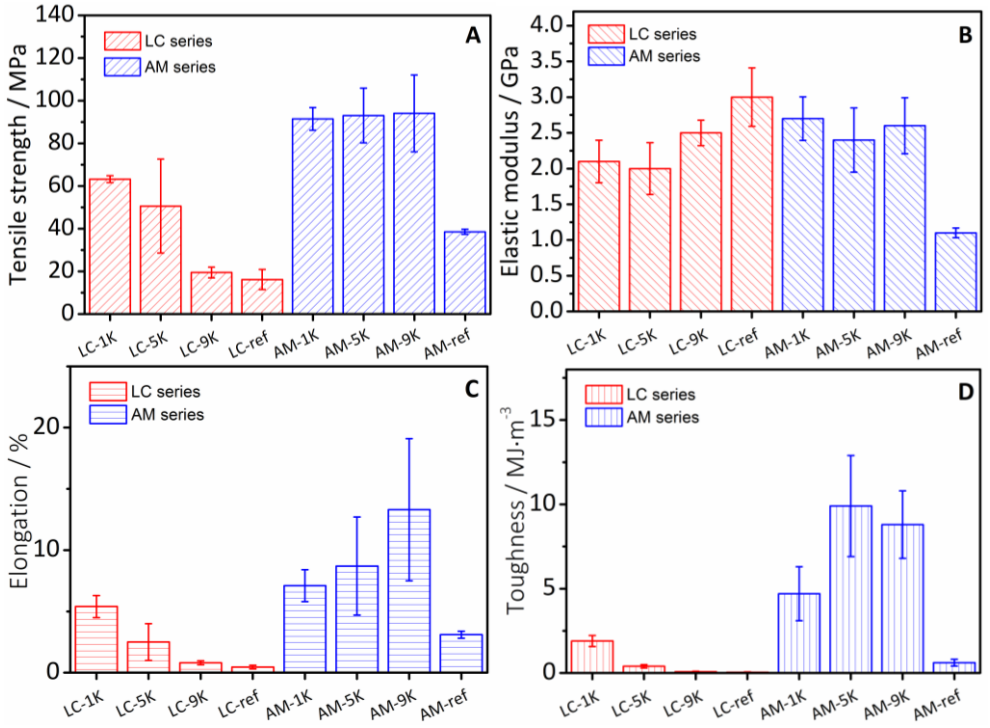

Fig. 3.14. Summarized tensile properties of the cured LC and AM oligomers and their reference polymers. Data shown is the average of 5 experiments; ***A-*** Tensile strength; ***B-*** Elastic modulus; ***C-*** Elongation at break; ***D-*** toughness.

Compared to the cured AM thermosets, the cured LC thermosets generally exhibit poorer mechanical properties. The tensile strength of the LC analogs ranges from 20 MPa to 60 MPa (with ε_{max} of ~5%), while the AM thermoset systems all displayed tensile strengths of over 90 MPa and strains varying between 7% and 13%. In contrast with the cured LC thermosets where the elongation at break decreased

going to longer oligomer lengths, the elongation at break in the AM series increased throughout the series. This is obviously due to the different semi-crystalline and amorphous nature of the two series of polymers, as confirmed by XRD analysis. Similarly, the toughness of the two sets of cured thermosets show the same trend throughout the series. The elastic modulus is comparable for all tested polymers, being approximately 2 GPa, which is a typical value for all aromatic main chain thermosets.[35-37] The AM cured samples, especially AM-5K and AM-9K thermosets, show a significant improvement with respect to elongation at break and toughness over their LCP thermoset analogs reported above.[35-37] The high elongation and toughness of the cured AM oligomer samples are possibly due to their amorphous nature and larger free volume comparing with the LC polyesters.

3.4 Conclusion

The LC and AM oligomers, as reported in Chapter 2, are cured into films and the cure behavior and (thermo)mechanical properties were investigated. Due to the introduction of phenyl groups, the main-chain LC and AM oligomers and their reference polymers show improved solubilities in common organic solvents over their non-substituted analogs. Because of the high aromatic content, the cured oligomers show high thermal stabilities with $T_d^{5\%}$ > 390 °C. The DSC, POM and XRD results confirm the liquid crystalline and amorphous nature of the different oligomers. The uncured LC oligomers and reference polymer shows T_gs of 136 – 157 ˚C, whereas the T_gs of the AM series are in the 130 – 134 ˚C range. After cure, the T_gs of the oligomers increased to 140 – 190 ˚C, depending on the concentration of reactive end-groups. The cure behavior was studied by following the evolution of viscosity and FTIR band intensity of the maleimide functionality as function of time and temperature. These measurements confirm curing degrees of approximately 70% to 99% depending on the curing temperature and nature (AM vs LC) of the polymer backbone. The crosslink density study shows that the two series of oligomers with M_n of 1 and 5 kg·mol^{-1} are highly crosslinked, while those with M_n of 9 kg·mol-1 are only partly crosslinked. DMTA experiments indicate that the cured oligomers can be used up to 150 °C, without a significant loss in modulus (E'). The films cured at 250 or 300 °C were tested for their tensile behavior, where the LC series performed inferior to the AM series, possibly caused by the brittleness induced by the high degree of crystallinity. The cured AM oligomer films show good

mechanical properties with high tensile strengths (> 90 MPa), elastic moduli (~2 GPa), elongation at break (~10%) and toughness (~8 $MJ \cdot m^{-3}$). In conclusion, we have demonstrated that the phenyl substituted poly(phenylene terephthalate) can be crosslinked using maleimide reactive end-groups. The two series of oligomers show different behavior with respect to their crosslinking chemistry, phase behavior and (thermo)mechanical properties, making them perfect rigid segment candidates for preparing high-performance block copolymers with soft PDMS blocks.

3.5 References

1 T. Dingemans, in *Polymer Science: A Comprehensive Reference*, ed. M. Möller, Elsevier, Amsterdam, 2012, pp. 753-769.

2 W. J. Jackson, *Brit. Polym. J.*, 1980, **12**, 154-162.

3 N. P. Cheremisinoff, *Handbook of Polymer Science and Technology*, Taylor & Francis, 1989.

4 W. R. Krigbaum, H. Hakemi and R. Kotek, *Macromolecules*, 1985, **18**, 965-973.

5 G. T. Kwiatkowski, L. M. Robeson, G. L. Brode and A. W. Bedwin, *J. Polym. Sci. Pol. Chem.*, 1975, **13**, 961-972.

6 G. D. Lyle, D. K. Mohanty, J. A. Cecere, S. D. Wu, J. S. Senger, D. H. Chen, S. Kilic and J. E. McGrath, *ACS Polym. Prepr.*, 1987, **28**.

7 G. D. Lyle, D. K. Mohanty, J. A. Cecere, S. D. Wu, J. S. Senger, D. H. Chen, S. Kilic and J. E. McGrath, *ACS Polym. Prepr.*, 1988, **19**.

8 G. D. Lyle, J. S. Senger, D. H. Chen, S. Kilic, S. D. Wu, D. K. Mohanty and J. E. McGrath, *Polymer*, 1989, **30**, 978-985.

9 M. Acevedo, J. G. de la Campa and J. de Abajo, *J. Appl. Polym. Sci.*, 1989, **38**, 1745-1759.

10 M. S. Chisholm, J. G. Carey, M. E. B. Jones and P. Wade, *Polymer*, 1992, **33**, 838-841.

11 L. R. Dix, J. R. Ebdon, N. J. Flint, P. Hodge and R. O'Dell, *Eur. Polym. J.*, 1995, **31**, 647-652.

12 P. Mison and B. Sillion, in *Progress in Polyimide Chemistry I*, ed. H. R. Kricheldorf, Springer Berlin Heidelberg, Berlin, Heidelberg, 1999, DOI: 10.1007/3-540-49815-x_5, pp. 137-179.

13 W. Hatke, H.-T. Land, H.-W. Schmidt and W. Heitz, *Macromol. Rapid Commun.*, 1991, **12**, 235-243.

14 M. A. Meador, *Annu. Rev. Mater. Sci.*, 1998, **28**, 599-630.

15 H. Han and P. K. Bhowmik, *Prog. Polym. Sci.*, 1997, **22**, 1431-1502.

16 J.-I. Jin and C.-S. Kang, *Prog. Polym. Sci.*, 1997, **22**, 937-973.

17 T. Takeichi, Y. Saito, T. Agag, H. Muto and T. Kawauchi, *Polymer*, 2008, **49**, 1173-1179.
18 J. D. Ferry, *Viscoelastic properties of polymers*, John Wiley & Sons, 1980.
19 G. Levita, S. De Petris, A. Marchetti and A. Lazzeri, *J. Mater. Sci.*, 1991, **26**, 2348-2352.
20 M. E. De Rosa and H. H. Winter, *Rheol. Acta*, 1994, **33**, 220-237.
21 A. V. Tungare and G. C. Martin, *J. Appl. Polym. Sci.*, 1992, **46**, 1125-1135.
22 A. A. Goodwin, *Polym. Int.*, 1993, **32**, 87-92.
23 M. S. Chandran, M. Krishna, S. Rai, M. S. Krupashankara and K. Salini, *ISRN Polymer Science*, 2012, **2012**, 8.
24 Y. Xiong, F. Y. C. Boey and S. K. Rath, *J. Appl. Polym. Sci.*, 2003, **90**, 2229-2240.
25 L. Zhang, P. Chen, M. Gao, L. Na, X. Xiong and S. Fan, *Designed Monomers and Polymers*, 2014, **17**, 637-646.
26 X. Liu, Y. Yu and S. Li, *Polymer*, 2006, **47**, 3767-3773.
27 J. C. Phelan and C. S. P. Sung, *Macromolecules*, 1997, **30**, 6845-6851.
28 Z. Luo, L. Wei, W. Li, F. Liu and T. Zhao, *J. Appl. Polym. Sci.*, 2008, **109**, 525-529.
29 X. Xiong, P. Chen, J. Zhang, Q. Yu and B. Wang, *Thermochim. Acta*, 2011, **514**, 44-50.
30 D. Calloway, *J. Chem. Educ*, 1997, **74**, 744.
31 J. Liu, H. Ishida and J. Maia, *Polym. Int.*, 2014, **63**, 521-528.
32 S. N. Chvalun, M. Ishaq, J. Blackwell and A. Y. Bilibin, *J. Macromol. Sci. B*, 1998, **37**, 451-462.
33 D. K. Deak, R. W. Lenz and S. W. Kantor, *J. Polym. Sci., Part A: Polym. Chem.*, 1997, **35**, 197-209.
34 C. de Ruijter, E. Mendes, H. Boerstoel and S. J. Picken, *Polymer*, 2006, **47**, 8517-8526.
35 M. Iqbal and T. J. Dingemans, *Compos. Sci. Technol.*, 2011, **71**, 863-867.
36 M. Iqbal, B. Norder, E. Mendes and T. J. Dingemans, *J. Polym. Sci., Part A: Polym. Chem.*, 2009, **47**, 1368-1380.
37 M. Iqbal and T. J. Dingemans, *Eur. Polym. J.*, 2010, **46**, 2174-2180.

Chapter 4 Synthesis of siloxane-based multiblock copolymers with all-aromatic rigid units

Abstract

In this Chapter we will describe the synthesis of two series high molecular weight $(AB)_n$ multiblock copolymers from all-aromatic liquid crystal (LC) or amorphous (AM) telechelic ester-based maleimide-functionalized oligomers and telechelic thiol-terminated poly(dimethylsiloxane) (PDMS), *via* highly efficient thiol-ene click chemistry. The maleimide-functionalized LC and AM precursors used have a M_n of 5 kg·mol^{-1}, and the telechelic thiol-terminated PDMS was prepared from commercial hydroxy-functionalized PDMS oligomers, with an M_n of 1, 5 and 10 kg·mol^{-1}. The molecular structure and molecular weight of the PDMS block, before and after end-group modification, was confirmed using ^{1}H NMR and GPC. ^{1}H NMR analysis of the AM- and LC-series showed that all multiblock copolymers have M_ns ranging from 22 to 58 kg·mol^{-1}, confirming that this chemistry can be used to prepare high molecular weight $(AB)_n$ multiblock copolymers based on all-aromatic rigid rods and PDMS flexible linkers.

4.1 Introduction

In the field of polymers, two ordered non-crystalline states are known, *i.e.* the liquid crystalline (LC) state and microstructures arising from block copolymers.[1, 2] Liquid crystalline polymers have attracted a lot of attention due to their outstanding properties in terms of high modulus, low thermal expansion, low melt viscosity, and flame retardant behavior.[3] On the other hand, block copolymers consisting of two or more chemically distinct polymer blocks display the beneficial effects of both blocks, in a microstructure which depends on miscibility, size and mobility of the different blocks.[4] Among block copolymers, multiblock copolymers of the $(AB)_n$ type, as shown in Figure 4.1, are important because of their outstanding mechanical properties, like multiblock polyurethane based thermoplastic elastomer (TPE) (B. F. Goodrich Co.), multiblock polyesters-based TPEs (TPES (Du Pont), and polyamides-based $(AB)_n$ multi-block copolymers TPEs or TPAs (Huls and Ato Chimie), etc.[5] Commercial $(AB)_n$ multiblock copolymers have found wide application in consumer applications, such as shoe soling formulations or toothbrushes and in industrial applications such as wire coating, flexible hoses and tubing, electrical connectors and automotive parts. The incorporation of LC precursors into $(AB)_n$ multiblock copolymers opens the possibility to combine the two different self-organization phenomena. Substantial research[1, 3, 6-12] has been conducted in this field since the first report[13] of combining liquid crystalline segments with amorphous segments in block copolymers in 1985. Considering the unique self-organizing behavior of liquid crystalline polymers, the main effort and interest of our research is focused on accessing $(AB)_n$ multiblock copolymers to induce liquid crystallinity and self-organization in block copolymers at the same time.

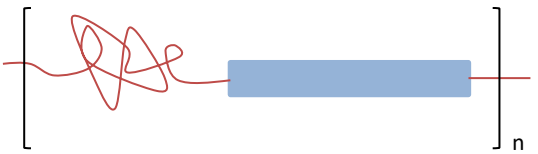

Fig. 4.1. Schematic representation of the molecular structure of an $(AB)_n$ multiblock copolymer. This multiblock copolymers consists of soft flexible blocks (red) and rigid all-aromatic (blue) fragments, connected *via* covalent bonds.

A versatile and very efficient route towards preparing $(AB)_n$ type multiblock copolymers is utilizing the well-known thiol-ene reaction.[14] This reaction, shown in Scheme 4.1, has been used as the hydrothiolation of a reactive C=C bond for over 100 years[15] and has attracted researchers in the area of polymer synthesis due to the recognition of its "click" characteristics, enabling the facile and efficient covalent bond formation between different types of polymers .[16-18]

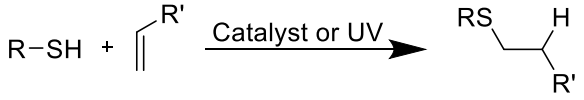

Scheme 4.1. The hydrothiolation reaction of a C=C bond, catalyzed by a catalyst (often a base) or UV light.

The "click" feature allows for the use of cheap or no catalyst, a wide range of reaction conditions and R-groups, a high reaction rate, high conversion and yield and a high tolerance towards air, oxygen and moisture.[14, 19] Comparing to other alkene candidates like (meth)acrylates and fumarate esters, maleimides are intrinsically activated substrates for base catalyzed thiol-ene reactions. Due to the presence of two activating carbonyl groups in a *cis*-conformation coupled with ring-strain/bond angle distortion, the C=C bond in maleimides is very reactive and thiol-ene reactions can take place extremely fast.[14]

In Chapter 2, the synthesis and molecular composition of the bis-maleimide functionalized all-aromatic telechelic oligomers is described. In this Chapter, a facile approach towards the preparation of $(AB)_n$ multiblock copolymers with rigid segments and PDMS chains *via* the highly efficient thiol-ene click reaction is presented. The multiblock copolymers were synthesized from 5,000 $g \cdot mol^{-1}$ (5K) bis-maleimide functionalized telechelic rigid (LC or AM) oligomers, with three telechelic thiol-terminated PDMS blocks (1.0, 5.0 and 10 $kg \cdot mol^{-1}$). A full description of the synthetic conditions will be provided together with the molecular weight characterization results (NMR, GPC and viscometry).

4.2 Experimental

4.2.1 Materials

In Chapter 2, the large-scale synthesis of the LC and AM all-aromatic bismaleimide-functionalized telechelic oligomers with a number average molecular weight of approximately 5 kg·mol^{-1} is described. The amorphous (AM) and liquid crystalline (LC) oligomers are labeled as AM-5K and LC-5K, respectively. Molecular weights and polydispersity index (PDI) are reported in Chapter 2.

All other chemicals were obtained from commercial sources and used as received unless state otherwise. 1,1,2,2-tetrachloroethane (TCE, 98.5%) was purchased from Acros Organics, dried over CaH_2 at 120 °C for 5h and distilled from CaH_2 under reduced pressure. Triethylamine (NEt_3, 99%) was obtained from Alfa Aesar, dried by refluxing with CaH_2 at 100 °C and distilled prior to use. Telechelic hydroxyl-functionalized poly(dimethyl siloxane)s with various number average molecular weights ($\overline{M}_n$), around 1.0, 5.0 and 10 kg·mol^{-1} were purchased from Gelest Inc. The PDMS oligomers were labelled as PDMS-OH-1K, PDMS-OH-5K and PDMS-OH-10K, respectively, where PDMS-OH reflects the main-chain and end-groups and the integers refer to the molecular weight, *i.e.* 1K = 1.0 kg·mol^{-1}. Anhydrous toluene (99.8%), anhydrous tetrahydrofuran (THF, 99.9%), mesyl chloride (99.7%), N,N-dimethylformamide (DMF, 99.8%), magnesium sulfate ($MgSO_4$, 98%), Celite 545, hydrochloric acid (30%) and *n*-propylamine (98%) were all purchased from Sigma-Aldrich and used as received. Potassium thioacetate (98%) was purchased from Acros Organics. Dichloromethane, Sodium chloride and diethyl ether were purchased from VWR. NMR solvents such as $CDCl_3$ (99.8 % D) and TCE-d_2 (99.5 % D) were purchased from Sigma Aldrich and used as received for NMR measurements.

4.2.2 Characterization

Nuclear magnetic resonance (NMR)

^{1}H and ^{13}C NMR spectra were recorded on a 400 MHz Agilent-400 MR DD2 at 25 °C. All samples were dissolved in deuterated solvents and the recorded spectra were referenced to the residual solvent resonance ($CDCl_3$: ^{1}H, 7.24 ppm and ^{13}C, 77.0 ppm. TCE-d_2: ^{1}H, 6.00 ppm and ^{13}C, 73.78 ppm).

Fourier transform infrared spectroscopy (FTIR)

FTIR spectra were recorded using a Perkin Elmer Spectrum 100 FTIR spectrometer.

Gel permeation chromatography (GPC)

GPC measurements on the polymers and oligomers were performed using a Shimadzu GPU DGU-20A3, equipped with Shodex LF-801 column and refractive index detector. THF was used as the eluent at a flow rate of 1.0 ml·min^{-1} and at a temperature of 40 °C. Calibration was based on monodisperse polystyrene standard (S1: Mn of 5800 and PDI of 1.05; S2: Mn of 12200 and PDI of 1.09; S3: Mn of 23700 and PDI of 1.09; S4: Mn of 48000 and PDI of 1.07; S5: Mn of 100000 and PDI of 1.13; S6: Mn of 186000 and PDI of 1.09; S7: Mn of 380000 and PDI of 1.12; S8: Mn of 853000 and PDI of 1.23) and the data analyses were performed with labSolutions software from the refractive index detector data. All polymers and oligomers were filtered through a 0.45 µm PTFE filter prior to a GPC run.

Viscometry

An Ubbelohde viscometer was used to measure the flow time of pure solvent and polymer or oligomer solutions. All viscosity measurements were carried out at 21 ± 0.01 °C in a water bath equipped with automatic temperature controller. The flow time of pure solvent in the clean dry viscometer was first measured. Subsequently, the flow time of an oligomer or polymer solution with known weight concentration (~0.5 g·dL^{-1}) was measured in the same viscometer. The ratio of flow time of solution to that of solvent was regarded as the relative viscosity (η_{rel}). Inherent viscosity (η_{inh}) was calculated according to Equation 4.1.

$$\eta_{inh} = \frac{\ln \eta_{rel}}{c} \qquad \text{(eqn. 4.1)}$$

Where *c* is the concentration of polymer solution (g·dL^{-1}).

4.2.3 Synthesis of telechelic thiol-terminated PDMS (PDMS-SH)

The synthesis of telechelic thiol-functionalized PDMS from hydroxyl-terminated PDMS, as shown in Scheme 4.2, has been reported by Du Prez *et al*.[20] Generally, the preparation of telechelic thiol-terminated PDMS with molecular weights of approximately 1.0, 5.0 and 10 kg·mol^{-1} were performed using the same procedure, however different molar ratios of reactants according to the various end-groups contents in PDMS were used. The synthesized samples were labelled as

PDMS-SH-1K, PDMS-SH-5K and PDMS-SH-10K, respectively, where PDMS-SH reflects the oligomer main-chain and end-groups and the integers refer to the molecular weight, *i.e.* 1K = 1.0 kg·mol^{-1}.

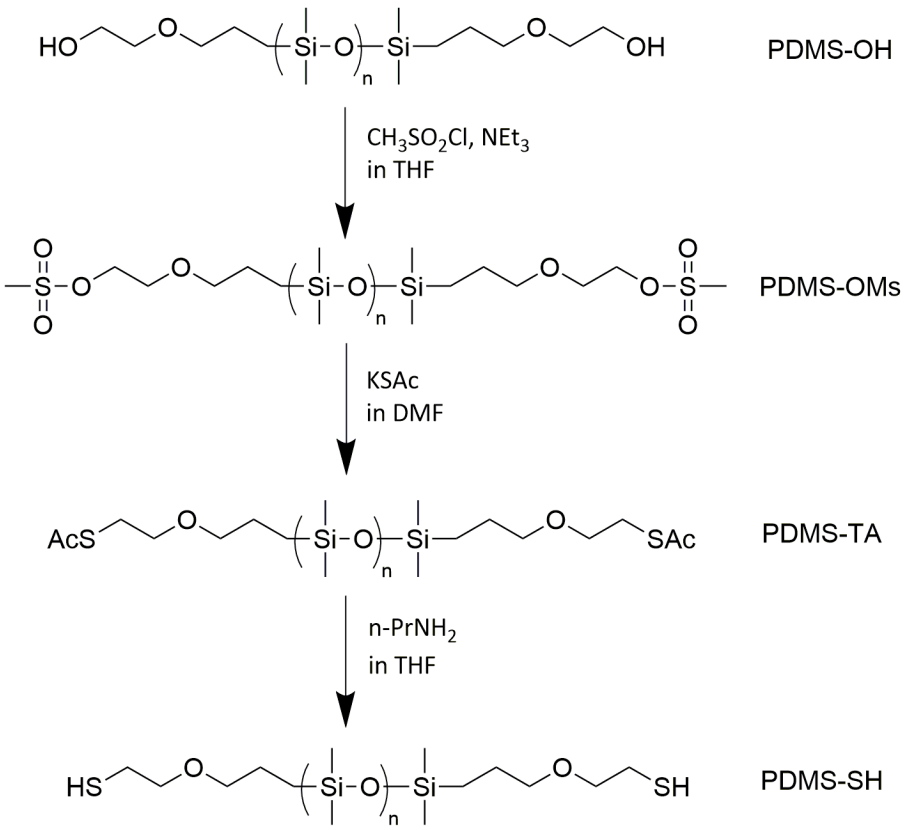

Scheme 4.2. Synthetic approach towards telechelic thiol-terminated PDMS oligomers. Three commercially available telechelic hydroxy-terminated PDMS oligomers with different molecular weights of approximately 1.0, 5.0 and 10 kg·mol^{-1} were used. The repeat unit (n) of the polydimethylsiloxane equals 14, 68 and 135 for PDMS-1K, -5K and -10K, respectively.

Synthesis of telechelic methylsulfonyl-terminated PDMS (PDMS-OMs)

Telechelic PDMS-OMs-1K: Into a 100 mL three-necked flask, 27.76 g (20.00 mmol) PDMS-OH-1K and 30 mL dry toluene was charged and the resulting solution was stirred under a nitrogen atmosphere. Azeotropic distillation was carried out on

this clear solution at 90 °C with vigorous stirring under a steady nitrogen flow to remove traces of water. Then 60 mL anhydrous THF was added and the solution was kept under argon and cooled to 0 °C. 4.86 g (48.00 mmol) dry NEt_3 was added followed by a dropwise addition of 5.50 g (48.00 mmol) mesyl chloride during 10 min under vigorous stirring. Stirring was continued for 1 h at 0 °C and another 4 h at room temperature. The white precipitate was filtered off and the filtrate was diluted with diethyl ether (200 mL), washed with brine (3 × 200 mL), dried on anhydrous $MgSO_4$ and finally filtered through celite 545. After removal of the solvent by in vacuo and drying in vacuum at room temperature, a clear colorless viscous liquid was obtained. Yield: 29.24 g, 95%. ^{1}H NMR (400 MHz, $CDCl_3$, ppm): 4.35 (t, C***H₂***OMs), 3.68 (t, OC***H₂***CH_2OMs), 3.43 (t, C***H₂***OCH_2CH_2OMs), 3.04 (s, SO_2C***H₃***), 1.56 − 1.63 (m, OCH_2C***H₂***CH_2), 0.49 - 0.53 (broad t, C***H₂***Si), -0.08 – 0.20 (m, (C***H₃***)$_2$Si).

Telechelic PDMS-OMs-5K: The same procedure as for telechelic PDMS-OMs-1K was used, except that 23.60 g (5.00 mmol) PDMS-OH-5K was treated with 1.38 g (12.00 mmol) mesyl chloride and 1.21 g (12.00 mmol) NEt_3. A clear colorless viscous liquid was obtained after work-up. Yield: 24.37 g, 100%. ^{1}H NMR (400 MHz, $CDCl_3$, ppm): 4.37 (t, C***H₂***OMs), 3.69 (t, OC***H₂***CH_2OMs), 3.45 (t, C***H₂***OCH_2CH_2OMs), 3.05 (s, SO_2C***H₃***), 1.56 − 1.63 (m, OCH_2C***H₂***CH_2), 0.49 - 0.53 (broad t, C***H₂***Si), -0.08 – 0.22 (m, (C***H₃***)$_2$Si).

Telechelic PDMS-OMs-10K: The same procedure as for telechelic PDMS-OMs-1K was used, except that 31.20 g (3.60 mmol) PDMS-OH-10K was treated with 0.99 g (8.64 mmol) mesyl chloride and 0.87 g (8.64 mmol) NEt_3. A clear colorless viscous liquid was obtained after work-up. Yield: 30.51 g, 97%. ^{1}H NMR (400 MHz, $CDCl_3$, ppm): 4.36 (t, C***H₂***OMs), 3.70 (t, OC***H₂***CH_2OMs), 3.45 (t, C***H₂***OCH_2CH_2OMs), 3.05 (s, SO_2C***H₃***), 1.56 − 1.63 (m, OCH_2C***H₂***CH_2), 0.49 - 0.53 (broad t, C***H₂***Si), -0.08 – 0.22 (m, (C***H₃***)$_2$Si).

Synthesis of telechelic thioacetyl-terminated PDMS (PDMS-TA)

Telechelic PDMS-TA-1K: To a solution of 29.24 g (18.94 mmol) telechelic *PDMS-OMs-1K* oligomer in 140 mL DMF, 8.65 g (75.75 mmol) potassium thioacetate was added all at once under a nitrogen atmosphere. The light red mixture was allowed to stir at 80 °C overnight. After cooling to room temperature, 200 mL water was added, which dissolved the precipitated salt to form a two-phase system. Subsequently, the mixture was extracted with diethyl ether (3 × 100 mL) and the combined organic layers were washed with brine (3 × 200 mL), dried with anhydrous $MgSO_4$ and filtered through celite 545. After concentrating in vacuo, a clear slightly

yellow viscous liquid was obtained, which was dried under vacuum at room temperature overnight. A clear slightly yellow viscous liquid was obtained after work-up. Yield: 28.10 g, 98%. ^{1}H NMR (400 MHz, $CDCl_3$, ppm): 3.53 (t, OC***H₂***CH_2SAc), 3.39 (t, C***H₂***SAc), 3.07 (t, C***H₂***OCH_2CH_2SAc), 2.32 (s, SCOC***H₃***) 1.54−1.62 (m, OCH_2C***H₂***CH_2), 0.49 - 0.53 (broad t, C***H₂***Si), -0.08 – 0.22 (m, (C***H₃***)$_2$Si).

Telechelic PDMS-TA-5K: The same procedure as for telechelic PDMS-TA-1K was used, except that 24.37 g (5.00 mmol) *PDMS-OMs*-5K was treated with 2.28 g (20.00 mmol) potassium thioacetate. A clear slightly yellow viscous liquid was obtained after work-up. Yield: 23.68 g, 98%. ^{1}H NMR (400 MHz, $CDCl_3$, ppm): 3.54 (t, OC***H₂***CH_2SAc), 3.40 (t, C***H₂***SAc), 3.08 (t, C***H₂***OCH_2CH_2SAc), 2.33 (s, SCOC***H₃***) 1.54−1.62 (m, OCH_2C***H₂***CH_2), 0.49 - 0.53 (broad t, C***H₂***Si), -0.08 – 0.22 (m, (C***H₃***)$_2$Si).

Telechelic PDMS-TA-10K: The same procedure as for telechelic PDMS-TA-1K was used, except that 24.57 g (2.80 mmol) *PDMS-OMs-10K* was treated with 1.28 g (11.20 mmol) potassium thioacetate. A clear colorless viscous liquid was obtained after work-up. Yield: 23.92 g, 98%. ^{1}H NMR (400 MHz, $CDCl_3$, ppm): 3.54 (t, OC***H₂***CH_2SAc), 3.40 (t, C***H₂***SAc), 3.09 (t, C***H₂***OCH_2CH_2SAc), 2.33 (s, SCOC***H₃***) 1.54−1.62 (m, OCH_2C***H₂***CH_2), 0.49 - 0.53 (broad t, C***H₂***Si), -0.08 – 0.22 (m, (C***H₃***)$_2$Si).

Synthesis of PDMS-SH oligomers

Telechelic PDMS-SH-1K: Into a three-necked round bottom flask equipped with condenser and gas inlet, a solution of 28.00 g (18.62 mmol) telechelic *PDMS-TA*-1K in 30 mL anhydrous THF was charged under argon atmosphere. Subsequently, 22.00 g (372.30 mmol) *n*-propylamine was added using a syringe. The solution was refluxed at 40 °C under argon atmosphere overnight. When the mixture was cooled to room temperature, 40 mL dilute hydrochloric acid (10%) and brine (300 mL) were added under a steady stream of argon. The mixture was then extracted with diethyl ether (3 × 100 mL) and the combined organic layers were washed with brine (3 × 200 mL), dried over anhydrous magnesium sulfate and filtered over cellite 545. After concentrating in vacuo, a clear slightly yellow viscous liquid was obtained and dried under vacuum at room temperature overnight. A clear slightly yellow viscous liquid was obtained after work-up. Yield: 26.09 g, 96%. ^{1}H NMR (400 MHz, $CDCl_3$, ppm): 3.55 (t, OC***H₂***CH_2SH), 3.40 (t, C***H₂***OCH_2CH_2SH), 2.66 (q, C***H₂***SH), 1.54−1.70 (m, OCH_2C***H₂***CH_2 and S***H***), 0.51 - 0.55 (broad t, C***H₂***Si), -0.08 – 0.22 (m, (C***H₃***)$_2$Si).

Telechelic PDMS-SH-5K: The same procedure as for telechelic PDMS-SH-1K was used, except that 22.89 g (4.74 mmol) telechelic *PDMS-TA*-5K was treated with

5.56 g (94.72 mmol) *n*-propylamine. A clear slightly yellow viscous liquid was obtained after work-up. Yield: 21.83 g, 97%. ^{1}H NMR (400 MHz, $CDCl_3$, ppm): 3.56 (t, OC***H₂***CH_2SH), 3.40 (t, C***H₂***OCH_2CH_2SH), 2.67 (q, C***H₂***SH), 1.54−1.70 (m, OCH_2C***H₂***CH_2 and S***H***), 0.51 - 0.55 (broad t, C***H₂***Si), -0.08 – 0.22 (m, $(C$***H₃***$)_2Si$).

Telechelic PDMS-SH-10K: The same procedure as for telechelic PDMS-SH-1K was used, except that 22.74 g (2.6 mmol) telechelic *PDMS-TA*-10K was treated with 3.07 g (52 mmol) *n*-propylamine. A clear colorless viscous liquid was obtained after work-up. Yield: 21.46 g, 96%. ^{1}H NMR (400 MHz, $CDCl_3$, ppm): 3.56 (t, OC***H₂***CH_2SH), 3.40 (t, C***H₂***OCH_2CH_2SH), 2.67 (q, C***H₂***SH), 1.54−1.70 (m, OCH_2C***H₂***CH_2 and S***H***), 0.51 - 0.55 (broad t, C***H₂***Si), -0.08 – 0.22 (m, $(C$***H₃***$)_2Si$).

4.2.4 Synthesis of multiblock copolymer

The all-aromatic AM oligomers with PDMS segments based $(AB)_n$-multiblock copolymers were labelled, AM5K-*b*-PDMS1K, AM5K-*b*-PDMS5K and AM5K-*b*-PDMS10K, respectively, where AM5K-*b*-PDMS reflects the composition of the $(AB)_n$-multiblock copolymer main-chain (A = the aromatic AM or LC block and B = the PDMS flexible block) and the integers refer to the molecular weight of the PDMS units, *i.e.* 1K = 1.0 kg·mol^{-1}. A similar convention was applied to the $(AB)_n$-multiblock copolymers composed of LC units and PDMS flexible blocks, labelled as LC5K-*b*-PDMS1K, LC5K-*b*-PDMS5K, LC5K-*b*-PDMS10K, respectively. The synthetic approach is shown in Scheme 4.3.

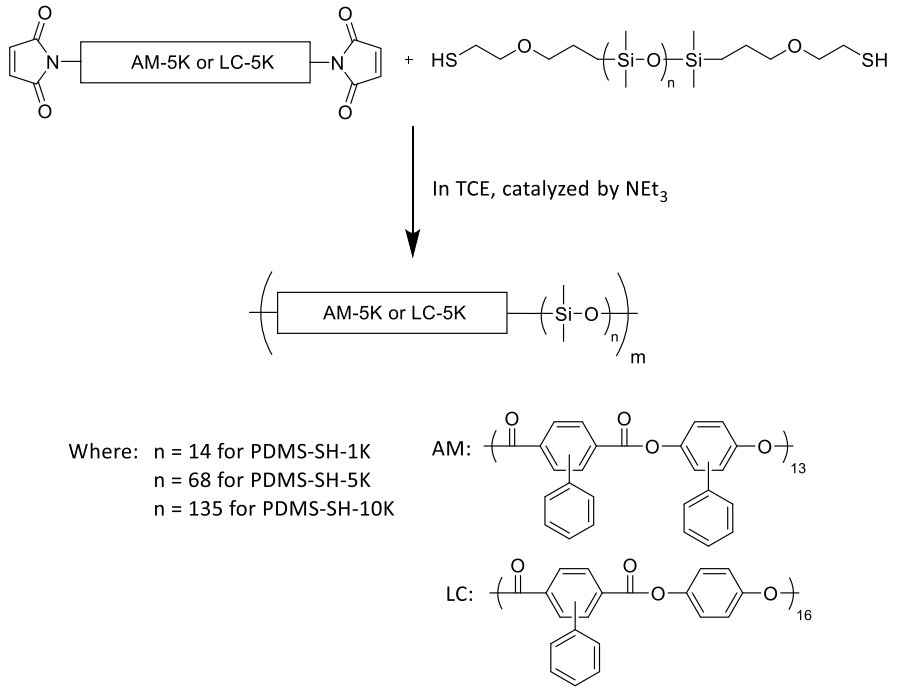

Scheme 4.3. Synthetic approach towards the $(AB)_n$-multiblock copolymers from thiol-terminated PDMS oligomers and maleimide terminated AM or LC oligomers.

Synthesis of AM5K-b-PDMS block copolymer

AM5K-b-PDMS1K: Into a 250 mL three-necked flask equipped with an overhead mechanical stirrer and argon gas inlet, 3.68 g (0.75 mmol) AM-5K and 36 mL TCE were charged under an argon atmosphere. Mechanical stirring at room temperature was applied until all the white solid dissolved, subsequently 1.04 g (0.71 mmol) PDMS-SH-1K and 0.50 mL triethylamine was added. After evacuation and back filling with argon, the clear solution was stirred at 60 °C for 2 h. When the reaction mixture was cooled to room temperature, the viscous solution was precipitated in ethanol. The filtered white product was re-dissolved in dichloromethane (100 mL) and re-precipitated in ethanol (500 mL), which was repeated one more time. After drying under vacuum at 60 °C overnight, a white solid was obtained. Yield: 4.71 g (99%). ^{1}H NMR (400 MHz, $CDCl_3$, ppm): 6.50 – 8.50 (aromatic), 4.05 (COC***H***S), 3.73 ($SCH_2C\boldsymbol{H_2}O$), 3.43 ($SCH_2CH_2OC\boldsymbol{H_2}CH_2$), 3.25 ($SC\boldsymbol{H_2}CH_2O$), 2.72 and 2.97 ($COC\boldsymbol{H_2}CHCO$), 1.60 ($OCH_2C\boldsymbol{H_2}CH_2$), 0.53 ($C\boldsymbol{H_2}Si$), -0.07 – 0.22 ($(C\boldsymbol{H_3})_2Si$).

AM5K-b-PDMS5K: The same procedure as for AM5K-*b*-PDMS1K was used, except that 2.45 g (0.50 mmol) AM-5K in 36 mL TCE was treated with 2.52 g (0.50 mmol) PDMS-SH-5K and 0.5 mL NEt_3. A white solid was obtained. Yield: 4.93 g (99%). ^{1}H NMR (400 MHz, $CDCl_3$, ppm): 6.50 – 8.50 (aromatic), 4.03 (COC***H***S), 3.69 ($SCH_2C\boldsymbol{H_2}O$), 3.43 ($SCH_2CH_2OC\boldsymbol{H_2}CH_2$), 3.24 ($SC\boldsymbol{H_2}CH_2$), 2.69 and 2.96 ($COC\boldsymbol{H_2}CHCO$), 1.62 ($OCH_2C\boldsymbol{H_2}CH_2$), 0.52 ($C\boldsymbol{H_2}Si$), -0.07 − 0.22 ($(C\boldsymbol{H_3})_2Si$).

AM5K-b-PDMS10K: The same procedure as for AM5K-*b*-PDMS1K was used, except that 1.96 g (0.40 mmol) AM-5K in 36 mL TCE was treated with 4.63 g (0.40 mmol) PDMS-SH-10K and 0.50 mL NEt_3. A white solid was obtained. Yield: 6.55 g (99%).^{1}H NMR (400 MHz, $CDCl_3$, ppm): 6.50 – 8.50 (aromatic), 4.06 (COC***H***S), 3.73 ($SCH_2C\boldsymbol{H_2}O$), 3.43 ($SCH_2CH_2OC\boldsymbol{H_2}CH_2$), 3.24 ($SC\boldsymbol{H_2}CH_2$), 2.71 and 2.96 ($COC\boldsymbol{H_2}CHCO$), 1.61 ($OCH_2C\boldsymbol{H_2}CH_2$), 0.53 ($C\boldsymbol{H_2}Si$), -0.08 − 0.22 ($(C\boldsymbol{H_3})_2Si$).

Synthesis of LC5K-b-PDMS block copolymer

Due to the limited solubility of the LC-5K oligomer and the high molecular weight block copolymers thereof, the amount of solvent (TCE) and/or the final reaction temperature was adjusted in order to avoid premature precipitation and phase separation during synthesis.

LC5K-b-PDMS1K: Into a 250 mL three-necked flask equipped with an overhead mechanical stirrer and argon gas inlet, 3.73 g (0.70 mmol) LC-5K and 36 mL TCE were charged under an argon atmosphere. The mixture was heated to 60 °C and stirred until all the white solid dissolved, subsequently 1.07 g (0.74 mmol) PDMS-SH-1K and 0.50 mL triethylamine was added. After degassing and back filling with argon, the clear solution was stirred at 90 °C for 2 h. When the reaction mixture was cooled to room temperature, the viscous solution was precipitated in ethanol. The filtered white product was washed with hot dichloromethane and ethanol for two times. After drying under vacuum at 60 °C overnight, a white solid was obtained. Yield: 4.71 g (98%). ^{1}H NMR (400 MHz, $CDCl_3$ + TCE-d_2 50/50, ppm): 6.50 – 8.60 (aromatic), 4.07 (COC***H***S), 3.70 ($SCH_2C\boldsymbol{H_2}O$), 3.42 ($SCH_2CH_2OC\boldsymbol{H_2}CH_2$), 3.20 ($SC\boldsymbol{H_2}CH_2$), 2.70 and 2.95 ($COC\boldsymbol{H_2}CHCO$), 1.68 ($OCH_2C\boldsymbol{H_2}CH_2$), 0.52 ($C\boldsymbol{H_2}Si$), -0.09 − 0.21 ($(C\boldsymbol{H_3})_2Si$).

LC5K-b-PDMS5K: The same procedure as for LC5K-*b*-PDMS1K was used, except that 2.66 g (0.50 mmol) LC-5K in 60 mL TCE was treated with 1.01 g (0.50 mmol) PDMS-SH-5K and 0.50 mL NEt_3. A white solid was obtained. Yield: 3.60 g (98%). ^{1}H NMR (400 MHz, $CDCl_3$ + TCE-d_2 50/50, ppm): 6.50 – 8.60 (aromatic), 4.07 (COC***H***S),

3.70 ($SCH_2C\boldsymbol{H_2}O$), 3.42 ($SCH_2CH_2OC\boldsymbol{H_2}CH_2$), 3.21 ($SC\boldsymbol{H_2}CH_2$), 2.70 and 2.96 ($COC\boldsymbol{H_2}CHCO$), 1.62 ($OCH_2C\boldsymbol{H_2}CH_2$), 0.51 ($C\boldsymbol{H_2}Si$), -0.09 − 0.20 ($(C\boldsymbol{H_3})_2Si$).

LC5K-b-PDMS10K: The same procedure as for LC5K-*b*-PDMS1K was used, except that 1.60 g (0.30 mmol) LC-5K in 60 mL TCE was treated with 3.47 g (0.30 mmol) PDMS-SH-10K and 0.50 mL NEt_3. A white solid was obtained. Yield: 5.01 g (99%). ^{1}H NMR (400 MHz, $CDCl_3$ + TCE-d_2 50/50, ppm): 6.50 – 8.60 (aromatic), 4.07 ($COC\boldsymbol{H}S$), 3.70 ($SCH_2C\boldsymbol{H_2}O$), 3.42 ($SCH_2CH_2OC\boldsymbol{H_2}CH_2$), 3.21 ($SC\boldsymbol{H_2}CH_2$), 2.70 and 2.97 ($COC\boldsymbol{H_2}CHCO$), 1.67 ($OCH_2C\boldsymbol{H_2}CH_2$), 0.52 ($C\boldsymbol{H_2}Si$), -0.09 − 0.21 ($(C\boldsymbol{H_3})_2Si$).

4.3 Results and discussion

4.3.1 Synthesis and characterization of PDMS-SH

The telechelic thiol-functionalized PDMS was successfully synthesized starting from commercial telechelic hydroxyl-functionalized PDMS with molecular weights of 1.0, 5.0 and 10 kg·mol^{-1}, respectively. The synthetic procedure was based on literature[20], however, an optimized approach was developed, aiming for high conversion of end-group functionalities. The hydroxyl functionalities were first converted into mesylate groups, followed by a nucleophilic substitution with potassium thioacetate in DMF. Afterwards, the thioacetate-functionalized PDMS was treated with an excess amount of *n*-propylamine to yield the telechelic thiol-terminated PDMS oligomers as slightly yellow oils with overall yields of over 90%, see Scheme 4.2. For the thiol-functionalized PDMS-10K oligomer, due to a much lower content of thiol end-groups, a nearly colorless and odorless viscous oil was received after work-up, with a similar high yield. The 5.0 and 10 kg·mol^{-1} PDMS oligomers were only partly soluble in DMF, and vigorous stirring was needed to solubilize the oligomers and obtain a high conversion of the end-groups. During the work-up of all reactions, a fine emulsion was formed while washing the product with brine. Small portions of acetone were added to promote phase separation. All solutions of the final PMDS product in ether were filtered over a celite 545 column to remove traces of $MgSO_4$.

^{1}H-NMR was used to follow the progress of the reactions and to confirm conversion of hydroxyl functionalities into thiol groups. In Figure 4.2, the ^{1}H NMR spectra of PDMS-OH-1K and PDMS-SH-1K are shown. The α protons of hydroxyl group at δ = 3.41 ppm (*f* triplets in Figure 4.2) shifted to 2.67 ppm (*f'* triplets in Figure

4.2) of the thiol *α* protons, clearly showing the conversion to telechelic thiol-terminated PDMS. The observed peaks at δ = 2.9 ppm (*i.e.* peaks *h* in Figure 4.2) arise from a slight and almost unavoidable formation of disulfide in the telechelic dithiol when exposed to atmospheric oxygen during work-up, which is reported to occur in similar systems.[20, 21]

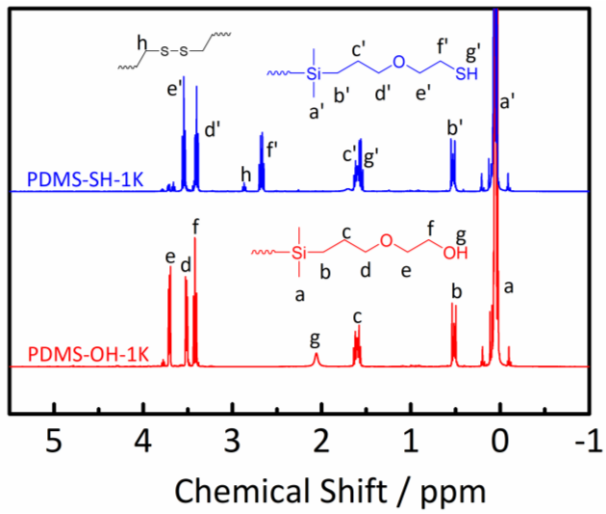

Fig. 4.2. [1]H NMR spectra and peak assignments of PDMS-OH-1K and PDMS-SH-1K oligomers. The labelling scheme of the peaks is included in the Figure. The spectra are offset for clarity.

The number average molecular weights($\overline{M}_n$s) for the PDMS-SH oligomers were calculated based on the signals of protons in end-groups and in the main-chain of PDMS. The average number of dimethylsiloxane repeating units ($\overline{DP}$) in PDMS can be calculated from the integration ratios of the *α* protons in the methylene group adjacent to Si ($I_{b'}$, corresponding to 4 protons of *b'* peak at δ = 0.5 ppm in Figure 4.2) to that of the methyl group on Si in the PDMS main-chain ($I_{a'}$, corresponding to 6 protons of *a'* peaks at around 0 ppm in Figure 4.2), using the following Equation 4.2.

$$\frac{I_{a'}}{I_{b'}} = \frac{4}{6\times\overline{DP}} \qquad \text{(eqn.4.2)}$$

Therefore $\overline{M}_n$ can be calculated by Equation 4.3.

$$\overline{M}_n = \left(\overline{DP} \times M_0\right) + M_{end} \times 2 \quad \text{(eqn. 4.3)}$$

Where M_0 is the molar mass of the dimethylsiloxane repeating unit (equals 74 for PDMS), $M_{end}$is the molecular weight of end-groups (equals 119 in this case). Using this method, all the $\overline{M}_n s$ were calculated and summarized in Table 4.1. The molecular weights for the 5K and 10K oligomers match the target molecular weights quite closely, only the 1K oligomer is somewhat higher. This is because the commercial source of PDMS-OH-1K has a $\overline{M}_n$ of 1.4 kg·mol^{-1}.

For comparison purposes the PDMS-OH and PDMS-SH GPC traces are shown in Figure 4.3, observing a slight increase of the molecular weight and polydispersity going from the hydroxyl terminated to the thiol terminated oligomer. For example, the number average molecular weights before and after end-group modification of PDMS-OH-1K and PDMS-SH-1K are 1.8 (PDI of 1.4) and 2.2 (PDI of 1.5) kg·mol^{-1}, respectively, relative to polystyrene standards. This slight increase was observed for all PDMS oligomers and might be the result of disulfide formation, as was also observed in the NMR experiments. The bimodal peak for PDMS-SH-1K in Figure 4.3 is due to an instrument artifact.

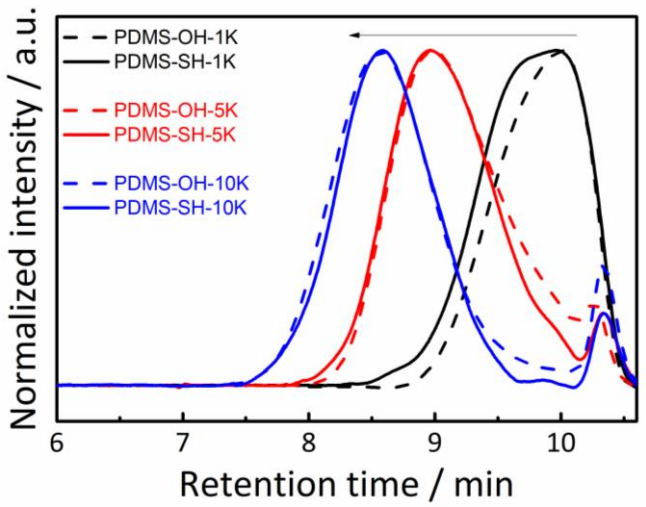

Fig. 4.3. GPC traces of PDMS-OH and PDMS-SH oligomers. All curves are normalized to maximum intensity. The small increase in molecular weight and PDI observed for the PDMS-SH oligomers is due to the formation of disulfides.

The resulting $\overline{M}_n$s, $\overline{M}_w$s, as well as PDI derived from the GPC traces are listed in Table 4.1, and are found to be consistently higher than the NMR results, due to the calibration of the GPC with polystyrene, giving an overestimation of the $\overline{M}_n$. The fact that the trends are similar proves the validity of both characterization methods.

Table 4.1. Molecular weights of the PDMS oligomers as determined by GPC, ^{1}H-NMR and viscometry.

Samples	*GPC results*[1]			$\overline{M}_n$ *(kg·mol^{-1}, NMR)*[2]	η_{inh} *(dL·g^{-1})*[3]
	$\overline{M}_n$ *(kg·mol^{-1})*	$\overline{M}_w$ *(kg·mol^{-1})*	*PDI*		
PDMS-OH-1K	1.8	2.5	1.4	1.4	0.030
PDMS-OH-5K	6.0	9.0	1.4	4.8	0.059
PDMS-OH-10K	13	20	1.5	11.2	-[4]
PDMS-SH-1K	2.2	3.4	1.5	1.53	0.032
PDMS-SH-5K	7.8	12	1.4	5.03	0.063
PDMS-SH-10K	13	18	1.4	11.6	-[4]

[1] Molecular weight and polydispersity index was measured by GPC with THF as eluent at a flow rate of 1 mL·min^{-1}, calibrated using monodisperse polystyrene standards.

[2] Molecular weights were calculated from ^{1}H NMR results (Measured in $CDCl_3$ at room temperature).

[3] Inherent viscosities were measured by capillary viscometer in TCE at a concentration of 0.5 g·dL^{-1} at 21 °C.

[4] Not determined due to low solubility in TCE.

4.3.2 Synthesis and characterization of multiblock copolymer

Optimization of synthetic conditions

The observation of disulphide formation may prohibit a straightforward stoichiometric polymerisation, therefore besides solvent, reaction time and temperature, the stoichiometry had to be optimized as well. A typical polymerization was performed with triethylamine (NEt_3) as a catalyst under a dry nitrogen atmosphere.

Due to the poor solubility of the LC-5K oligomer at room temperature, TCE seemed to be the only convenient solvent for synthesizing LC5K-*b*-PDMS block copolymers *via* solution-based thiol-ene click reaction. Satisfactory polymerization results were also obtained for the copolymerization of the AM5K-*b*-PDMS series in chloroform, but for the sake of direct comparison, all syntheses were performed in TCE.

As frequently reported[14, 16, 22], thiol-ene click reactions proceed extremely rapid and the conversions can reach up to 90% within minutes at room temperature. In our case, the reaction time was extended to 2 hours to ensure full conversion and formation of high molecular weight polymer. The reaction temperature was set to 60 °C for the AM5K-*b*-PDMS series, however in the case of LC5K-*b*-PDMS analogues, the reaction temperature had to be raised to 90 °C due to the limited solubility of both starting materials and the resulting block copolymers. No precipitation or gelation was observed during the syntheses, indicating that no premature crosslinking of maleimide end-groups has taken place.

After optimizing the solvent selection, reaction time and temperature, the preferred ratio of both reactive oligomers was explored. With the optimized conditions followed by drying in vacuum at 60 °C overnight, the final product was collected and analysed using either GPC in THF (AM5K-*b*-PDMS) or viscometry in TCE at 21 °C (LC5K-*b*-PDMS), depending on the solubility of the copolymers. Figure 4.4 shows the results of the stoichiometry optimisation, where the preferred stoichiometry of most of the polymerization reactions was close to 1:1, underlining the effectiveness of the end-group analysis and molecular weight calculation of the oligomers. Besides, this also implies that dithiol formation has a rather small influence on the molecular weight of the final block copolymers. The molar ratios of both reactants showing the highest molecular weights or highest inherent viscosity were selected as the optimal stoichiometry for scaling up the block copolymer

synthesis. These results also show the applicability of the thiol-ene click in the synthesis of the block copolymers.

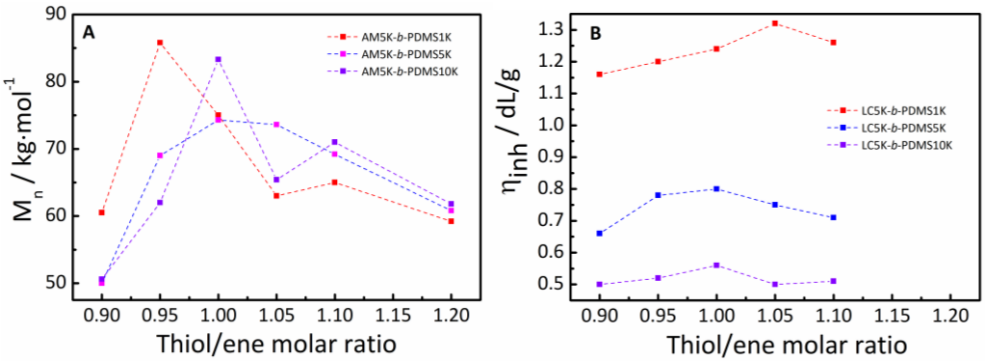

Fig. 4.4. Optimisation of thiol-ene feed ratios for the AM5K-*b*-PDMS series (***A***) and LC5K-*b*-PDMS series (***B***). Note that GPC results (THF as eluent) are only available for the AM-series. The LC series is soluble in TCE only and was therefore analysed using viscometry.

FTIR spectra of the oligomers and polymers

FTIR was performed to confirm the presence or absence of functional groups in the oligomers and polymers. Figure 4.5 shows the spectra of PDMS-SH-1K, AM-5K and the resulting $(AB)_n$ multiblock copolymer AM5K-*b*-PDMS1K, as representative examples. The spectrum of PDMS-SH-1K shows two peaks at 1083 cm^{-1} and 1010 cm^{-1}, corresponding to the asymmetric and symmetric stretching vibration of the two neighbouring siloxane groups, respectively.[23] The bands at 1259 cm^{-1} and 795 cm^{-1} are assigned to the in-plane bending and out-of-plane oscillations of the $Si–CH_3$ bond, respectively.[24] The peak located at 2960 cm^{-1} is due to the asymmetric stretching of $Si-CH_3$.[25] The spectrum of AM-5K oligomer shows a strong peak at 1720 cm^{-1} (ester C=O stretching). The weak peak at 828 cm^{-1} is associated with the out-of-plane bending of the maleimide =C-H end-group.

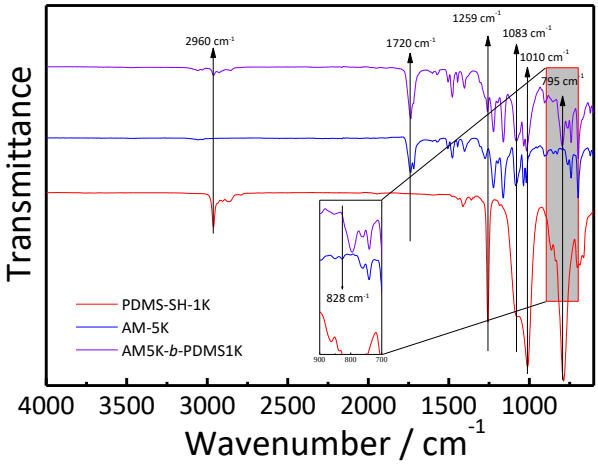

Fig. 4.5. FTIR spectra of PDMS-SH-1K, AM-5K and AM5K-*b*-PDMS1K copolymer. The inset shows the decrease of the 828 cm^{-1} peak, associated with the maleimide double bond after thiol-ene reaction. The spectra are offset for clarity.

As expected, the characteristic peak at 828 cm^{-1}, associated with the maleimide double bond [17] decreased dramatically going from the AM-5K oligomer to the final copolymer (AM5K-*b*-PDMS1K), showing the successful reaction of the maleimide. All the other peaks that can be assigned to the PDMS oligomers and the rigid aromatic oligomers peaks remain unchanged, indicating the final copolymer contains all functional groups present in the original oligomers. All the other oligomers and polymers show similar results.

Molecular composition and Molecular weight of $(AB)_n$ multiblock copolymers

For ^{1}H NMR analysis, different deuterated solvents were selected depending on the solubility of the prepared block copolymers. All the AM5K-*b*-PDMS series were measured in $CDCl_3$, whereas the LC5K-*b*-PDMS analogues were measured in a 50/50 mixture of $CDCl_3$ and TCE-d_2. In Figure 4.6, the ^{1}H NMR spectra of the AM-5K oligomer and AM5K-*b*-PDMS1K are shown as examples to verify the thiol-ene click reaction. A dramatic decrease in the proton signal of the maleimide (at δ = 6.84 ppm) was observed, while at the same time the appearance of peaks h, d and d', assigned to protons in the hydrothiolated maleimide, imply a successful thiol-ene Michael addition.

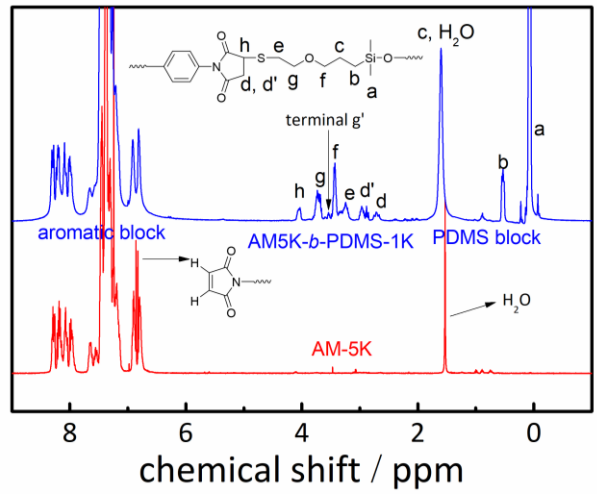

Fig. 4.6. ^{1}H NMR of the AM-5K oligomer and resulting multiblock copolymer AM5K-*b*-PDMS1K, as a representative example. The assignment of peaks is shown in the Figure. The spectra are offset for clarity. The maleimide peak at δ = 6.84 ppm has disappeared after the thiol-ene click reaction. The proton peak of g' at 3.53 ppm in the terminal end-groups are integrated to calculate the molecular weights of the block copolymers.

With the aim of estimating the molecular weight ($\overline{M}_n$) of the final $(AB)_n$ multiblock copolymers, the starting materials, *i.e.*, AM-5K and PDMS oligomers are treated as difunctional macromonomers in the calculation for the sake of simplicity. The number of macromonomer segments in the final $(AB)_n$ multiblock copolymers can be determined by end-group analysis from ^{1}H NMR data. For a well-defined structured $(AB)_n$ main-chain type multiblock copolymer, the number of repeat units (n) and the number of unreacted end-groups at block ***A*** (N_t) and main-chain linkage (N_c) of the reacted end-group has a relationship[26, 27] of:

$$\frac{N_t}{N_c} = \frac{I_t}{I_c} = \frac{1}{2\times n-1} \qquad \text{(eqn. 4.4)}$$

Where I_t and I_c represent the integrals of the peaks of the terminal end-group and the linkage within the polymer chain, respectively. Therefore $\overline{M}_n$ of the $(AB)_n$ multiblock copolymer can be calculated by Equation 4.5,

$$\overline{M}_n = \left(\overline{M}_A + \overline{M}_B\right) \times n \qquad \text{(eqn. 4.5)}$$

Where $\overline{M}_A$ and $\overline{M}_B$ are number average molecular weights ($\overline{M}_n$) of each block ***A*** and ***B***, respectively.

As an example, the number of repeat units (n) of AM5K-*b*-PDMS1K is calculated using Equation 4.4, based on the NMR spectrum of integrated areas of the peaks of the terminal end-group (g' peak at 3.53 ppm in Figure 4.6) and the aliphatic bridge (g peak at 3.70 ppm in Figure 4.6), equals 5.07. The $\overline{M}_n$s of the AM-5K oligomer ($\overline{M}_A$) and the PDMS-SH-1K precursor ($\overline{M}_B$) are 4.9 and 1.5 kg·mol^{-1}, respectively, as determined previously. Therefore, the $\overline{M}_n$ of AM5K-*b*-PDMS1K is calculated to be approximately 32 kg·mol^{-1}.

Table 4.2 lists the molecular weights and PDMS contents of the block copolymers calculated by ^{1}H NMR and as determined by GPC. The GPC traces of the soluble AM5K-*b*-PDMS block copolymers are shown in Figure 4.7 (Note: the LC-based block copolymers are not soluble in THF and therefore could not be analysed using GPC). The PDMS content as determined by ^{1}H NMR is quite close to the theoretical values, confirming the efficiency of the thiol-ene click chemistry and the right molecular composition. The results from the different techniques show a similar trend and have the same order of magnitude. Although the absolute values observed by the two techniques are different, the results obtained are quite satisfying also considering the fact that polystyrene, a random coil polymer, was used as the internal standard for the GPC measurements. As expected, the polydispersity of the block copolymers is slightly higher than that of the oligomers, which can be attributed to the polydispersity of the starting oligomers.

The inherent viscosity of both the block copolymers and oligomers was measured in TCE. Since the block copolymers have different molecular compositions, a direct comparison of their inherent viscosity cannot be made. A higher inherent viscosity of different polymers does not necessarily imply a higher molecular weight.

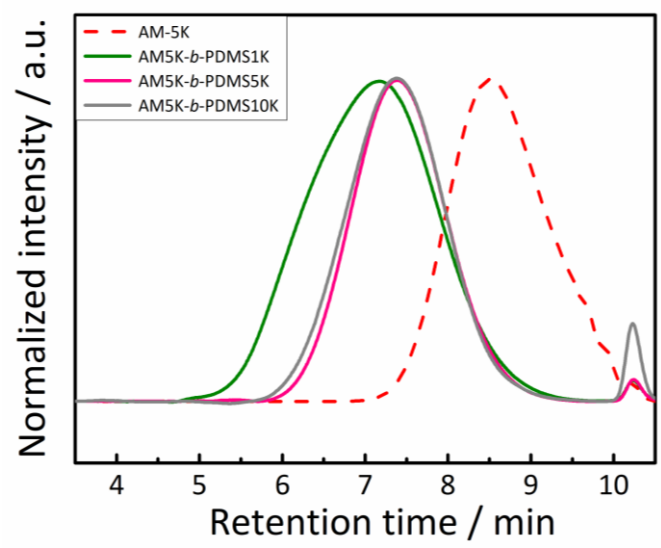

Fig. 4.7. GPC curves obtained for the soluble (THF) AM-5K oligomer and AM5K-*b*-PDMS1K, -5K and -10K block copolymers. All curves are normalized to maximum intensity. Note that the LC-series could not be analyzed using GPC because of the limited solubility in THF.

Table 4.2. Molecular weight and composition results of the oligomers and final $(AB)_n$-multiblock copolymers.

Samples	*GPC results*[1]			$\overline{M}_n$ *(kg·mol^{-1}, NMR)*	η_{inh} *(dL·g^{-1})*[4]	*PDMS content (theoretical)*[5]	*PDMS content (NMR)*[6]
	$\overline{M}_n$ *(kg·mol^{-1})*	$\overline{M}_w$ *(kg·mol^{-1})*	*PDI*				
AM-5K	8.7	22	2.3	4.9[2]	0.52	0%	0%
LC-5K	N/A[7]	N/A	N/A	5.3[2]	0.70	0%	0%
AM5K-*b*-PDMS1K	93	417	4.4	32[3]	1.74	22%	25%
AM5K-*b*-PDMS5K	72	168	2.3	46[3]	1.71	51%	52%
AM5K-*b*-PDMS10K	77	189	2.5	58[3]	0.97	69%	70%
LC5K-*b*-PDMS1K	N/A[7]	N/A	N/A	22[3]	1.20	22%	26%
LC5K-*b*-PDMS5K	N/A[7]	N/A	N/A	37[3]	0.96	49%	46%
LC5K-*b*-PDMS10K	N/A[7]	N/A	N/A	44[3]	0.56	66%	65%

[1] Molecular weight and polydispersity index was measured by GPC with THF eluent at a flow rate of 1 mL·min^{-1}, calibrated using polystyrene standards (S1: Mn of 5800 and PDI of 1.05; S2: Mn of 12200 and PDI of 1.09; S3: Mn of 23700 and PDI of 1.09; S4: Mn of 48000 and PDI of 1.07; S5: Mn of 100000 and PDI of 1.13; S6: Mn of 186000 and PDI of 1.09; S7: Mn of 380000 and PDI of 1.12; S8: Mn of 853000 and PDI of 1.23). [2] Molecular weights were calculated from ^{13}C NMR results (Chapter 2).
[3] Molecular weights were calculated from ^{1}H NMR results (Equation 4.4 and 4.5).
[4] Inherent viscosities were measured by capillary viscometer in TCE at a concentration of 0.5 g·dL^{-1} at 21 °C.
[5] PDMS content was calculated from feed ratios. [6] PDMS content was collected from ^{1}H NMR results.
[7] Not determined due to limited solubility in THF.

4.4 Conclusion

Three different thiol-terminated PDMS oligomers with molecular weights of 1, 5 and 10 kg·mol^{-1} were synthesized and characterized using ^{1}H-NMR and GPC. ^{1}H NMR and GPC studies confirmed that the thiol functionalities undergo a slight degree of oxidation during the work-up of the oligomers. However, all thiol-terminated PDMS oligomers could be successfully copolymerized with either LC- or AM-maleimide end-capped rigid all-aromatic blocks (M_n = 5 kg·mol^{-1}), *via* thiol-ene Michael click chemistry. The structure of the resulting block copolymers was validated with ^{1}H NMR and FTIR. ^{1}H NMR measurements confirmed that the block copolymers exhibited high molecular weights (M_n), in the range of 22 – 58 kg·mol^{-1}. The soluble AM-5K based multiblock copolymers could be analysed using GPC and we found polydispersity indices ranging from 2.3 to 4.4, which is a consequence of using polydisperse macromonomers as starting materials. The M_ns of the AM-based block copolymer series ranges from 72 to 93 kg·mol^{-1}. The molecular composition, as calculated from ^{1}H NMR experiments, are consistent with the theoretical values, suggesting the effectiveness of preparing high molecular weight block copolymers *via* thiol-ene click chemistry. The morphology and (thermo)mechanical properties of the new amorphous and liquid crystalline $(AB)_n$ block copolymers will be discussed in detail in the next Chapter.

4.5 References

1 J. Adams and W. Gronski, *Macromol. Rapid Commun.*, 1989, **10**, 553-557.
2 H. Fischer and S. Poser, *Acta Polym.*, 1996, **47**, 413-428.
3 W. Heitz, *Makromol. Chem. M. Symp.*, 1989, **26**, 1-8.
4 M. J. Fasolka and A. M. Mayes, *Annu. Rev. Mater. Res.*, 2001, **31**, 323-355.
5 N. Hadjichristidis, S. Pispas and G. Floudas, in *Block Copolymers*, John Wiley & Sons, Inc., 2003, DOI: 10.1002/0471269808.ch21, pp. 383-408.
6 D. Pospiech, L. Häußler, K. Eckstein, H. Komber, D. Voigt, D. Jehnichen, P. Friedel, A. Gottwald, W. Kollig and H. R. Kricheldorf, *High Perform. Polym.*, 2001, **13**, S275-S292.
7 A. M. Nelson, G. B. Fahs, R. B. Moore and T. E. Long, *Macromol. Chem. Phys.*, 2015, **216**, 1754-1763.
8 B. C. Auman and V. Percec, *Polymer*, 1988, **29**, 938-949.

9 V. Percec, B. C. Auman, H. Nava and J. P. Kennedy, *J. Polym. Sci., Part A: Polym. Chem.*, 1988, **26**, 721-741.
10 N. Reichelt, U. Schulze and H.-W. Schmidt, *Macromol. Chem. Phys.*, 1997, **198**, 3907-3930.
11 A. Gottschalk and H. W. Schmidt, *Liq. Cryst.*, 1989, **5**, 1619-1627.
12 S. Brenda, W. Heitz, A. Karback and R. Wehrmann, *Macromol. Chem. Phys.*, 1994, **195**, 1327-1339.
13 J. M. Lambert, E. Yilgor, G. I. Wilkes and J. E. McGrath, *Polym. Prepr. (Am. Chem. Soc., Div. Polym. Chem.)*, 1985, **26**, 275.
14 A. B. Lowe, *Polym. Chem.*, 2010, **1**, 17-36.
15 T. Posner, *Ber. Dtsch. Chem. Ges.*, 1905, **38**, 646-657.
16 B. H. Northrop and R. N. Coffey, *J. Am. Chem. Soc.*, 2012, **134**, 13804-13817.
17 C. E. Hoyle and C. N. Bowman, *Angew. Chem. Int. Ed.*, 2010, **49**, 1540-1573.
18 C. E. Hoyle, A. B. Lowe and C. N. Bowman, *Chem. Soc. Rev.*, 2010, **39**, 1355-1387.
19 B. D. Mather, K. Viswanathan, K. M. Miller and T. E. Long, *Prog. Polym. Sci.*, 2006, **31**, 487-531.
20 O. van den Berg, L.-T. T. Nguyen, R. F. A. Teixeira, F. Goethals, C. Özdilek, S. Berghmans and F. E. Du Prez, *Macromolecules*, 2014, **47**, 1292-1300.
21 R. Mahou and C. Wandrey, *Polymers*, 2012, **4**, 561.
22 C. E. Hoyle, T. Y. Lee and T. Roper, *J. Polym. Sci., Part A: Polym. Chem.*, 2004, **42**, 5301-5338.
23 J. N. Chazalviel and U. P. Rodrigues-Filho, *Thin Solid Films*, 2012, **520**, 3918-3921.
24 L. F. Wang, Q. Ji, T. E. Glass, T. C. Ward, J. E. McGrath, M. Muggli, G. Burns and U. Sorathia, *Polymer*, 2000, **41**, 5083-5093.
25 L. M. Johnson, L. Gao, C. W. Shields IV, M. Smith, K. Efimenko, K. Cushing, J. Genzer and G. P. López, *J Nanobiotechnology*, 2013, **11**, 1-8.
26 W. Huang, Y. Wan, J. Chen, Q. Xu, X. Li, X. Yang, Y. Li and Y. Tu, *Polym. Chem.*, 2014, **5**, 945-954.
27 H. Li, S. Thanneeru, L. Jin, C. J. Guild and J. He, *Polym. Chem.*, 2016, **7**, 4824-4832.

Chapter 5 Thermo-mechanical properties of siloxane-based multiblock copolymers with all-aromatic rigid units

Abstract

In this Chapter, the phase behavior and (thermo)mechanical properties of our aromatic/PDMS $(AB)_n$ multiblock copolymers will be presented. The AM5K-based multiblock copolymers show good solubility in common solvents, whereas the LC5K-based analogs show limited solubility. All block copolymers films were prepared *via* a standard solution casting technique, using either TCE or chloroform as the casting solvent. With the incorporation of PDMS segments, the multiblock copolymers show a reduction in thermal stability when compared to their all-aromatic starting materials, with $T_d^{5\%}$ >346 °C. The $(AB)_n$ multiblock copolymers prepared from mesogenic (LC) units show micro-phase separation and liquid crystallinity even with a PDMS content as high as 65 wt%. The AM5K-based series, on the other hand, is completely amorphous. All the multiblock copolymers show two T_gs at approximately -120 °C and 120 °C, respectively, in DMTA measurements, implying the presence of a (micro)phase separated system. The multiblock copolymers built from AM-5K and PDMS-1K display excellent stress–strain behavior at 25 °C, with a tensile strength of ~125 MPa, an elastic modulus of ~3.5 GPa, an elongation at break of ~30% and toughness of ~30 $MJ \cdot m^{-3}$. The LC-5K based multiblock copolymer films exhibit poor stress–strain behavior comparing to their AM-5K based analogous, which is the results of a higher degree of phase separation and low phase intermixing, as confirmed by TEM and SEM measurements.

5.1 Introduction

Multiblock copolymers are a set of polymers containing at least two chemically distinct blocks, which are connected by covalent bonds. Compared with polymer blends, block copolymers show properties that are a combination of the individual building blocks without macroscopic scale phase separation. When a rigid high-performance polymer block is employed as one of the constituents, a block copolymer with potentially high mechanical properties is anticipated. Extensive work on block copolymers containing high-performance polymer units has been reported, including amorphous, semi-crystalline or liquid crystalline high-performance polymers.[1]

With different types of high-performance polymer units utilized in preparing block copolymers, the phase behavior obviously varies on the nature of the rigid unit, as well as on the soft blocks. Various parameters, including the thermodynamic interaction parameter χ, the temperature, the molecular weight and molecular weight distribution and the volume fraction of the different components, have an effect on the phase separation of the two blocks.[2, 3] Pospiech *et al.* studied the phase separation behavior of $(AB)_n$ type multiblock copolymers containing segments with different degrees of flexibility and different molecular weights.[4] The systematic variation of the chemical structure and molecular weights of the individual blocks revealed that the onset of phase separation in such rather complex systems can be understood using Flory–Huggins χ-parameters. While using a LCP as the high-performance block, the block copolymers may exhibit liquid crystallinity, depending on the chain composition. In the work reported by Schmidt *et al.*, the block copolymers from a liquid crystalline polyester with poly(ethylene glycol) (PEG) or polystyrene (PS) show thermotropic liquid crystalline behavior up to 50 wt% PEG or 65 wt% PS. [5, 6]

Polydimethylsiloxane (PDMS) is a unique inorganic material with extremely low T_g *(-125 °C)*, which can be used to prepare organic/inorganic hybrid block copolymers. With the incorporation of PDMS into a block copolymer, several improvements in properties can be noted, such as processability, toughness, and flexibility.[7] Several different types of dianhydrides and diamines, including 4,4'-oxydiphthalic anhydride (ODPA), bisphenol-A-dianhydride (BPADA), 2,2-bis(4-[4-aminophenoxyl]phenyl)propane (BAPP), 4,4(-bis(3-trifluoromethyl-*p*-aminobiphenyl ether) biphenyl have been utilized to prepare block copolymers of poly(imidesiloxane).[7-14] Fluorinated poly(imide-siloxane)s show T_gs of 107 – 203 ˚C,

and a film tensile strength at break of 24 - 75 MPa, depending on the siloxane loading. The elongation at break of the block copolymers ranges from 24 to 144%, with the increase in siloxane loading.[9] Block copolymers based on PDMS and aromatic amides were first developed by Yoshio Imai *et al*.[15] The mechanical properties also shows a dependence on the PDMS concentration. The final block copolymers behave as rubber-toughened aramid plastics, having tensile strength and fracture elongation of 60 MPa and 9%, respectively at low PDMS loading. With higher PDMS contents introduced, the materials are analogous to thermoplastic elastomers, showing tensile strength and fracture elongation of up to 6 MPa and 140%, respectively.[15] In further studies, an extensive range of properties of this set of material, like phase behavior, tensile properties, thermo-mechanical properties, thermal stability, bio-compatibility, gel permeability, was studied.[16-28] The synthesis and properties of block copolymers based on hexafluoroisopropylidene bisphenol poly(arylene ether sulfone) and PDMS have also been reported by Turner *et al.*[29] A similar structure-properties relationship was reported. The highest and lowest tensile strength of the block copolymers are 23 and 8 MPa, respectively. However, in all the cases reported, none of them exhibited the expected real high mechanical performance (> 80 MPa). The mechanical properties of the material are somehow compromised by the soft region and weakened by phase separation.[4]

In Chapter 4, the synthesis and molecular characterization of the block copolymers from all-aromatic maleimide end-capped polyesters (LC-5K and AM-5K) and thiol-functionalized PDMS (-1K, -5K and -10K) are discussed, as shown in Figure 5.1. In this Chapter we will report on the morphological, thermal and mechanical properties of the block copolymers. The temperature dependent mechanical performance of LC5K-*b*-PDMS5K and AM5K-*b*-PDMS5K are also presented.

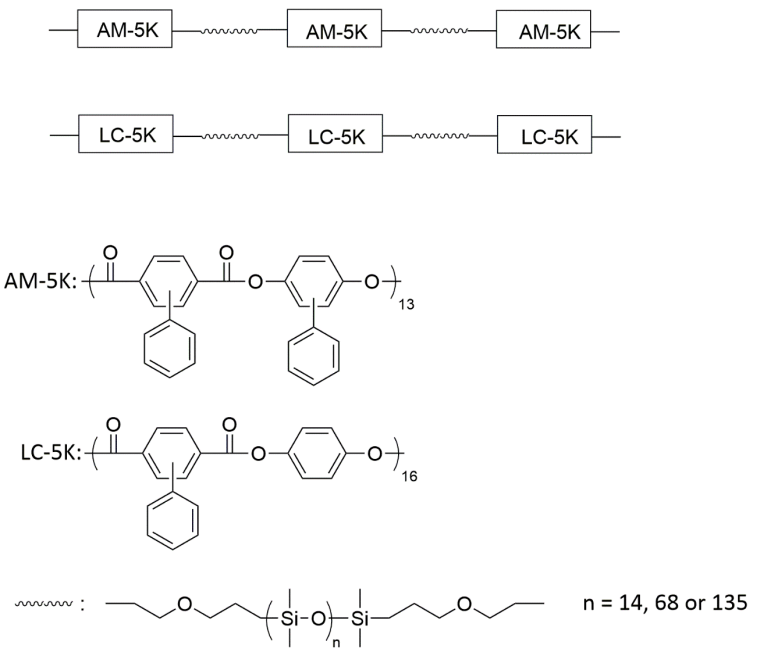

Fig. 5.1. Schematic representation of the molecular composition of the multiblock copolymers under investigation (the AM5K-*b*-PDMS series and LC5K-*b*-PDMS series). The multiblock copolymers are labeled as AM5K-*b*-PDMS1K, AM5K-*b*-PDMS5K, AM5K-*b*-PDMS10K, and LC5K-*b*-PDMS1K, LC5K-*b*-PDMS5K, LC5K-*b*-PDMS10K.

5.2 Experimental

5.2.1 Materials

The block copolymers used here were prepared as described in Chapter 4. All other chemicals were obtained from the indicated sources and used as received. 1,1,2,2-tetrachloroethane (98.5%, TCE), tetrahydrofuran (99%, THF), dimethylformamide (99%, DMF), anhydrous N-Methyl-2-pyrrolidone (99.5%, NMP) were all purchased from Acros Organics. Chloroform (95%, $CHCl_3$) was obtained from VWR international BV.

Commercial polymers polyetheretherketone (PEEK, TenCate Cetex® TC1200), polyetherimide (PEI, TenCate Cetex® TC1000) and polyphenylenesulfide (PPS, TenCate Cetex® TC1100) are purchased from Koninklijke Ten Cate NV. Thin films (~0.2 mm thickness) were prepared by stacking three layers of as-purchased

0.08 mm-thick neat polymer film in a hot platen press at a pre-determined temperature and 2 MPa for 10 min. The processing temperature used to prepare PEI, PPS and PEEK films are 250, 260 and 320 ˚C.

5.2.2 Characterization

Differential scanning calorimetry (DSC)

The transition temperatures of the block copolymers were determined by DSC using a Perkin Elmer DSC 8000 with a heating rate of 40 °C·min^{-1} under helium atmosphere.

X-ray diffraction (XRD)

X-ray diffraction (XRD) analysis was conducted on a PANalytical X'pert Pro PW3040/60 diffractometer, using a Cu-K_α radiation source. Data was collected in an angular 2Θ range of 4 - 40˚ at a rate of 2˚·min^{-1} and a step size of 0.008˚.

Transmission electron microscopy (TEM)

Transmission electron microscopy (TEM) was performed using a Jeol 100CX and operating at 80 kV at room temperature. All of the samples were prepared by cryo microtome using a Leica UT7/UTC at -80 ˚C, and transferred onto a copper grid.

Tensile tests

An Instron 3365 universal tensile machine with a 1 kN force cell was used to investigate the stress-strain behavior of the thin polymer films. Tensile tests were performed by fixing the films with an adhesive onto a rectangular frame with the side arms cut. The specimens have dimensions of approximately 50 mm × 5 mm × 0.2 mm. All experiments were performed at room temperature at a strain rate of 0.1 mm/mm·min^{-1}. The data is reported as an average of 5 samples. The elastic modulus was measured by calculating the slope of the stress-strain curve between 0.1% and 0.3% strain.

The temperature dependent tensile test was also performed on an Instron 3365 universal tensile machine with a 1 kN force cell, with the same specimen dimensions and strain rate. The testing temperatures other than room temperature were controlled by an Instron 3119-506 environmental chamber, which was cooled by liquid nitrogen.

SEM

The fracture surfaces of the tested films after stretching was studied by a high-resolution JEOL scanning electron microscope (HR-SEM) operating at 5 kV. The facture surfaces of the samples were sputtered with gold and the electron beam was focused on the fracture surface along the stretching axis.

The details of the remaining characterization techniques (solubility test, thermogravimetric analysis, polarized optical microscope, dynamic mechanical analysis) are the same as reported in Chapter 3.

5.2.3 Film preparation

All AM5K-*b*-PDMS block copolymers (amorphous) thin films were prepared by casting a ~10 %w/v solution of copolymers in chloroform, filtered through a PTFE syringe filter (pore size: 5 µm), in a level 8 cm diameter petri dish. The solvent was allowed to evaporate slowly at 30 °C in an oven overnight. When most of the solvent was removed, the transparent film that was obtained was dried at 100 °C under vacuum for 2 h, to remove residual solvent. Due to the different solubility, the thin films from LC5K-*b*-PDMS block copolymers were prepared via a similar fashion, but TCE was used as the solvent. The filtered solution was dried in oven at 60 °C overnight and the possible residual solvent was removed by drying at 150 °C under vacuum for 2h. All the freestanding films were obtained after soaking the petri dish in lukewarm water. Figure 5.2 shows the freestanding films of the block copolymers.

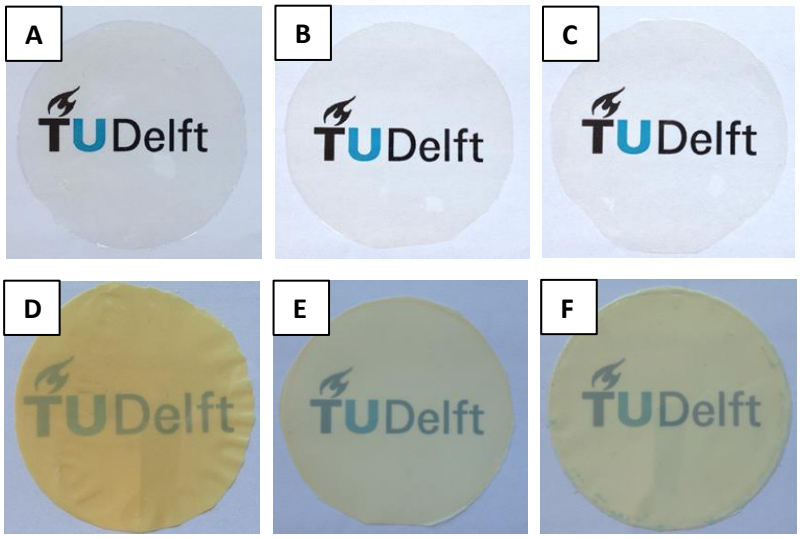

Fig. 5.2. Freestanding films of all 6 block copolymers. ***A***- AM5K-*b*-PDMS1K; ***B***- AM5K-*b*-PDMS5K; ***C***- AM5K-*b*-PDMS10K; ***D***- LC5K-*b*-PDMS1K; ***E***- LC5K-*b*-PDMS5K; ***F***- LC5K-*b*-PDMS10K. Films' diameter: 8 cm, thickness: ~50 μm.

5.3 Results and Discussion

5.3.1 Solubility test

The effects of different contents of PDMS blocks on the solubility of the block copolymers are summarized in Table 5.1. Following the same trend observed in Chapter 3, the AM block copolymers with PDMS blocks show good solubility in most of the tested solvents. Due to the high PDMS content (70%), AM-5K-*b*-PDMS10K is not soluble in DMF and NMP.[30] The LC analogues are only soluble in TCE at temperatures above 60 °C. Compared to the LC-5K oligomer, no significant improvement in solubility in either chloroform or THF was achieved by introducing a PDMS block. As all the AM block copolymers are soluble in chloroform, this solvent was chosen as the processing solvent for the reason of ease of processing. Since LC block copolymers are soluble only in TCE, this solvent was used as the solvent for film casting.

Table 5.1. Solubility of block copolymers in several common solvents.

Samples	$CHCl_3$	THF	TCE	DMF	NMP
AM-5K-*b*-PDMS1K	++	++	++	++	++
AM-5K-*b*-PDMS5K	++	++	++	+-	+-
AM-5K-*b*-PDMS10K	++	++	++	--	--
LC5K-*b*-PDMS1K	--	--	+-	--	--
LC5K-*b*-PDMS5K	--	--	+-	--	--
LC5K-*b*-PDMS10K	--	--	+-	--	--

Solubility test were conducted by dissolving film samples (~10 mg) in the different solvents.

++: soluble at room temperature,

+-: soluble at elevated temperature (60 °C for $CHCl_3$, 65 °C for THF, 140 °C for TCE, 180 °C for DMF and 200 °C for NMP, close to their boiling temperature),

--: insoluble or partly soluble at high temperature.

5.3.2 Dynamic thermogravimetric analysis

The thermal stability of the $(AB)_n$ block copolymers was evaluated using dynamic thermogravimetric analysis (TGA) at a heating rate of 10 °C·min^{-1}. The TGA thermograms of the block copolymers are shown in Figure 5.3, and $T_d^{5\%}$ and char yields are summarized in Table 5.2.

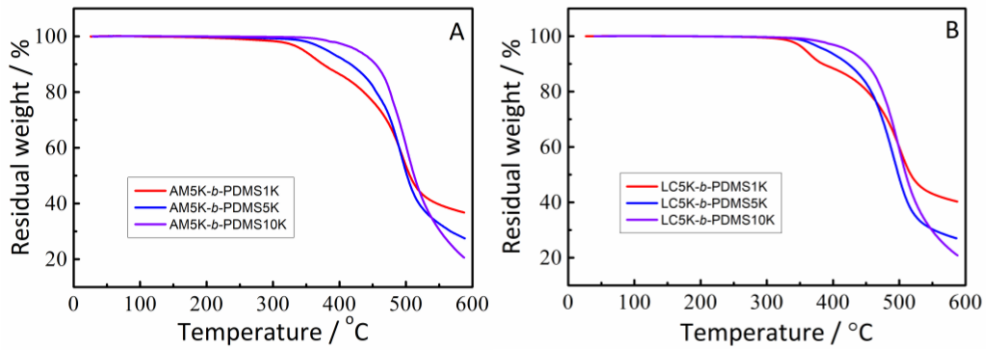

Fig. 5.3. TGA thermograms of the $(AB)_n$ block copolymers recorded under nitrogen atmosphere with a heating rate of 10 °C·min^{-1}.

With the introduction of PDMS segments, the thermal stability of the block copolymers slightly decreased, depending on the molecular weight of the PDMS blocks. The PDMS blocks have short aliphatic chains at the link with the aromatic block, which is the weak point in the block copolymers and will thermally degrade first during heating. This is reflected in both series where the polymers with most of these links (PDMS 1K) will decompose first, in the order of PDMS 1K, PDMS 5K, PDMS 10K. The char yield follows the trend in PDMS contents as well, where the polymers

with lower PDMS loading have a higher char yield at 600 °C, due to the fact that PDMS is fully pyrolyzed at 600 °C.[31]

Table 5.2. Summary of thermal stability collected by TGA experiment and glass transition temperatures revealed by DSC measurements.

Sample	*TGA*[a]		*DSC*	
	$T_d^{5\%}$ *(°C)*	*Char yield (wt%)*	T_g[b] *(°C)*	T_g[c] *(°C)*
AM5K-*b*-PDMS1K	346	37	-	120
AM5K-*b*-PDMS5K	381	28	-129	120
AM5K-*b*-PDMS10K	427	20	-124	124
LC5K-*b*-PDMS1K	358	40	-	-
LC5K-*b*-PDMS5K	390	27	-128	-
LC5K-*b*-PDMS10K	423	21	-119	-

[a] $T_d^{5\%}$ represents the 5% weight loss under nitrogen at a heating rate of 10 ˚C·min^{-1}, *Char yield* is defined as the residual weight at 600 ˚C under nitrogen atmosphere;

[b] Glass transition of PDMS blocks at a heating rate of 40 ˚C·min^{-1}, under a helium atmosphere;

[c] Glass transition of aromatic blocks at a heating rate of 40 ˚C·min^{-1}, under a helium atmosphere.

5.3.3 Transitions of the block copolymers

As discussed in Chapter 3, the LC-5K reactive oligomer shows a broad nematic window from 295 to 400 °C (the decomposition temperature). The liquid crystalline behavior of the block copolymers was investigated with respect to the molecular weight of PDMS blocks using polarized optical microscope with cross polarizers. With

the introduction of PDMS blocks, the liquid crystalline window was maintained and the crystal to nematic transition temperatures ($T_{K\text{-}N}$) of LC5K-*b*-PDMS1K, 5K and 10K are hardly affected and are all at around 270 °C. Upon further heating, the block copolymers show a nematic to isotropic transition ($T_{N\text{-}I}$) at 390 °C, which is close to the $T_d^{5\%}$. It is somewhat remarkable to observe liquid crystalline behavior in LC5K-*b*-PDMS10K with the LC segment content as low as 30 wt%. All AM block copolymers from AM-5K oligomer and PDMS segments show isotropic phase behavior as a function of temperature. The microphotographs of the liquid crystalline and amorphous multiblock copolymer are shown in Figure 5.4.

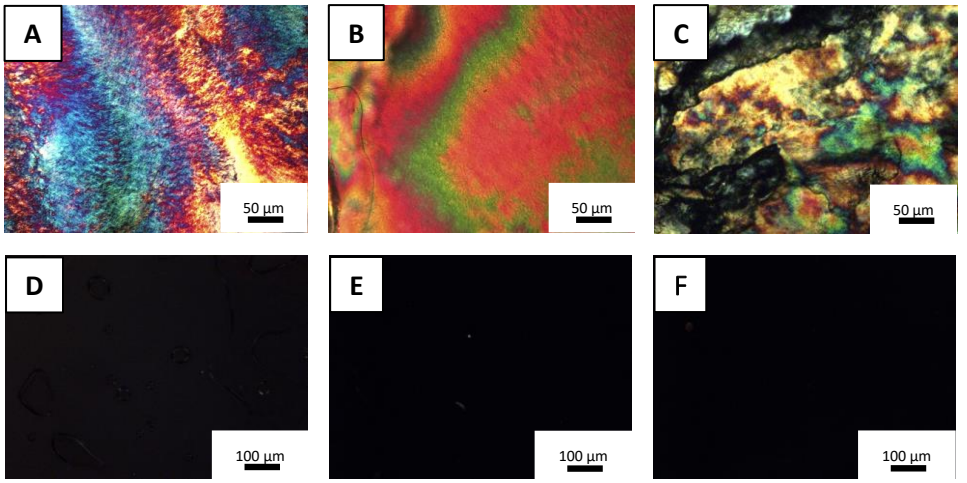

Fig. 5.4. Microphotographs of the $(AB)_n$ multiblock copolymers observed between cross polarizers at 300 °C at a heating rate of 20 °C·min^{-1}. ***A-*** LC5K-*b*-PDMS1K; ***B-*** LC5K-*b*-PDMS5K; ***C-*** LC5K-*b*-PDMS10K; ***D-*** AM5K-*b*-PDMS1K; ***E-*** AM5K-*b*-PDMS1K; ***F-*** AM5K-*b*-PDMS10K.

Differential scanning calorimetry (DSC) experiments were carried out to record the glass transition temperatures of the $(AB)_n$ multiblock copolymers. As discussed in Chapter 3, LC-5K shows a $T_{K\text{-}N}$ at 280 °C, while the AM-5K exhibited a glass transition temperature at 131 °C, with no additional thermal transitions. The DSC curves of the block copolymers are shown in Figure 5.5 and the results are summarized in Table 5.2. The PDMS oligomers, show T_gs at approximately -120 °C. This value is reflected in the AM5K-*b*-PDMS5K and -PDMS10K. Here, two glass transitions, originating from the PDMS segment (around -120 °C) and the all-

aromatic block are observed, indicating the presence of a (micro)phase separated system. In contrast, the DSC curve of AM5K-*b*-PDMS1K shows only one T_g, possibly as a result of the short PDMS segments.

Similarly, the T_gs of the PDMS blocks are clearly discernable in the DSC curves collected from the LC5K-*b*-PDMS5K and -PDMS10K samples, while that of the LC5K-*b*-PDMS1K shows no clear T_g. The glass transition of the LC segment is hardly observed, since glass transitions are only displayed by amorphous regions. Similar to literature reports[32], the DSC curves of the block copolymers of both AM5K-*b*-PDMS10K and LC5K-*b*-PDMS10K show crystallization and melting peaks of the PDMS blocks at -82 and -48, -85 and -48 °C, respectively.

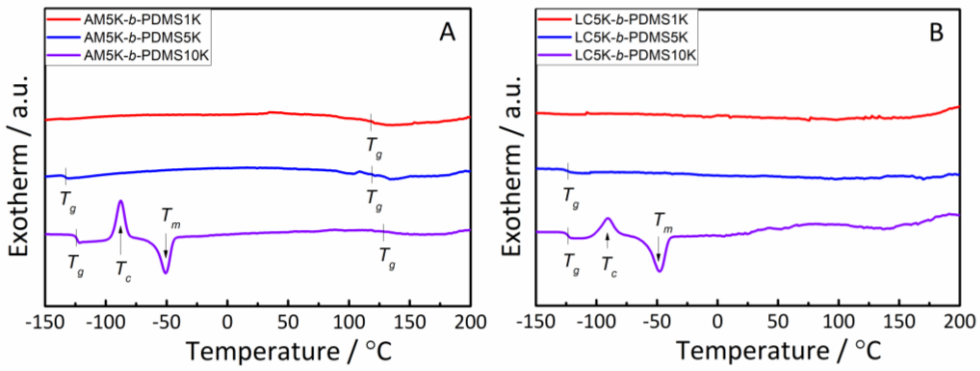

Fig. 5.5. DSC curves of the $(AB)_n$ block copolymers. In the graphs the glass transitions (T_gs) are marked with a vertical bar. ***A-*** AM5K-*b*-PDMS series; ***B-*** LC5K-*b*-PDMS series. All of the data was collected from the first heating cycle at a heating rate of 40 °C·min^{-1} of as-prepared samples under a helium atmosphere. The graphs are offset for clarity.

5.3.4 Thermo-mechanical properties

DMTA experiments were performed on all the casted films from the $(AB)_n$ multiblock copolymers, to study the storage modulus (E') and loss modulus (E") as a function of the temperature, as shown in Figure 5.6. Table 5.3 summarizes the DMTA results.

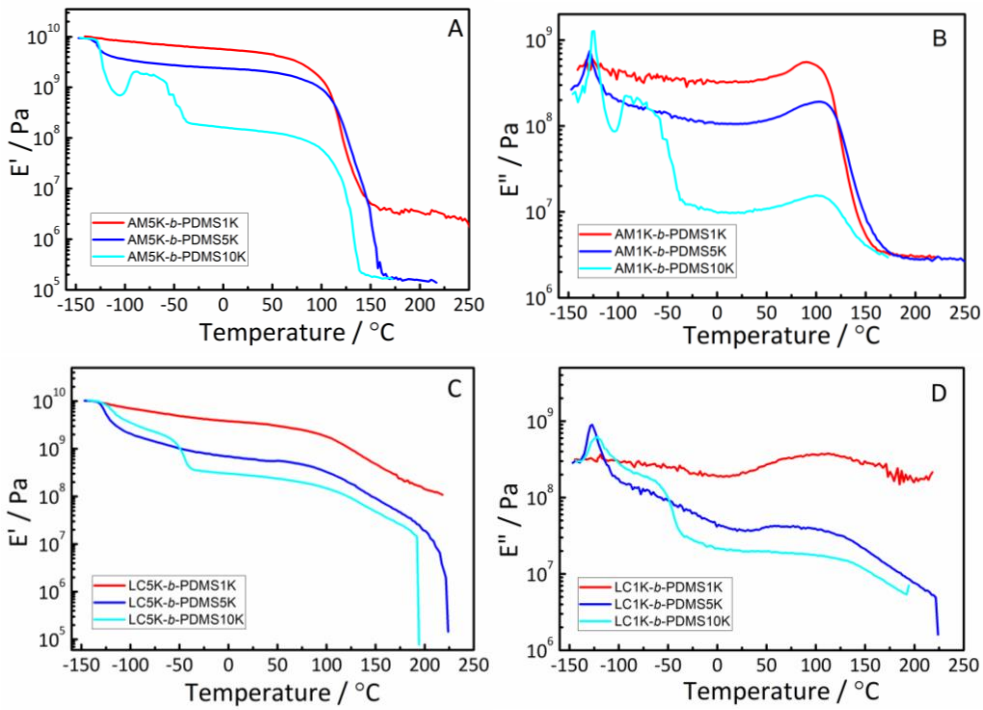

Fig. 5.6. DMTA analysis of the multiblock copolymers. ***A-*** and ***C-*** Storage modulus (E') as a function of temperature for the AM5K-*b*-PDMS series and LC5K-*b*-PDMS series, respectively; ***B-*** and ***D-*** loss modulus (E") as function of temperature for the AM5K-*b*-PDMS series and LC5K-*b*-PDMS series, respectively. All analyses were conducted using a heating rate of 2 ˚C·min^{-1} under N_2 atmosphere and at a frequency of 1 Hz.

The AM series of the $(AB)_n$ multiblock copolymers shows similar storage moduli at -150 °C, at approximately 10 GPa (Figure 5.6), indicating the hard nature of the block copolymer at low temperatures. The storage moduli are hardly affected by the block copolymer compositions at temperatures below T_g of PDMS. No obvious decrease in modulus at around -125 ˚C was observed for AM5K-*b*-PDMS1K, indicative of the low PDMS content. The drop in E' of AM5K-*b*-PDMS5K and AM5K-PDMS10K was at the same temperature, but much larger. The T_gs of the aromatic blocks of the three AM multiblock copolymers was observed at approximately 100 ˚C. Between the two T_gs, a stable plateau was observed, characteristic of thermoplastic elastomers (TPEs).[33] The AM5K-*b*-PDMS10K film exhibited a cold crystallization of PDMS when the film was heated above the T_g of the PDMS segments, at -89 ˚C.

Subsequent heating induced melting of the formed PDMS crystals, as was also observed in the DSC experiments.

For the LC5K-*b*-PDMS multiblock copolymer series, similar results were obtained in the DMTA tests. Only one T_g originated from the rigid block was observed for LC5K-*b*-PMDS1K, due the very low content of PDMS. LC5K-*b*-PDMS5K shows two obvious T_gs, again indicative of (micro)phase separation.[5, 6, 33] The curve of LC5K-*b*-PDMS10K appears to exhibit three T_gs, however, the transition at ~ -50 ˚C is attributed to the melting of the PDMS crystals, as confirmed by our DSC results.

It is remarkable to observe that the storage moduli of AM5K-*b*-PDMS multiblock copolymers are superior to those of the LC 5K-*b*-PDMS analogs. This is likely due to the intermixing of the two blocks in the block copolymers. The degree of intermixing in phase-separated multiblock copolymers depends in part on the flexibility of the segments. The block copolymers combining two amorphous phases typically show a higher degree of intermixing between the phases than those with based on amorphous/nematic phases.[4] By a larger degree of mixing, the properties of the aromatic (stiff) units are better distributed in the material, resulting in bulk properties resembling a mixed character of the two constituents.

Table 5.3. Summary of thermo-mechanical properties collected from DMTA analysis.

Samples	*E' (GPa)*[a] *(25 °C)*	*E' (GPa)*[a] *(100 °C)*	T_g[b] *(°C)*
AM5K-*b*-PDMS1K	5.2	1.4	96
AM5K-*b*-PDMS5K	2.3	0.9	-127, 102
AM5K-*b*-PDMS10K	1.5	0.06	-126, 103
LC5K-*b*-PDMS1K	3.5	1.8	112
LC5K-*b*-PDMS5K	0.6	0.3	-127, 112
LC5K-*b*-PDMS10K	0.3	0.1	-124, 115

[a] Storage modulus (E') collected by DMTA at 1Hz, using a heating rate of 2 ˚C·min^{-1}.

[b] Glass transition temperature (T_g) reported as the maximum of loss modulus (E") at 1 Hz.

5.3.5 WAXD analysis of multiblock copolymers

The morphology of the aromatic/PDMS multiblock copolymer films was analyzed by room temperature WAXD experiments and the results are shown in Figure 5.7.

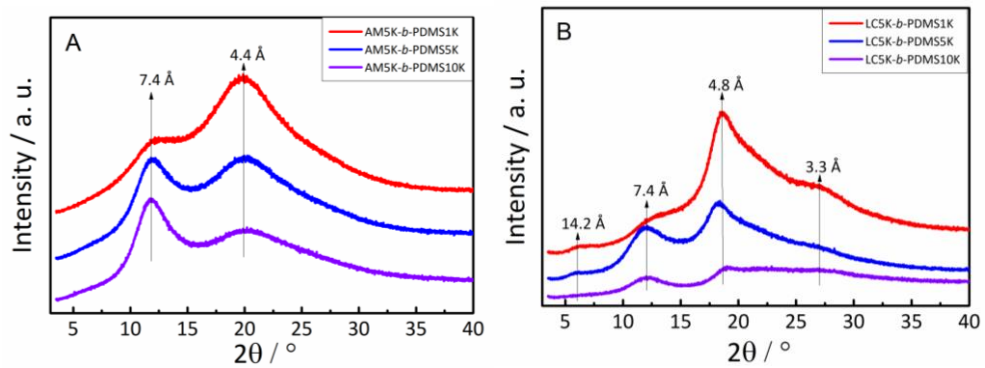

Fig. 5.7. WAXD analysis of the AM and LC block copolymers. 1-dimensional WAXD diffraction intensity profiles of ***A-*** AM multiblock copolymer films, and ***B-*** LC multiblock copolymer films at room temperature. The curves are offset for clarity.

From the one-dimensional X-ray diffraction intensity profiles of the AM multiblock copolymers in Figure 5.7A, the intense diffraction peak at 2Θ = 12° corresponds to the original d-spacing (d = 7.4 Å) of the PDMS tetragonal crystal lattice.[34] The characteristic peak at 2Θ = 20° of amorphous polymers is attributed to the inter-chain d-spacing (d = 4.4 Å), a value similar to the interchain spacing of 4.6 Å as observed for liquid crystalline co-poly(HBA/HNA).[35, 36]

Similar to the AM multiblock copolymer, LC multiblock copolymer films show an intense diffraction peak at 2Θ = 12° (d = 7.4 Å) of the PDMS tetragonal crystal lattice, see Figure 5.7B. The intense diffraction peak at 2Θ = 18° (d = 4.8 Å) is again attributed to the interchain d-spacing, similar to the AM series. The diffraction peak located at 2Θ = 6.2° (d = 14.2 Å) is associated with the projection length of one repeating unit in the crystalline unit cell. The reflection at around 27° is ascribed to d_{310}, as reported in literature.[35]

The existence of distinct diffraction peaks for PDMS and the aromatic domains again indicates (micro)phase separation, as was also observed in DMTA and DSC experiments.

5.3.6 Morphology

As confirmed by DSC, DMTA and WAXD experiments, (micro)phase separation might occur in this type of aromatic/PDMS multiblock copolymers. Figure 5.8 shows the transmission electron micrographs of ultrathin sections of the AM5K-*b*-PDMS and LC5K-*b*-PDMS multiblock copolymers prepared by cryo-microtome. Due to the high electron density of PDMS compared to the aromatic polyester, no staining is needed and the black and white areas indicate a PDMS-rich and an ester-rich domain, respectively.[37]

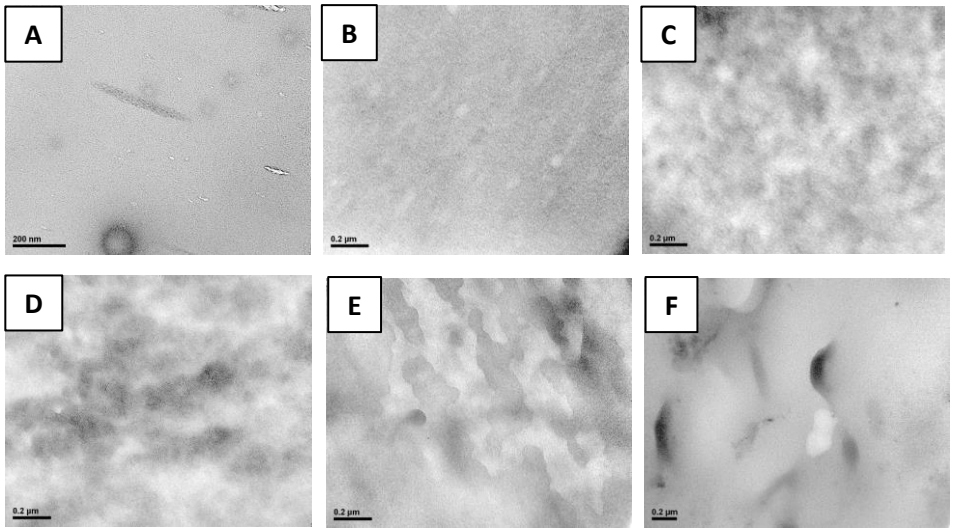

Fig. 5.8. Cryo-TEM images of the multiblock copolymers. ***A-*** AM5K-*b*-PDMS1K; ***B-*** AM5K-*b*-PDMS5K; ***C-*** AM5K-*b*-PDMS10K; ***D-*** LC5K-*b*-PDMS1K; ***E-*** LC5K-*b*-PDMS1K; ***F-*** AM5K-*b*-PDMS10K.

In the TEM microphotographs of the AM5K-*b*-PDMS multiblock copolymers, the microphase separation is much harder to observe than in the LC5K-*b*-PDMS multiblock copolymers. No obvious phase separation was observed for AM5K-*b*-PDMS1K, while in AM5K-*b*-PDMS5K, a blurred micro-phase separation, with domains

in the order of ~50 nm, can be seen. A somewhat larger feature size (~100 nm) is observed for AM5K-*b*-PDMS10K, although the image is highly blurred. In the LC5K-*b*-PDMS series, LC5-*b*-PDMS5K shows a solid proof of phase separation with elongated contours, with clear lines indicating the phase boundaries. The LC5K-*b*-PDMS1K and 10K do not show clear phase separation edges.

It was reported by Pospiech and colleagues that block copolymer systems combining two different amorphous phases typically show a high degree of intermixing between the phases, while in the systems of an amorphous phase and an nematic phase, less intermixing is observed.[4] Compared to the high intermixing of AM5K and PDMS domains, the LC5K and PDMS should have a higher degree of phase separation, as shown in the examples of AM5K-*b*-PDMS5K and LC5K-*b*-PDMS5K.

5.3.7 Tensile properties at room temperature

The tensile behavior of the thin films tested at around 22 ˚C is shown in Figure 5.9, 5.10 and 5.11. Prior to film casting, a filtration of the casting solution over a 5 µm syringe filter was performed to remove insoluble particulates and to avoid any irregularities in the resulting films. The films are flexible and easy to handle, and can be cut into test specimen without difficulty. The best tensile properties of the as-prepared films out of 5 experiments are shown in Figure 5.9.

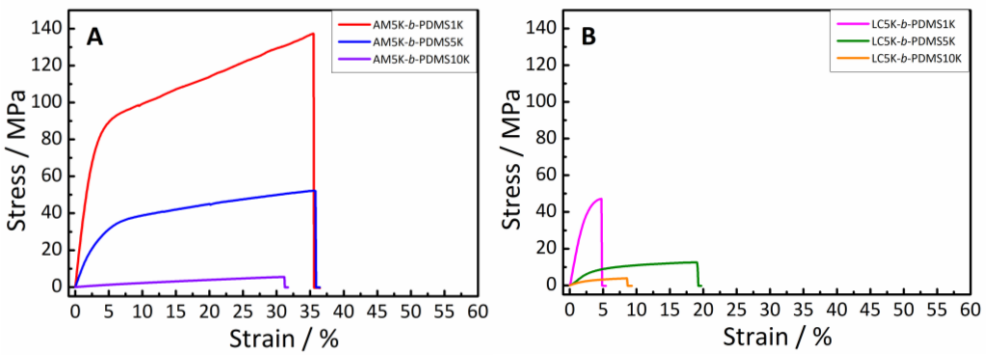

Fig. 5.9. Room temperature stress-strain curves of multiblock copolymers. ***A***- AM5K-*b*-PDMS and ***B***- LC5K-*b*-PDMS multiblock copolymers. Shown are the best results out of 5 stress-strain experiments. All experiments were performed at a strain rate of 0.1 mm/mm·min^{-1}.

Overall, the tensile properties of the thin films are highly dependent on the PDMS chain length (associated with PDMS contents) in the multiblock copolymers. With the increase in PDMS content, the tensile strength and modulus of the multiblock copolymers decrease dramatically. Take the AM5K-*b*-PDMS series as an example, a significant drop in both tensile strength and tensile modulus is observed by increasing the PDMS chain length from 1K to 10K. The fracture elongation stays similar with the variation of PDMS segments, which is rather remarkable. In the case of LC5K-*b*-PDMS analogs, a similar trend in tensile properties *vs* PDMS contents is observed. Similar structure-tensile property relationships were reported in several other multiblock copolymers, such as polysulfone-*b*-PDMS, polyamide-*b*-PDMS, polyether-*b*-polyamide, polybutadiene-*b*-polyamide.[15, 21, 28, 29, 38, 39] The stress-strain behavior of the AM5K-based multiblock copolymer films is much better than the LC5K-based films. Notable, the AM5K-*b*-PDMS1K film shows a very high mechanical tensile strength and elastic modulus in the test.

Since the mechanical performance of polymer materials are highly dependent on the testing conditions, a comparison of the tensile behavior with some commercial high-performance polymer films was made under the same testing parameters. Figure 5.10 shows the best performing data out of 5 tensile experiments of PEEK (TenCate Cetex® TC1200), PEI (TenCate Cetex® TC1000) and PPS (TenCate Cetex® TC1100) films, as well a AM5K-*b*-PDMS1K film. It is clear that the AM5K-*b*-PDMS1K film shows the highest tensile strength and elastic modulus, with a high elongation at break (~ 35%). The PEEK film shows a high fracture elongation (~ 130%) due to necking.

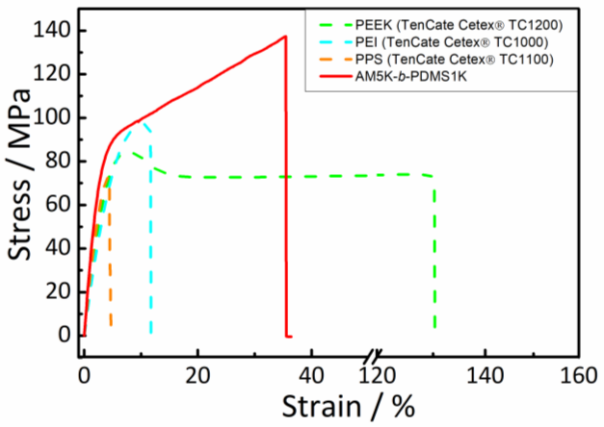

Fig. 5.10. Comparing the tensile properties of a AM5K-*b*-PDMS1K film with commercial high-performance polymer films, *i.e.,* PEEK (TenCate Cetex® TC1200), PEI (TenCate Cetex® TC1000) and PPS (TenCate Cetex® TC1100).

Figure 5.11 shows the average data of the tensile strength (***A***), elastic modulus (***B***), elongation at break (***C***) and toughness (***D***) of the as-prepared AM5K-based and LC5K-based films of 5 experiments, as well as the commercial polymer films.

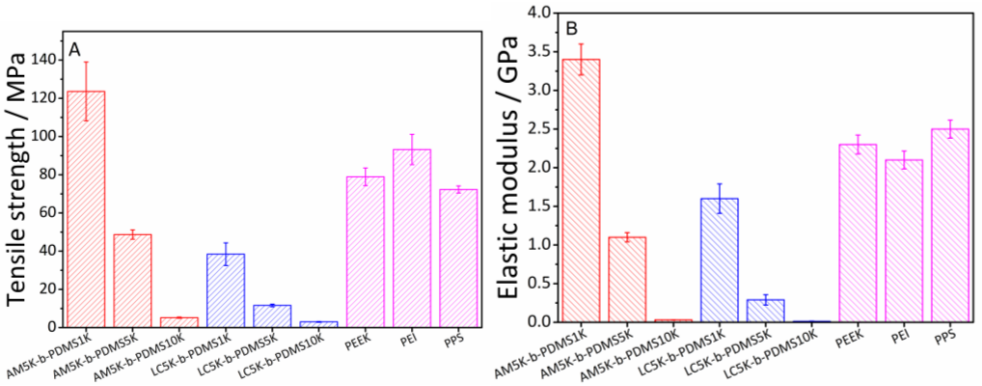

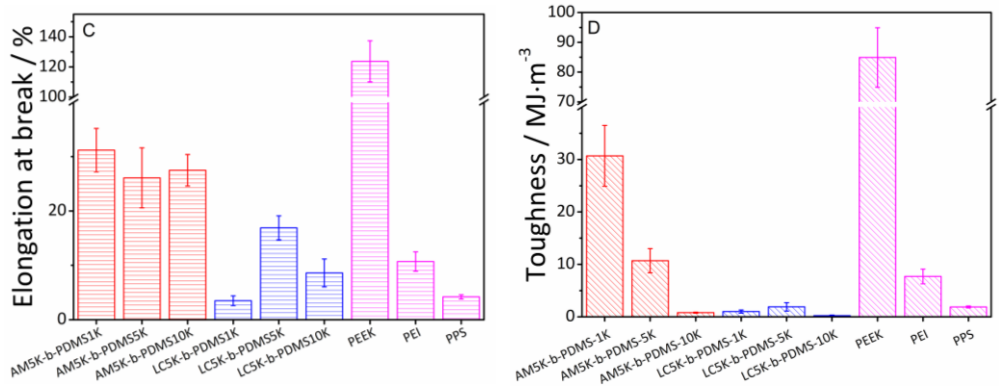

Fig. 5.11. Average data (including error bars) of tensile properties of 5 specimens of block copolymers and commercial polymers. ***A*-** Tensile strength; ***B*-** Elastic modulus; ***C*-** Elongation at break; ***D***- toughness.

Over the whole composition range, the AM5K-*b*-PDMS block copolymer films show average tensile strength and elastic moduli ranging from 5.2 to 123.6 MPa and 0.031 to 3.4 GPa, respectively. In sharp contrast, the LC5K-*b*-PDMS series shows much-lowered average tensile data. The LC5K-*b*-PDMS1K displays an average tensile strength and elastic modulus of 38.4 MPa and 1.6 GPa, respectively. With the PDMS chain length increasing to 10K, the LC5K-*b*-PDMS10K shows an average tensile strength and elastic modulus of 0.29 and 0.013 GPa, respectively. It is also clear that the hard segments have a great effect on the tensile properties of the block copolymer films. In general, the AM5K-based multiblock copolymers show superior mechanical properties (elastic moduli, tensile strength, fracture strain and toughness) over their LC5K-based analogs. Take AM5K-*b*-PDMS1K and LC5K-*b*-PDMS1K as examples, the tensile strength is 123.6 and 38.4 MPa, respectively, and the elastic moduli are 3.4 and 1.6 GPa, respectively. Besides, the AM5K-*b*-PDMS1K film exhibits a much higher fracture elongation (32%) and toughness (30.7 $MJ \cdot m^{-3}$) than those of LC5K-*b*-PDMS1K (5% and 1 $MJ \cdot m^{-3}$, respectively). This is because the LC5K-based multiblock copolymers have a higher degree of microphase separation, as revealed by TEM results in Figure 5.8. Typically, a non-phase separated multiblock copolymer show higher modulus than their phase separated analogs.[40, 41] The higher mechanical properties of the AM5K-*b*-PDMS1K are due to a higher degree of phase intermixing, as depicted in Figure 5.8.

The AM5K-*b*-PDMS1K shows excellent mechanical properties, with best tensile strength/elastic modulus/elongation/toughness at break of 137

MPa/35%/3.7 GPa/ 38 MJ·m^{-3} out of 5 tensile experiments. The results are found to be much higher than those of PDMS-based high-performance multiblock copolymers reported in the literature.[15, 21, 28] It is also obvious that AM5K-*b*-PDMS1K shows superior mechanical properties, with respect to tensile strength/elastic modulus/fracture elongation/toughness, over commercially available high-performance polymers such as PEI and PPS. Even through PEEK shows a higher elongation at break and toughness (130% and 85 MJ·m^{-3}) due to necking, the AM5K-*b*-PDMS1K film performs better in terms of tensile strength and elastic modulus, with a value of 125 MPa and 3.4 GPa, respectively.

The SEM analysis of the fracture surfaces of the best performing samples reveals highly different fracture behavior of the different samples, as shown in Figure 5.12, which also (in part) explains the difference in observed tensile properties.

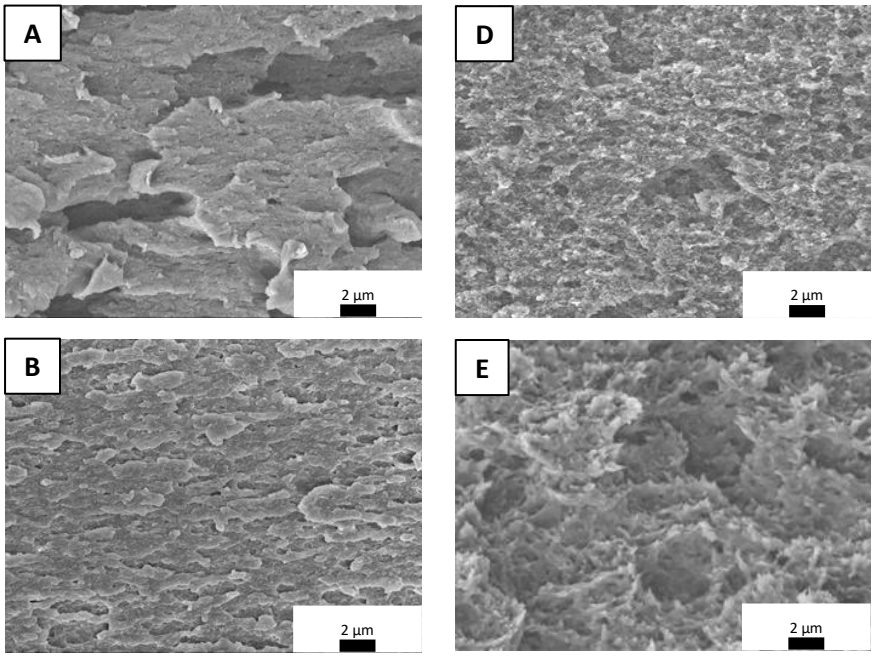

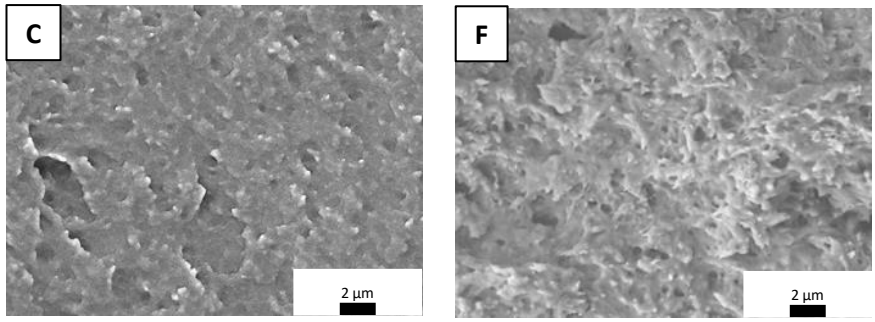

Fig. 5.12. SEM images of the fracture surface of ***A-*** AM5K-*b*-PDMS1K; ***B-*** AM5K-*b*-PDMS5K; ***C-*** AM5K-*b*-PDMS10K; ***D-*** LC5K-*b*-PDMS1K; ***E-*** LC5K-*b*-PDMS5K; ***F-*** LC5K-*b*-PDMS10K, along the stretching axis.

The improvement in tensile properties of AM5K-*b*-PDMS1K illustrates that the stress transfer is better in this material over its LC5K-based analogs. Comparing to the rough and block-like consolidated fracture surface of AM5K-*b*-PDMS1K (Figure 5.12***A***), the SEM image for the AM5K-*b*-PDMS5K (Figure 5.12***B***) and -PDMS10K (Figure 5.12***C***) films show smooth, poorly consolidated brittle fracture surface. In the SEM images of LC5K-*b*-PDMS series, the fracture surfaces are much rougher than the AM analogs, showing ribbon-like fracture surfaces. This is due to the lower degree of intermixing of the two components and higher degree of phase separation. The different fracture surfaces of AM5K-*b*-PDMS and LC5K-*b*-PDMS multiblock copolymers are in high consistency with the TEM observations.

5.3.8 Temperature dependent tensile test

Temperature plays an important role in the mechanical performance of high temperature elastomers. Generally, multiblock copolymers composed of a hard segment and a soft segment are elastomers with a relatively low yield stress, high fracture stress and high fracture strain. Upon heating, the modulus, yield stress, and the fracture stress decrease, while the fracture strain increases, as is usual for most polymers.[42-44] The tensile and elastic properties of TPEs are sensitive to the type, concentration and morphology of the hard phase.[1, 45]

Figure 5.13 ***A*** and ***B*** shows the temperature dependent tensile data of AM5K-*b*-PDMS5K and LC5K-*b*-PDMS5K, which was collected from tensile experiments over a temperature range of -70 to 110 °C. This temperature range was selected well between the two glass transitions of the individual blocks. The data of all

experiments are summarized in Table 5.4. The yield point is generally seen as the point of onset at which substantial plastic deformation takes place.[44, 46, 47] Below the yield point, the material deforms elastically under an applied external stress, while after the yield point, plastic deformation takes place. In order to calculate the yield point, plots of (dσ/dε) as a function of strain were made. The yield point was defined as the inflection point, as shown in Figure 5.13 ***C*** and ***D***.

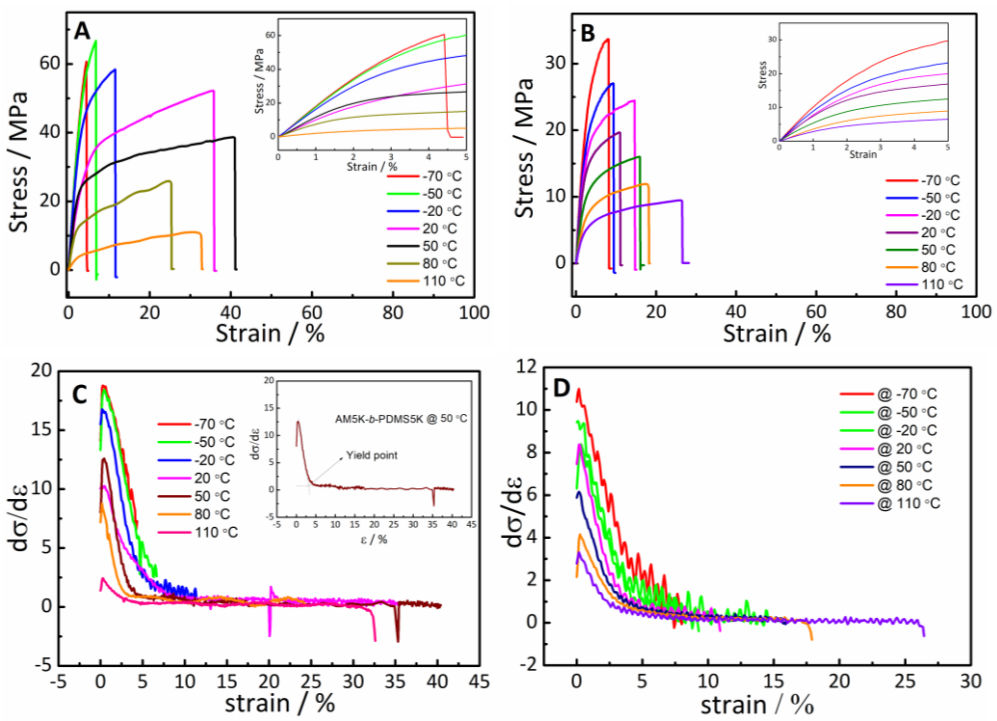

Fig. 5.13. Temperature dependent tensile test results. ***A-*** AM5K-*b*-PDMS5K and ***B-*** LC5K-*b*-PDMS5K. The insets provided in both Figures show the stress-strain curves at low strain values; ***C-*** and ***D-*** shows the stress of AM5K-*b*-PDMS5K and LC5K-*b*-PDMS5K differentiating stress with respect to strain. The inset in the ***C*** plot depicts the definition of the yield point in a stress-strain curve.

Table 5.4. Temperature dependent tensile results for AM5K-*b*-PDMS5K and LC5K-*b*-PDMS5K at various temperatures.

Samples	*T (˚C)*	*Elastic modulus (E, MPa)*	*Stress at 5% strain ($\sigma_{5\%}$ MPa)*	*Yield stress [b] (σ_y, MPa)*	*Yield strain[b] (ε_y, %)*	*Fracture stress (σ_b, MPa)*	*Fracture strain (ε_b, %)*
	-70	2990	-[a]	-[c]	-[c]	60.1	4.4
	-50	2740	60.3	-[c]	-[c]	66.8	6.7
	-20	2500	48.2	46.3	4.4	58.6	11.5
AM5K-*b*-PDMS5K	20	2260	31.3	28.0	4.0	52.1	35.7
	50	1990	26.6	23.8	3.0	38.9	41.1
	80	1470	15.0	12.6	2.5	26.0	25.4
	110	542	5.1	3.5	2.1	10.8	32.7
	-70	1350	27.2	-[c]	-[c]	33.7	8.2
	-50	1010	21.5	21.5	4.0	27.0	9.4
	-20	790	18.9	18.2	3.6	24.5	14.7
LC5K-*b*-PDMS5K	20	612	16.0	15.2	3.4	19.6	11.0
	50	556	11.7	10.6	3.0	16.0	16.0
	80	449	8.3	7.2	2.8	18.2	11.2
	110	267	6.0	5.0	2.5	9.3	26.5

[a] Sample broke before 5% strain;

[b] Yield point is defined as the inflection point in plots of (dσ/dε) as a function of strain;

[c] Samples broke before yield.

Young's modulus

Figure 5.14 plots the Young's moduli as a function of temperature for AM5K-*b*-PDMS5K and LC5K-*b*-PDMS5K. In general, for both polymers the Young's moduli of decreases in a linear fashion with increasing temperature. Before T_g (~100 ˚C) of the AM5K segments in AM5K-*b*-PDMS5K, the Young's modulus of AM5K-*b*-PDMS5K decreases roughly linear. There is also a dramatically decrease of the modulus observed at 110 ˚C, this is due to the glass transition of the AM5K units. At this temperature, the polymer chains segments become sufficiently mobile. Due to the higher T_g (115 ˚C) of LC5K, the elastic modulus of LC5K-*b*-PDMS5K decrease linearly over the test temperature range.

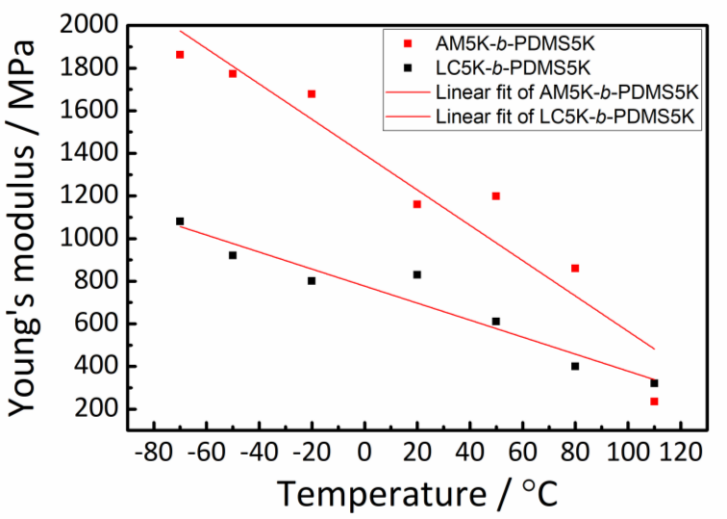

Fig. 5.14. Elastic moduli of AM5K-*b*-PDMS5K and LC5K-*b*-PDMS5K as a function of temperature, ranging from -70 to 110 °C. Both polymers show a linearly decrease in Young's modulus below their T_g.

Stress at 5%

Figure 5.15 shows the stress at 5% strain ($\sigma_{5\%}$) for both AM5K-*b*-PDMS5K and LC5K-*b*-PDMS5K at the test temperatures, and the data is summarized in Table 5.4. With the decrease in elastic modulus upon increasing the temperature from -70 to 110 ˚C, the stress at 5% strain decrease linearly and by approximately 90% and 80%

for AM5K-*b*-PDMS5K and LC5K-*b*-PDMS5K, respectively. This implies that upon increasing the temperature, the strain softening of both polymers is becoming more prominent, which makes sense as at higher temperatures the polymer chains become more mobile.

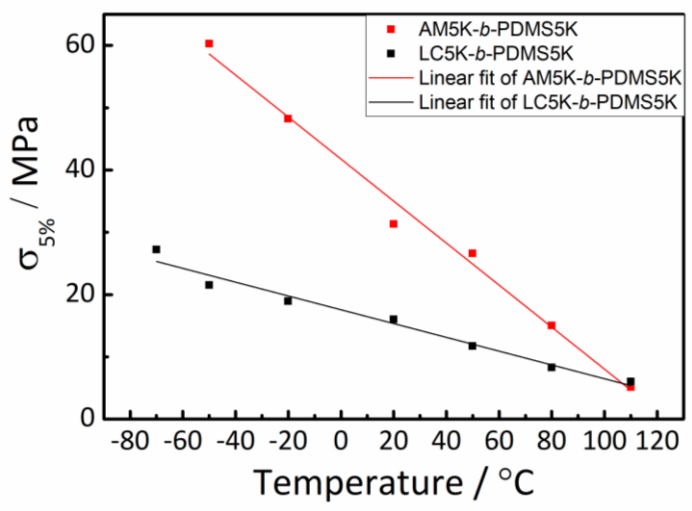

Fig. 5.15. The stress at 5% strain for AM5K-*b*-PDMS5K and LC5K-*b*-PDMS5K as a function of temperature, ranging from -70 to 110 °C.

Yield behavior

The yield point defines the limitation of mechanical loads, since it represents the upper stress limits of avoiding permanent plastic deformation. As shown in Figure 5.16 and table 5.4, the yield stress and strain of both polymers decrease linearly with increasing temperature. This again suggests strain-softening, which increased with temperature. Due to the higher temperature and hence a lower barrier for molecular mobility, the polymers deformed easier at lower applied stresses.

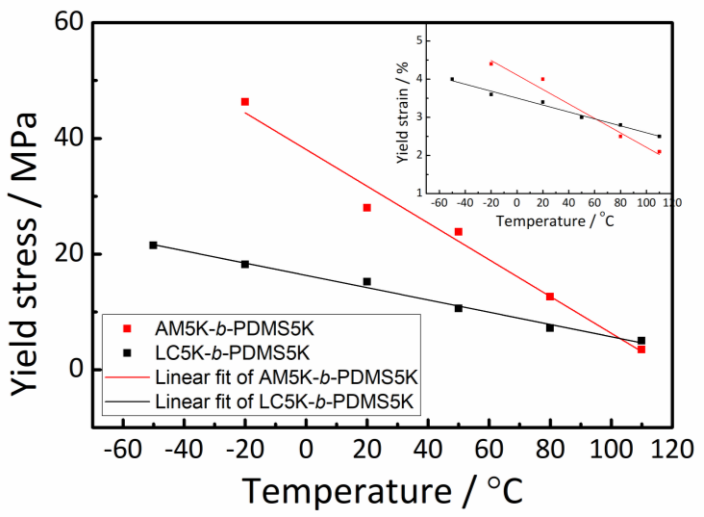

Fig. 5.16. Yield stress of AM5K-*b*-PDMS5K and LC5K-*b*-PDMS5K as a function of temperature (-70 to 110 °C). Inset shows the yield strain as a function of temperature, in the same temperature range.

The yield stress as a function of strain rate and temperature can be described by the Eyring relationship,[43, 44]

$$\frac{\sigma_y}{T} = \frac{R}{v}\left(\frac{\Delta H}{RT} + \ln\frac{2\dot{e}}{\dot{e}_0}\right) \qquad \text{eqn. 5.1}$$

Where σ_y is the yield stress, v is the activation volume, ΔH is the activation enthalpy, T is the temperature, R is the gas constant, $\dot{e}$ is the strain rate, $\dot{e}_0$ is a constant.

From equation 5.1, it is expected that a linear relationship is obtained if $\frac{\sigma_y}{T}$ is plotted as a function of the reciprocal temperature, *i.e.*, $\frac{\sigma_y}{T}$ *vs.* $\frac{1}{T}$. An Eyring plot was made for both AM5K-*b*-PDMS5K and LC5K-*b*-PDMS5K multiblock copolymers, and both of them show linear relationships, as shown in Figure 5.17. This indicates that the yield behavior can be described by this Eyring relationship.

The slope in this plot is calculated by $\frac{\Delta H}{v}$, *i.e.* the ratio of activation enthalpy to activation volume. A larger $\frac{\Delta H}{v}$ clearly indicates a higher energy barrier for yield. We observe that the slope for these two polymers are quite different, calculated to be 127 and 45 kJ·mol^{-1}·nm^{-3} for AM5K-*b*-PDMS5k and LC5K-*b*-PDMS5K, respectively.

This is most likely due to the different morphology, as we discussed above. As the amorphous rigid unit has a higher chance of intermixing with the PDMS segments. Comparing to the $\frac{\Delta H}{\nu}$ value of 64 and 60 kJ·mol^{-1}·nm^{-3} for polypropylene[48] and UHMWPE[49], that of AM5K-*b*-PDMS5K seems to be high, meaning that the polymer has more difficulty to yield.

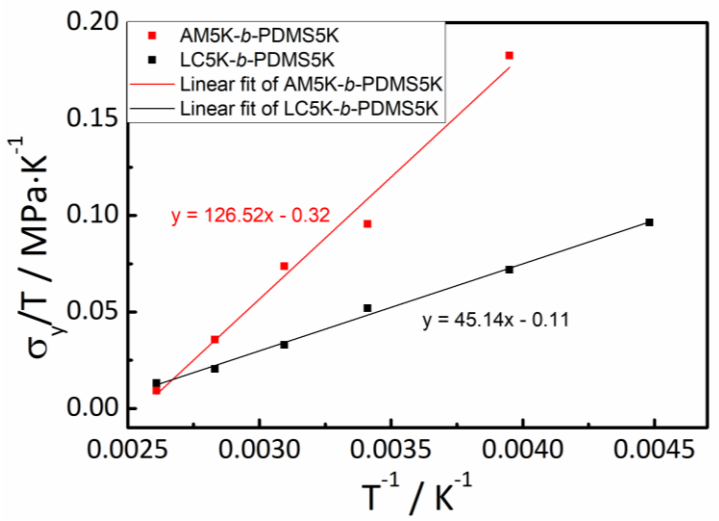

Fig. 5.17. An Eyring plot $\frac{\sigma_y}{T}$ *vs.* $\frac{1}{T}$ for AM5K-*b*-PDMS5K and LC5K-*b*-PDMS5K in the temperature range from -70 to 110 °C.

Fracture behavior

The fracture properties are very sensitive to the test temperature and specimen conditions. Typically, the fracture stress decreases with increasing temperature whereas the fracture strain increases.[43, 44, 47, 50] As depicted in Figure 5.18 and Table 5.4, generally the tensile stress decreases linearly with the increase in testing temperature, while the fracture strain only shows a non-ordered increase.

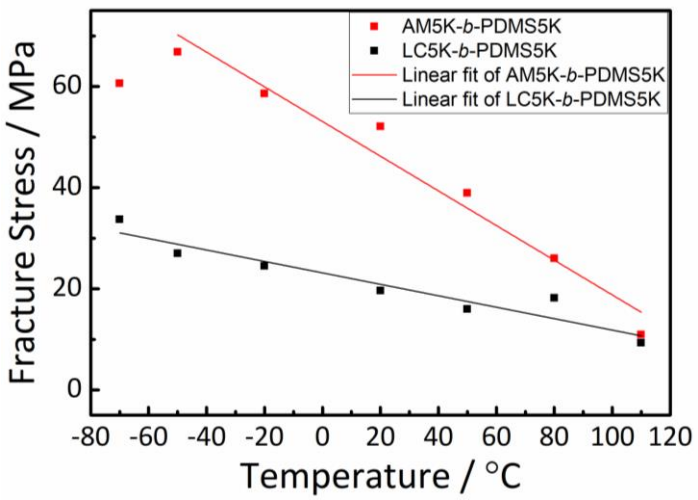

Fig. 5.18. Tensile strength of AM5K-*b*-PDMS5K and LC5K-*b*-PDMS5K as a function of temperature.

5.4 Conclusion

In this Chapter, we have presented the unique (thermo)mechanical properties of the multiblock copolymer from aromatic/PDMS units. With the introduction of PDMS segments, the amorphous ester-based multiblock copolymers show good solubility, while the liquid crystalline ester-based multiblock copolymers can only be dissolved in tetrachloroethane at elevated temperature. With the introduction of PDMS segments, a compromise of the thermal stability was observed for all multiblock copolymers, depending on the PDMS molecular weight. The multiblock copolymers show $T_d^{5\%}$ > 346 ˚C, and the char yield at 600 ˚C under nitrogen atmosphere are all higher than 20%. The AM5K-*b*-PDMS multiblock copolymers are amorphous, and the LC5K-*b*-PDMS multiblock copolymers retain their liquid crystallinity even with LC segments as low as 30 wt%. DSC and DMTA experiments confirmed that the multiblock copolymers with PDMS segments with M_n of 5K and 10K show two glass transitions, indicating the micro-phase separation, due to the incompatibility of the aromatic ester and PDMS units. However, due to the high polydispersity, the phase separation is difficult to observe by TEM. Only one T_g was observed in the samples based on PDMS-1K. In tensile test, the AM5K-*b*-PDMS multiblock copolymers show excellentmechanical properties, while the LC5K-*b*-PDMS multiblock copolymers performs much poorer. The AM5K-*b*-PDMS1K film

show outstanding tensile strength of ~125 MPa, elastic modulus of 3.4 GPa and elongation at break > 30%. The temperature dependent tensile properties of the AM/LC5K-*b*-PDMS multiblock copolymers were also studied, showing that the mechanical properties become compromised as the temperature increases. Due to the existence of two plateau regions (DMTA studies), the multiblock copolymers based on PDMS5K and 10K are expected to exhibit shape memory behavior over a 300 ˚C temperature range, i.e. from -150 to 150 ˚C.

5.5 References

1 S. Fakirov, *Handbook of Condensation Thermoplastic Elastomers*, Wiley, 2006.

2 M. W. Matsen and M. Schick, *Macromolecules*, 1994, **27**, 6761-6767.

3 S. L. Aggarwal, *Polymer*, 1976, **17**, 938-956.

4 D. Pospiech, L. Häußler, K. Eckstein, H. Komber, D. Voigt, D. Jehnichen, P. Friedel, A. Gottwald, W. Kollig and H. R. Kricheldorf, *High Perform. Polym.*, 2001, **13**, S275-S292.

5 U. Schulze and H.-W. Schmidt, *Polym. Bull.*, 1998, **40**, 159-166.

6 N. Reichelt, U. Schulze and H.-W. Schmidt, *Macromol. Chem. Phys.*, 1997, **198**, 3907-3930.

7 J. E. McGrath, D. L. Dunson, S. J. Mecham and J. L. Hedrick, in *Progress in Polyimide Chemistry I*, ed. H. R. Kricheldorf, Springer Berlin Heidelberg, Berlin, Heidelberg, 1999, pp. 61-105.

8 C. M. Mahoney, J. A. Gardella and J. C. Rosenfeld, *Macromolecules*, 2002, **35**, 5256-5266.

9 A. Ghosh and S. Banerjee, *Polym. Adv. Technol.*, 2008, **19**, 1486-1494.

10 A. Ghosh, S. K. Sen, S. Banerjee and B. Voit, *RSC Adv.*, 2012, **2**, 5900-5926.

11 A. Ghosh and S. Banerjee, *J. Appl. Polym. Sci.*, 2008, **109**, 2329-2340.

12 C.-K. Ku and Y.-D. Lee, *Polymer*, 2007, **48**, 3565-3573.

13 S. Andre, F. Guida-Pietrasanta, A. Rousseau and B. Boutevin, *J. Polym. Sci., Part A: Polym. Chem.*, 2001, **39**, 2414-2425.

14 C. A. Arnold, D. H. Chen, Y. P. Chen, R. O. Waldbauer, M. E. Rogers and J. E. McGrath, *High Perform. Polym.*, 1990, **2**, 83-94.

15 M. Kajiyama, M. Kakimoto and Y. Imai, *Macromolecules*, 1989, **22**, 4143-4147.

16 T. Matsumoto, Y. Koinuma, K. Waki, A. Kishida, T. Furuzono, I. Maruyama and M. Akashi, *J. Appl. Polym. Sci.*, 1996, **59**, 1067-1071.

17 K. Senshu, T. Furuzono, N. Koshizaki, S. Yamashita, T. Matsumoto, A. Kishida and M. Akashi, *Macromolecules*, 1997, **30**, 4421-4428.

18 T. Furuzono, K. Seki, A. Kishida, T.-A. Ohshige, K. Waki, I. Maruyama and M. Akashi, *J. Appl. Polym. Sci.*, 1996, **59**, 1059-1065.
19 T. Furuzono, K. Senshu, A. Kishida, T. Matsumoto and M. Akashi, *Polym. J.*, 1997, **29**, 201-203.
20 T. Matsumoto, T. Uchida, A. Kishida, T. Furuzono, I. Maruyama and M. Akashi, *J. Appl. Polym. Sci.*, 1997, **64**, 1153-1159.
21 E.-C. Kang, T. Kaneko, D. Shiino and M. Akashi, *J. Polym. Sci., Part A: Polym. Chem.*, 2003, **41**, 841-852.
22 A. Kishida, T. Kanda, T. Furuzono, I. Maruyama and M. Akashi, *J. Appl. Polym. Sci.*, 2000, **78**, 2198-2205.
23 A. Korematsu, T. Furuzono and A. Kishida, *Macromol. Mater. Eng.*, 2005, **290**, 66-71.
24 E.-C. Kang and M. Akashi, *Polym. J.*, 2002, **34**, 395-399.
25 T. Furuzono, E. Yashima, A. Kishida, I. Maruyama, T. MatsumotO and M. Akashi, *J. Biomater. Sci. Polym. Ed.*, 1994, **5**, 89-98.
26 M. Akashi, T. Furuzono, T. Matsumoto, A. Kishida and I. Maruyama, in *Advanced Biomaterials in Biomedical Engineering and Drug Delivery Systems*, eds. N. Ogata, S. W. Kim, J. Feijen and T. Okano, Springer Japan, Tokyo, 1996, pp. 183-187.
27 T. Furuzono, A. Kishida, M. Yanagi, T. Matsumoto, T. Kanda, T. Nakamura, T. Aiko, I. Maruyama and M. Akashi, *J. Biomater. Sci. Polym. Ed.*, 1996, **7**, 871-880.
28 T. Otsuki, M.-A. Kakimoto and Y. Imai, *J. Polym. Sci., Part A: Polym. Chem.*, 1991, **29**, 611-618.
29 L. T. Cureton, F. L. Beyer and S. R. Turner, *Polymer*, 2010, **51**, 1679-1686.
30 J. N. Lee, C. Park and G. M. Whitesides, *Anal. Chem.*, 2003, **75**, 6544-6554.
31 S. C. Moldoveanu, *Analytical Pyrolysis of Synthetic Organic Polymers*, Elsevier Science, 2005.
32 L. Feng, H. Fang, S. Zhou and L. Wu, *Macromol. Chem. Phys.*, 2006, **207**, 1575-1583.
33 Yi, X. Fan, X. Wan, L. Li, N. Zhao, X. Chen, J. Xu and Q.-F. Zhou, *Macromolecules*, 2004, **37**, 7610-7618.
34 G. Liu, W.-S. Hung, J. Shen, Q. Li, Y.-H. Huang, W. Jin, K.-R. Lee and J.-Y. Lai, *J. Mater. Chem. A*, 2015, **3**, 4510-4521.
35 S. N. Chvalun, M. Ishaq, J. Blackwell and A. Y. Bilibin, *J. Macromol. Sci. B*, 1998, **37**, 451-462.
36 J. Blackwell, A. Biswas, G. A. Gutierrez and R. A. Chivers, *Faraday Discuss. Chem. Soc.*, 1985, **79**, 73-84.
37 X. Chen, J. A. Gardella and P. L. Kumler, *Macromolecules*, 1992, **25**, 6631-6637.
38 Y. Imai, M. Kajiyama, S.-i. Ogata and M.-a. Kakimoto, *Polym. J.*, 1984, **16**, 267-272.

39 S. Ogata, M. Kakimoto and Y. Imai, *Macromolecules*, 1985, **18**, 851-855.

40 *Des. Monomers. Polym.*, 1998, **1**, 103-109.

41 *Des. Monomers. Polym.*, 1998, **1**, 187-206.

42 C. P. Rader, *Handbook of thermoplastic elastomers*, Springer, 1988.

43 I. M. Ward and J. Sweeney, *Mechanical properties of solid polymers*, John Wiley & Sons, 2012.

44 W. Brostow and R. D. Corneliussen, *Failure of plastics*, Hanser Pub.: Distributed in the United States of America by Macmillan Pub., 1986.

45 P. W. Dufton, *Thermoplastic Elastomers*, iSmithers Rapra Publishing, 2001.

46 R. W. Hertzberg, R. P. Vinci and J. L. Hertzberg, *Deformation and Fracture Mechanics of Engineering Materials, 5th Edition*, Wiley, 2012.

47 N. G. McCrum, C. P. Buckley and C. B. Bucknall, *Principles of Polymer Engineering*, Oxford University Press, 1997.

48 Y. Zhou and P. K. Mallick, *Polym. Eng. Sci.*, 2002, **42**, 2449-2460.

49 M. C. Galetz and U. Glatzel, *J. Mech. Behav. Biomed. Mater.*, 2010, **3**, 331-338.

50 J. Krijgsman, D. Husken and R. J. Gaymans, *Polymer*, 2003, **44**, 7573-7588.

Chapter 6 Shape memory behavior of PDMS-based multiblock copolymers

Abstract

In this Chapter we will discuss the shape memory performance of PDMS-containing $(AB)_n$ multiblock copolymers described in Chapter 5, in the temperature range of -150 to 150 °C, using a rheometer in torsion mode. The glass transitions originating from the rigid regions and PDMS domains were used as the reversible switches for designing T_g-based dual- or triple-shape memory polymers. The AM5K- and LC5K-*b*-PDMS1K multiblock copolymers show dual-shape memory effect in the range of 20–150 °C, while the PDMS-5K based analog shows triple-SME in the temperature range of -150 to 150 °C. Due to the low aromatic content, the PDMS-10K multiblock copolymers failed to show satisfying shape memory properties. We found that the phase morphology and the degree of crystallinity play an important role in the shape fixation and shape recovery rate.

6.1 Introduction

Shape memory polymers (SMPs) are stimuli-responsive materials, which can be triggered by various types of stimuli, such as heat, light or electricity, to recover from a temporary fixed shape to a permanent shape.[1] Since the discovery of SMPs in the 1940s of dental materials (methacrylic ester resin)[2] and the use of heat shrinkage polyethylene (*e.g.* films or tubings) in the 1960s,[3, 4] this type of material attracts more research interest in the past two decades due to the promising functionalities in various applications, for instance in biomedical applications, smart textiles and materials for aerospace engineering.[5-13] So far, thermally responsive SMPs are the most extensively investigated and widely used systems,[14-18] and in this Chapter we will also be focusing on thermal responsive polymers.

From a molecular architecture point of view, SMPs are elastic polymer networks, consisting of net-points and molecular switches.[13] The net-points can be of a chemical or physical nature. Chemical networks are crosslinked by covalent bonds, while physical crosslinking is obtained by chain entanglement, crystalline domains, or interpenetrating phases. The net-points play an important role in determining the permanent shape of the polymer network. The molecular switches are thermo response domains, which are responsible for the fixation of the temporary shape and the trigger for shape recovery.

The simplest and most well-known shape memory cycle involves a transformation between two shapes, *i.e.*, one temporary fixed shape is transformed into a permanent shape, a process known as a dual- shape memory effect (SME). As depicted in Figure 6.1***A***, for a thermo response dual SMP, a permanent shape is predetermined by an initial processing step (extrusion, spinning, pressing, etc.). Above the switch temperature (T_{sw}), the permanent shape is programmed with the help of an external force, and is fixed by lowering the temperature below T_{sw}. Upon exposure to a temperature higher than T_{sw}, the material will recover its initial permanent shape. The shape recovery is driven by the relaxation of the internal stress formed during the programming step(s). In principle, this cycle of programming and recovery can be repeated several times, with different temporary shapes in subsequent cycles.[19] A crosslinked epoxy based on oligo(bisphenol A) diglycidyl ether and Jeff amines was reported to show SME, triggered by the tunable T_gs in the temperature range of 31 to 93 ˚C.[20] Lendlein and coworkers reported the co(polyester-polyurethane) SMPs, which are based on star-shaped oligo[(*rac*-lactide)-co-glycolide] soft segments.[21] Similar to the chemically crosslinked networks

mentioned above, physically "crosslinked" polymer also shows T_g-based SME. A thermoplastic, semi-crystalline, engineering polymer such as polyetheretherketone (PEEK) can be modified to reveal SME with a switch temperature higher than 180 ˚C (above T_g but below T_m).[22] PUs with a thermoplastic elastomeric and shape memory behavior could be obtained by the polymerization of 1,3-butanediol and hexamethylene diisocyanate (soft block) together with 4,4'-bis-(6-hydroxy hexoxy)biphenyl and tolylene 2,4-diisocyanate (hard block).[23]

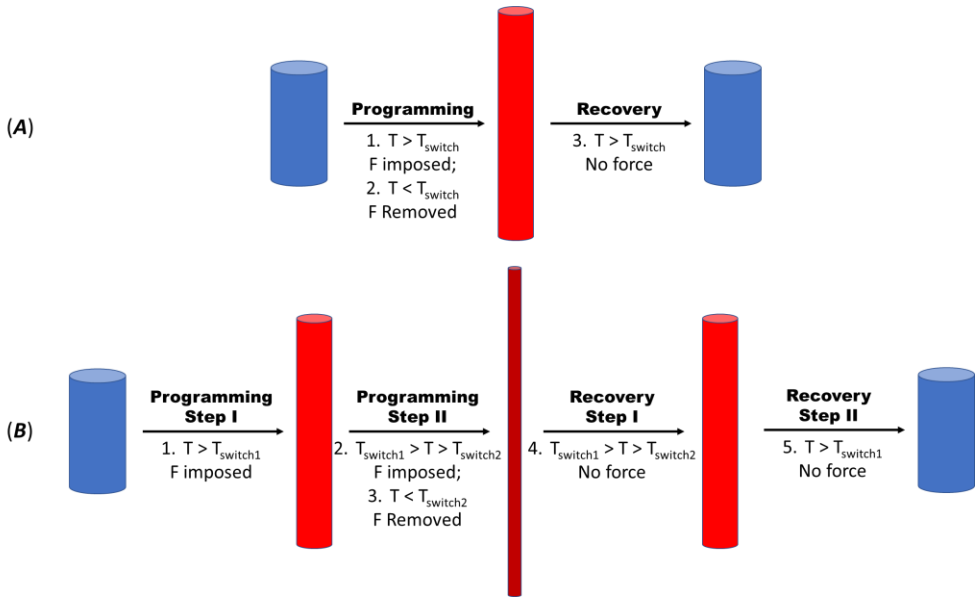

Fig. 6.1. Schematic representation of how shape memory works in polymeric systems. ***A*-** dual-SME; ***B*-** triple-SME. T_{swicth} is the switching temperature of the SMPs.

In addition to dual SMPs mentioned above, triple SMPs are capable of even more complex movements, due to the existence of two temporary states (*A* and *B*) as well as a permanent shape.[24, 25] Triple SMPs require two programming steps and show two recovery steps, as shown in Figure 6.1***B***. After a two-step programming of the material, the polymer will go from temporary shape *A* to temporary shape *B*, induced by a temperature increase, whereas a second temperature increase provokes the transformation back to the permanent shape. Triple SMPs are either polymers with a very broad glass transition or with multiphases, *i.e.*, a phase-separated polymer with different transitions, responsible for each fixation and

recovery step.[19] Generally, the latter generates better control over the SME and the required switching temperatures. Triple SMP based on a multiphase material was first reported by Lendlein's group.[26] This triple SMP is based on a system consisting of crosslinked poly(ε-caprolactone) (PCL) and polyethylene glycol network, where the two T_ms served as shape transformation triggers. The transition temperatures of this system can be tuned by adjusting the length of the corresponding segment. At a high PEO content (>70%), the material loses its triple SME and shows dual SME, even though two distinct transitions were observed in a DSC experiment. Perfluorosulphonic acid ionomer (PFSA, *i.e.* Nafion) was also reported to show triple SME, based on a broad glass transition temperature.[27-29] Interpenetrating networks (IPNs) based on polymethyl methacrylate (PMMA) and polyethylene oxide (PEO) were also reported to show one broad T_g, and the triple SME was studied by *Peng* and colleagues.[30]

Block copolymers are promising triple SMP materials, because they offer the possibility to generate a nanophase separated polymer morphology,[31] which can act as switches for the triple-shape changes. Besides, in the case of incorporating high-performance polymer segments, this type of polymer is likely to exhibit excellent mechanical properties and good shape memory properties at the same time. In a study by *Thorsten* and coworkers, a triple SMP from multiblock poly(ester urethane) was reported.[32] The material displays triple-shape functionality in the temperature range of -60 to 60 ˚C, with the use of crystallization temperature (T_c) of soft segment and glass transition temperature (T_g) of the rigid segment as the triggers. However, to the best of our knowledge, none of the reported materials show SME at high temperature (> 150 ˚C) and at low temperature (< -150 ˚C) at the same time, which is required for space applications. Another shortcoming is that all these materials have rather low moduli, due to the incorporation of high content of soft segments, which restrict the application of shape memory materials seriously.

$(AB)_n$ type multiblock copolymers from all-aromatic esters-based segments (AM5K and LC5K) and PDMS units (PDMS- 1K, -5K and -10K) have been synthesized, characterized and discussed in Chapter 4 and 5. (Thermo)mechanical analyses showed that AM5K-based multiblock copolymers show excellent (thermo)mechanical properties and excellent tensile performance at low PDMS loading (PDMS-1K). Depending on the selections of the molecular weights of the PDMS block, the multiblock copolymer exhibit one (PDMS-1K) or two T_gs (PDMS-5K and -10K) as determined by DMTA, which is one of the morphological requirements for designing SMPs. The one T_g (~110 ˚C) or two T_gs (~-120 ˚C and 110 ˚C) originated

from the aromatic and PDMS phases can be used as the switches for dual and triple SME, respectively. To the best of our knowledge, this is the first demonstration of a triple SME of a polymer that transforms shapes at both high (> 100 ˚C) and low temperature (< -100 ˚C) simultaneously.

6.2 Experimental

6.2.1 Materials

The synthesis and characterization of $(AB)_n$ multiblock copolymers (AM5K-*b*-PDMS and LC5K-*b*-PDMS) has been described in Chapter 4 and 5. The multiblock copolymers are composed of all-aromatic units (M_n = 5 kg·mol^{-1}) and soft PDMS segments (M_n = 1, 5 and 10 kg·mol^{-1}), as shown in Figure 6.2. The rectangular shape films specimens of multiblock copolymers (AM5K-*b*-PDMS series and the LC5K-*b*-PDMS series) for SM test were prepared by film casting in a petri dish, as described in Chapter 5.

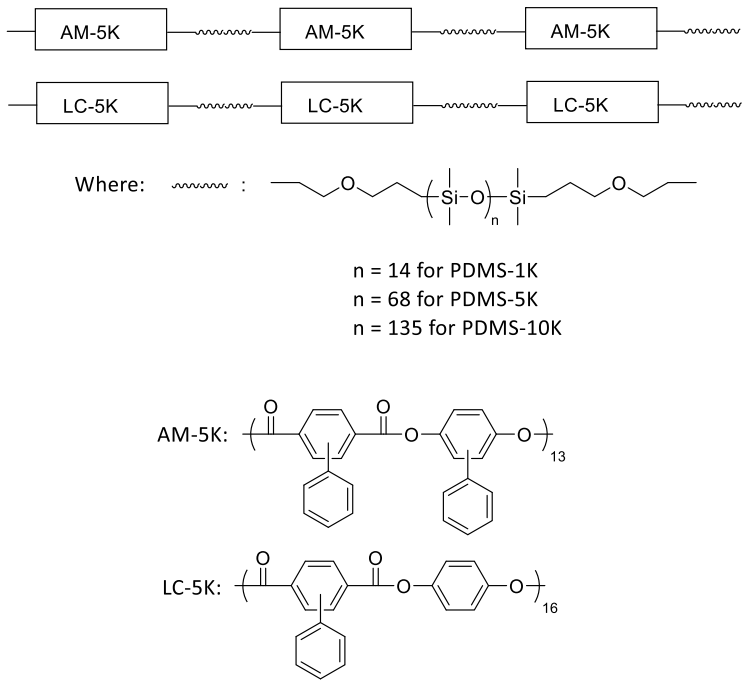

Fig. 6.2. Molecular compositions of the aromatic/PDMS-based $(AB)_n$-multiblock copolymers.

6.2.2 Characterization

Dual shape memory test of AM5K-b-PDMS1K and LC5K-b-PDMS1K

The dual shape memory test was performed on a Thermofisher Haake MARS III rheometer equipped with solid clamp geometry with rectangular thin films (approximately 25 × 5 × 0.2 mm^3) in controlled torsion mode. All tests were carried out under an air atmosphere and at a constant strain rate of 0.1%·s^{-1}, equivalent to a rotation speed of 3 °·s^{-1}. The heating and cooling rates are 10 °C·min^{-1}.

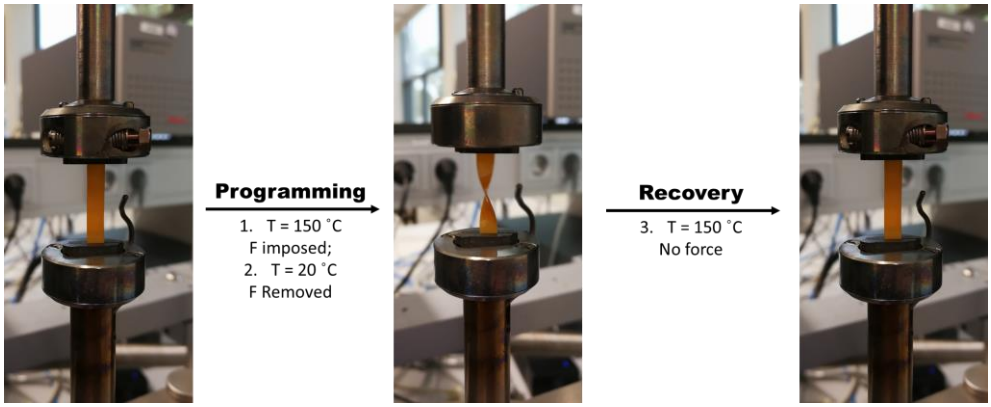

Fig. 6.3. Illustration of dual-SMP experiment performed using a rheometer in controlled torsion mode. Samples were tested between 20 to 150 °C and twisted 180°. Comparing to characterization under tension mode, with this set-up, samples are able to be exposed the large deformations but they experience little strain.

The dual torsion SMP experiment was conducted following the protocols shown in Figure 6.3. Generally, the experiment was conducted by a rotation of 180˚ and the recovery under stress-free condition was measured. The film was first kept at 150 ˚C for 10 min, which is well above T_g of the aromatic segments, and rotated by 180˚ from the original shape to a temporary deformed shape (φ_d). After a 10 min hold at this temperature, the sample was cooled to 20 ˚C at a cooling rate of 10 ˚C·min^{-1}, to fix the temporary shape. To quantify the shape memory effect, shape fixation rate (R_f) is defined as

$$R_f = \frac{\varphi_f}{\varphi_d} \times 100\% \qquad \text{eqn. 6.1}$$

and the shape recovery rate (R_r) is given by

$$R_r = \frac{\varphi_d - \varphi_r}{\varphi_d} \times 100\% \qquad \text{eqn. 6.2}$$

Where φ_d, φ_f and φ_r stand for he rotational angle after deformation, at the fixed temporary shape and after recovery, respectively. R_f and R_r are the percentage of shape fixation and shape recovery, respectively. The instantaneous recovery velocity V_r is defined as the time derivative of the angle as shown in Equation 6.3, to clarify the recovery temperature range corresponding to the shape recovery process.

$$V_r = \frac{\partial \varphi}{\partial \mathrm{t}} \qquad \text{eqn. 6.3}$$

Triple shape memory test of AM5K-b-PDMS5K and LC5K-b-PDMS5K

The triple shape memory test was also performed on a Thermofisher Haake MARS III rheometer equipped with solid clamp geometry with rectangular thin films in controlled torsion mode with the film dimensions of approximately 25 × 5 × 0.2 mm^3. The constant strain rate and the heating/cooling rate used for the test are described above. The triple torsion SMP experiment was conducted following the protocols shown in Figure 6.4.

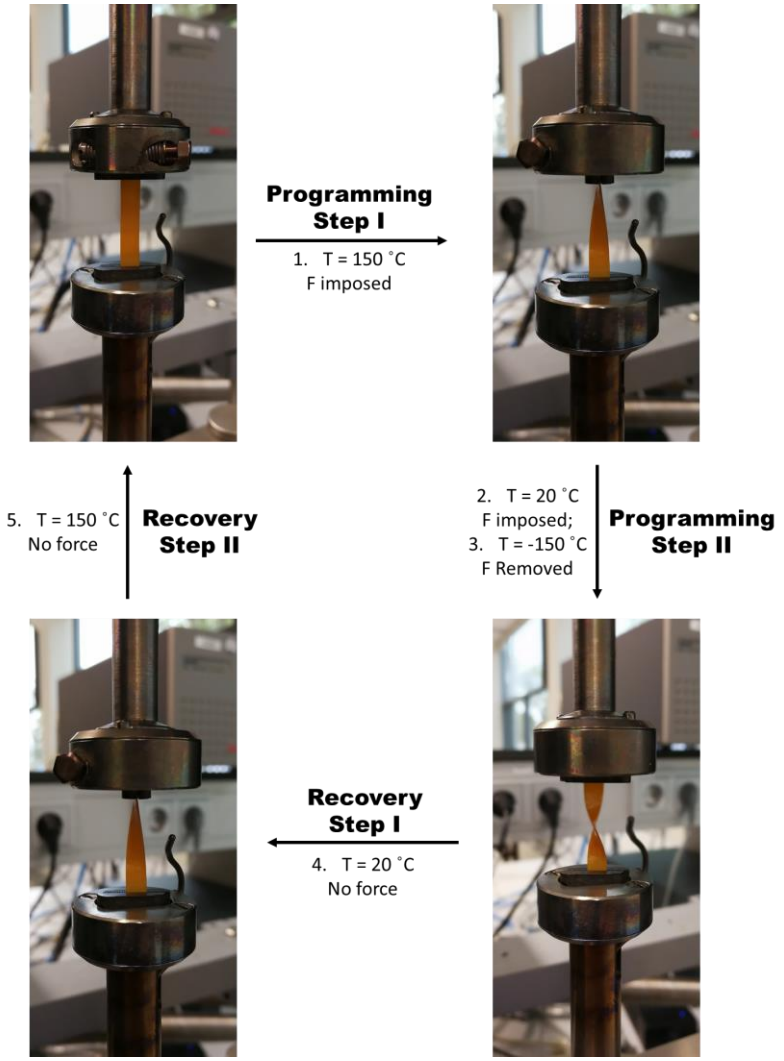

Fig. 6.4. Illustration of triple-SMP experiment performed using a rheometer in controlled torsion mode. Samples were tested between -150 to 150 °C and twisted 90° and 180°.

Generally, the experiment was conducted by two rotation steps (*e.g.*, 90˚ + 90˚), to a constant total rotation of 180˚. The sample was kept isothermal at 150 ˚C, which is well above T_g of the aromatic units, and rotated by 90˚ from the original shape *A* (φ_A) to a temporary shape *B* (φ_B). After held at the temperature for 10 min, the sample was cooled to 20 ˚C, which is between the two glass transitions. After

stabilize at this temperature for 10 min, a second stress was applied to rotate the sample to another temporary shape *C* (φ_C). The sample was subsequently cooled to -150 ˚C, which is well below the T_g of PDMS units, to fix a temporary shape *C*. During this two-step programing process, with the measurement of rotation degree φ_C and the final fixed rotation degree φ_f, the shape fixation rate (R_f) is defined as

$$R_f = \frac{\varphi_f}{\varphi_C} \times 100\% \qquad \text{eqn. 6.4}$$

In the subsequent recovery step, the sample was allowed to recover upon the temperature heating up with the release of external stress. The two-step recovery rates (R_r) can be calculated using the following equations:

$$R_{r(C\to B)} = \frac{\varphi_f - \varphi_{B/rec}}{\varphi_C - \varphi_B} \times 100\% \qquad \text{eqn. 6.5}$$

$$R_{r(B\to A)} = \frac{\varphi_{B/rec} - \varphi_{A/rec}}{\varphi_B - \varphi_A} \times 100\% \qquad \text{eqn. 6.6}$$

Where φ_A, φ_B and φ_C denote the degree of rotation after the torsion step, the degree of rotation of the fixed temporary shape, and the degree of rotation after recovery, respectively.

6.3 Results and Discussion

6.3.1 Dual shape memory properties of AM5K- and LC5K-*b*-PDMS1K

Traditionally, a quantitative characterization of the SME is conducted in a cyclic thermo-mechanical extension or bending test.[33] However, the multiblock copolymer materials are not chemically crosslinked, and the elastic deformations are only observed in the region with strain less than 5% in stress-strain curves, as discussed in Chapter 5. As a result, an orientation of the multiblock copolymer films could take place during SM test if a cyclic thermo-mechanical extension is applied, making SME characterization not possible. SME characterization using torsion mode was also reported by Diani *et al*.[34] The torsion mode tests involve non-homogeneous strains and stresses in the cross-section of a rectangular film sample, and enable the SMPs to reach large deformations with moderate strains.[35] Thus, a torsion mode setup was used to characterize the SME of the multiblock copolymer films. The deformation and fixation of the film samples are performed under strain control, and the recovery is in a stress-free condition.

Figure 6.5 shows the DSC traces and the storage moduli (E') obtained from DMTA experiments as a function of temperature, as illustration of the transformation triggers. As discussed in Chapter 5, the AM5K-*b*-PDMS1K multiblock copolymer shows one T_g from the rigid segments, in the temperature range from 100 to 150 ˚C (shown in Figure 6.5***A***). Two stable plateaus with E' of approximately 5 GPa and 4 MPa, respectively, can be observed before and after T_g. The presence of two plateau regions (< T_g and > T_g) is of interest, as this facilitates high-temperature shape memory behaviour.[36] Besides, this material shows excellent tensile strength (> 125 MPa) and elastic modulus (> 3.4 GPa) in tensile testing experiments at 25 ˚C, making this material a promising engineering SMP for industry. In the case of LC5K-*b*-PDMS1K, again only one T_g was observed (Figure 6.5***B***) from DMTA, but the glass transition temperature range is wider. Both AM5K-*b*-PDMS1K and LC5K-*b*-PDMS1K were tested for SME at their respective T_g.

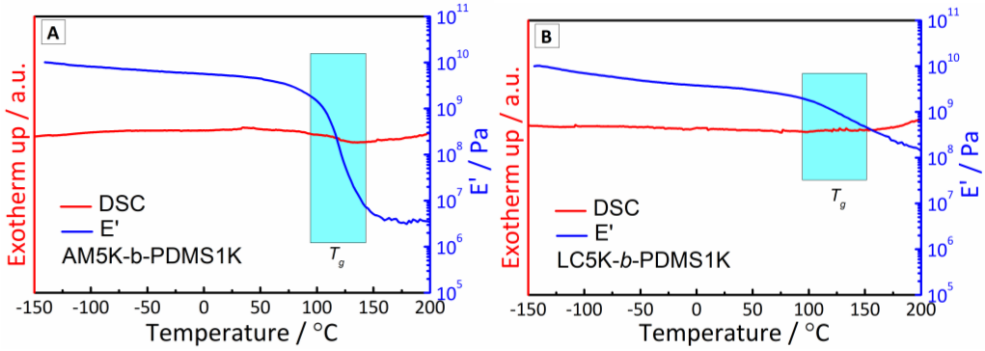

Fig. 6.5. DSC trace and storage modulus (E') as a function of temperature during heating. ***A-*** AM5K-*b*-PDMS1K; ***B-*** LC5K-*b*-PDMS1K. The shaded area indicates the glass transition (T_g).

Three consecutive deformation, fixation and recovery cycles were conducted for each sample to test the shape memory behaviour over multiple cycles. The results are shown in Figure 6.6, in which R_f and R_r are calculated using Equation 6.1 and 6.2, summarized in Table 6.1.

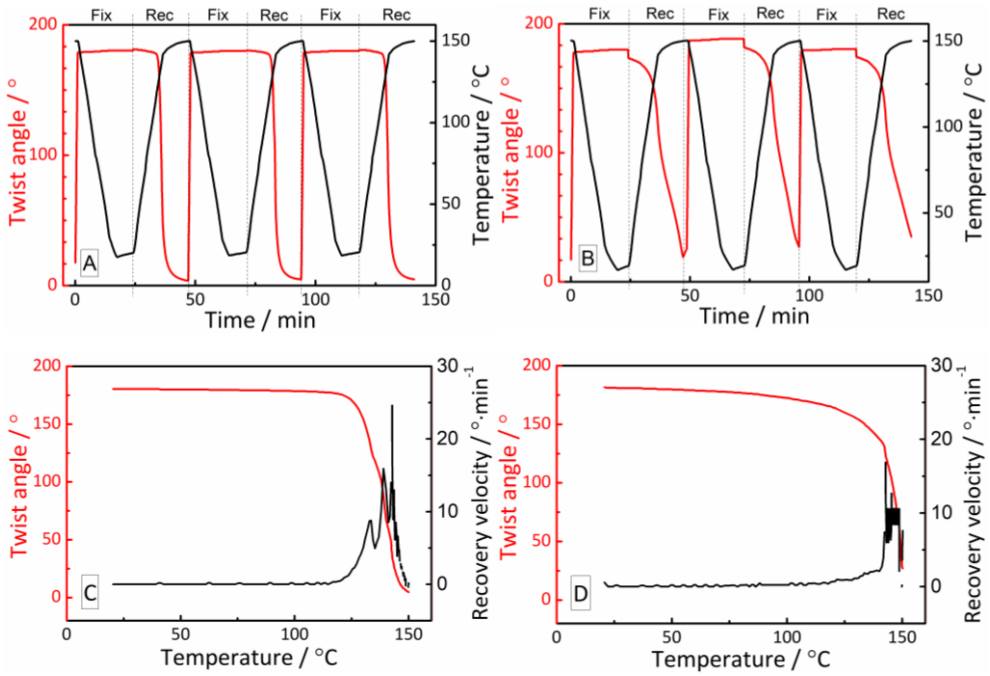

Fig. 6.6. Dual SM torsion test of the multiblock copolymer films with a rotation angle of 180˚. ***A-*** AM5K-*b*-PDMS1K; ***B-*** LC5K-*b*-PDMS1K. Shape recovery velocity as a function of temperature in the second cycle for ***C-*** AM5K-*b*-PDMS1K; ***D-*** LC5K-*b*-PDMS1K. The heating and cooling rates are 10 ˚C·min^{-1}.

As shown in Figure 6.6, the multiblock copolymer film samples were deformed at 150 °C, which is well above T_g (96 °C and 112 °C for AM5K-b-PDMS1K and LC5K-b-PDMS1K, respectively, as obtained by the maximum of loss modulus (E") in DMTA test in Figure 5.6 in Chapter 5), and the temporary shape was fixed at 20 °C. At this temperature, the mobility of the polymer chain segments is strongly restricted by the rigid domains. However, this is not sufficient to fix the deformation (torsion) and with the release of imposed force, a relaxation took place, resulting a slight instant retreat in the torsional angle. This was also observed in other physical scaffolds systems.[37] With the temperature increase to 150 °C, the temporary shape recovers to its original permanent shape, triggered by the glass transition of the rigid segments. The dual shape fixation and recovery results of the two materials are summarized in Table 6.1.

Table 6.1. Dual shape fixation and recovery results of the AM5K-*b*-PDMS1K and LC5K-*b*-PDMS1K multiblock copolymer films.

Samples	T_g[a] (°C)	T_{prog}[b] (°C)	T_r[c] (°C)	*Cycle 1*		*Cycle 2*		*Cycle 3*	
				R_f (%)	R_r (%)	R_f (%)	R_r (%)	R_f (%)	R_r (%)
AM5K-*b*-PDMS1K	96	150	143	100	98	100	97	100	97
LC5K-*b*-PDMS1K	112	150	143	97	88	97	85	97	81

[a] Glass transition temperature (T_g) reported as the maximum of loss modulus (E") at 1 Hz in a DMTA experiment (Figure 5.6 in Chapter 5).

[b] T_{prog} is the programming temperature.

[c] T_r is the temperature at the maximum recovery velocity.

The AM5K-*b*-PDMS1K film shows high R_f value of approximately 100% in the three cycles, whereas the R_r numbers of LC5K-*b*-PDMS1K film are slightly lower over the cycles (97% in the three cycles). In a similar fashion, the AM5K-*b*-PDMS1K film shows a high R_r of approximately 97% - 98% over the three cycles, while the LC5K-*b*-PDMS1K film shows poorer recovery, with a medium R_r value of 88% in the first cycle, and 81% in the third cycle. Most likely, this is because LC5K-*b*-PDMS1K is semi-crystalline and AM5K-*b*-PDMS1K is totally amorphous, as discussed in Chapter 5. The shape recovery originates from the relaxation of the amorphous chain segments (*i.e.* glass transition), which are restricted by the crystalline domains. The recovery of all samples cannot reach 100% because of the inevitable irreversible chain-segment orientation and relaxation effects, which partly dissipate the stored stress.[38] The shape recovery velocity of the second cycle is plotted as a function of temperature as shown in Figure 6.6. Both samples show relatively low velocity (< 25 °·min^{-1}) at 143 °C through the recovery process, which is a general phenomenon among T_g-based SMPs.[39] The shape recovery is triggered by the glass transition of the

amorphous chain segments, which is significantly slower than other transitions, such as melting.

6.3.2 Triple shape memory properties of AM5K- and LC5K-*b*-PDMS5K

In contrast to AM5K- and LC5K-*b*-PDMS1K, the PDMS5K-based analogous films exhibit three stable storage moduli (E') plateau regions (> T_{g1}, T_{g2} - T_{g1} and < T_{g2}), as shown in Figure 6.7. The T_g is very low for the PDMS segments (~-125 ˚C) and high for the rigid units (102 and 112 ˚C for AM5K and LC5K, respectively). The all-aromatic microphases act as physical net-points, together with the appearance of the two distinct glass transitions, making the two polymers potential triple SMPs. Moreover, the polymers exhibit high moduli making them potential candidates for space applications, which require extreme switching temperatures and good mechanical properties at the same time. The two T_gs of the two (micro)phases are used as the switching temperatures to explore the triple SME.

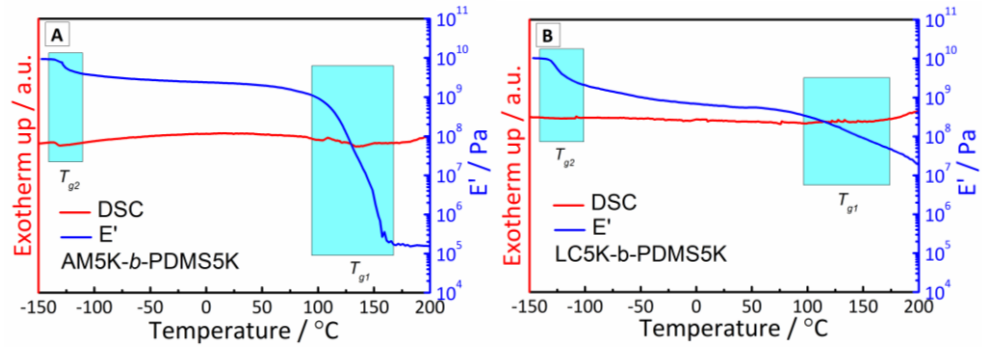

Fig. 6.7. DSC trace and storage modulus (E') as a function of temperature during heating. ***A*-** AM5K-*b*-PDMS5K; ***B*-** LC5K-*b*-PDMS5K. The blue shaded area indicates the glass transition (T_g) region of the PDMS and rigid aromatic block, respectively.

The experimental results of AM5K-*b*-PDMS series are shown in Figure 6.8***A***, and the shape memory properties of the multiblock copolymers are summarized in Table 6.2. In a typical experiment, after cooling to -150 ˚C, the shape fixation rate R_f of the multiblock copolymer films are 96 and 88% for AM5K-*b*-PDMS5K and LC5K-*b*-PDMS5K, respectively. While heating up to recovering temperature, both of the AM5K-*b*-PDMS5K and LC5K-*b*-PDMS5K show $R_{r(C\rightarrow B)}$ and $R_{r(B\rightarrow A)}$ values of 96 % and 99% for AM5K-*b*-PDMS5K, while those for LC5K-*b*-PDMS5K are 80% and 91%,

respectively. As listed in Table 6.2, the shape fixation and recovery rate remain comparable in the repeated experiments, indicating a potential high durability of this type of materials.

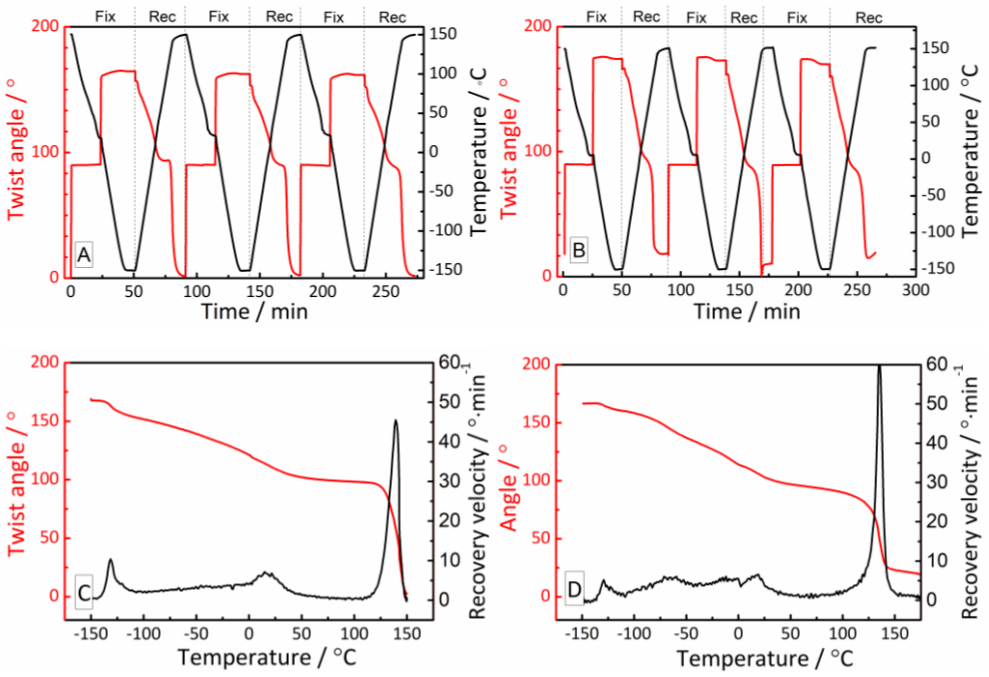

Figure 6.8. Triple SM torsion test of the multiblock copolymer films with a total rotation angle of 180˚. ***A*-** AM5K-*b*-PDMS5K; ***B*-** LC5K-*b*-PDMS5K. Shape recovery velocity as a function of temperature in the second cycle for ***C*-** AM5K-*b*-PDMS5K; ***D*-** LC5K-*b*-PDMS5K. Test conditions: the degree of rotation = 90 + 90˚, $T_{prog\ (A \rightarrow B)}$ = 150 °C, $T_{prog\ (B \rightarrow C)}$ = 20 °C, the heating and cooling rates are 10 ˚C·min^{-1}.

In Figure 6.8, the recovery velocity of the AM5K-*b*-PDMS5K and LC5K-*b*-PDMS5K is also presented, to show the validity of using the glass transitions as triggers for SME. The AM5K-*b*-PDMS5K multiblock copolymer film was heated up from the temporary shape *C* at -150 ˚C showing an obvious recovery velocity peak located at -125 ˚C, due to the glass transition of the PDMS blocks. Further heating to ~50 ˚C, the film is further recovering from shape *C* to *B* slowly, indicating a slow relaxation of the hindered PDMS block among the AM-5K blocks. A much higher

recovery velocity peak at ~130 ˚C due the glass transition of the AM-5K blocks is observed releasing all the stress from the system and restoring the original shape.

Similar to AM5K-*b*-PDMS5K, LC5K-*b*-PDMS5K exhibits slow recovery below 50 ˚C starting at the T_g of the PDMS phase, together with a high recovery velocity at ~130 ˚C. The experiment clearly shows the SME of this type of multiblock copolymers is triggered by glass transitions. With a similar trend as the PDMS-1K based multiblock copolymers, the AM5K-b-PDMS5K films shows superior fixation rate and recovery rate over its LC5K-based analogous, due to the same reason as mentioned above.

Table 6.2. Triple-shape fixation and recovery results of multiblock copolymer films.

Samples	T_{r1}[a] (˚C)	T_{r2}[a] (˚C)	*Cycle 1*			*Cycle 2*			*Cycle 3*		
			R_f (%)	R_{rec} (C→B) (%)	R_{rec} (B→A) (%)	R_f (%)	R_{rec} (C→B) (%)	R_{rec} (B→A) (%)	R_f (%)	R_{rec} (C→B) (%)	R_{rec} (B→A) (%)
AM5K-*b*-PDMS5K	-131	139	96	96	99	95	99	99	95	99	99
LC5K-*b*-PDMS5K	-129	136	93	88	80	91	87	89	92	85	83

[a] T_{r1} and T_{r2} refer to the temperature at the first and second maximum recovery velocity, respectively.

Noteworthy, even though the multiblock copolymers with PDMS-10K also show two T_gs in DMTA test (Figure 5.6 and Table 5.3), no triple or dual high temperature SME was observed. This is most likely due to the very low concentration of physical crosslinkers, *i.e.* the aromatic part of the polymer backbone, which is not sufficient to provide a scaffold that locks the temporary shapes.[13]

6.4 Conclusion

In summary, we have demonstrated that our $(AB)_n$ multiblock copolymers can be used as SMPs. The dual- and triple-shape fixation and recovery performances were investigated in torsion mode. Depending on the M_n of PDMS segments, the multi-block copolymers exhibit one (for PDMS1K) or two T_gs (for PDMS5K and PDMS10K) in DMTA test, which were used as shape memory triggers for exploring SME of this type of materials. AM5K- and LC5K-b-PDMS1K multiblock copolymers show high temperature dual-shape memory behavior (>150 °C) by using the T_gs of rigid segments. The AM5K-based multiblock copolymer shows high R_f (100%) and R_r (>97%), while the LC5K-based analog exhibits moderate shape memory performance, with R_f of 97% and R_r > 80%. The PDMS5K-based multiblock copolymers show triple-SME by using the two T_gs as temperature switches. High R_f (>95%) and high R_r (>96%) was measured for AM5K-b-PDMS5K, while the LC5K-based analog exhibits slightly lower R_f of >91% and R_r > 80%. Due to the very low aromatic content, the AM5K/LC5K-b-PDMS10K multiblock copolymers shows no satisfying high temperature dual- or triple SME. This is because the physical crosslinks are not sufficiently abundant in the polymer and cannot provide a scaffold that locks the shapes. Considering the excellent mechanical performance as discussed in Chapter 5, the excellent shape memory properties of AM5K-based multiblock copolymers makes them a promising candidate for applications requiring very high temperature and very low temperature at the same time.

6.5 References

1 A. Nelson, *Nat Mater*, 2008, **7**, 523-525.
2 *L. B. Vernon and H. M. Vernon, US Pat.,* US2234993, 1941.
3 *R. J. Perrone, US Pat.,* US3326869, 1967.
4 *J. J. Hitov, W. C. Rainer, E. M. Redding, A. W. Sloan and W. D. Stewart, US Pat.,* US3144398, 1964.
5 M. Behl, M. Y. Razzaq and A. Lendlein, *Adv. Mater.*, 2010, **22**, 3388-3410.
6 I. A. Rousseau, *Polym. Eng. Sci.*, 2008, **48**, 2075-2089.
7 J. Hu, Y. Zhu, H. Huang and J. Lu, *Prog. Polym. Sci.*, 2012, **37**, 1720-1763.
8 T. Xie, *Polymer*, 2011, **52**, 4985-5000.
9 H. Zhang, H. Xia and Y. Zhao, *ACS Macro Letters*, 2014, **3**, 940-943.
10 X. Lan, Y. Liu, H. Lv, X. Wang, J. Leng and S. Du, *Smart Mater. Struct.*, 2009, **18**, 024002.

11 J. Hu, H. Meng, G. Li and S. I. Ibekwe, *Smart Mater. Struct.*, 2012, **21**, 053001.
12 A. Lendlein, M. Behl, B. Hiebl and C. Wischke, *Expert Review of Medical Devices*, 2010, **7**, 357-379.
13 M. Behl and A. Lendlein, *Mater. Today*, 2007, **10**, 20-28.
14 A. Khaldi, J. A. Elliott and S. K. Smoukov, *J. Mater. Chem. C*, 2014, **2**, 8029-8034.
15 T. Xie, *Nature*, 2010, **464**, 267-270.
16 K. Kratz, S. A. Madbouly, W. Wagermaier and A. Lendlein, *Adv. Mater.*, 2011, **23**, 4058-4062.
17 A. M. Schmidt, *Macromol. Rapid Commun.*, 2006, **27**, 1168-1172.
18 T. F. Scott, R. B. Draughon and C. N. Bowman, *Adv. Mater.*, 2006, **18**, 2128-2132.
19 M. D. Hager, S. Bode, C. Weber and U. S. Schubert, *Prog. Polym. Sci.*, 2015, **49**, 3-33.
20 I. A. Rousseau and T. Xie, *J. Mater. Chem.*, 2010, **20**, 3431-3441.
21 A. Alteheld, Y. Feng, S. Kelch and A. Lendlein, *Angew. Chem. Int. Ed.*, 2005, **44**, 1188-1192.
22 X. L. Wu, W. M. Huang, Z. Ding, H. X. Tan, W. G. Yang and K. Y. Sun, *J. Appl. Polym. Sci.*, 2014, **131**, n/a-n/a.
23 H. M. Jeong, S. Y. Lee and B. K. Kim, *J. Mater. Sci.*, 2000, **35**, 1579-1583.
24 M. Behl and A. Lendlein, *J. Mater. Chem.*, 2010, **20**, 3335-3345.
25 Q. Zhao, M. Behl and A. Lendlein, *Soft Matter*, 2013, **9**, 1744-1755.
26 I. Bellin, S. Kelch, R. Langer and A. Lendlein, *Proceedings of the National Academy of Sciences*, 2006, **103**, 18043-18047.
27 T. Xie, *Nature*, 2010, **464**, 267.
28 J. Li and T. Xie, *Macromolecules*, 2011, **44**, 175-180.
29 T. S. Kustandi, W. W. Loh, L. Shen and H. Y. Low, *Langmuir*, 2013, **29**, 10498-10504.
30 J. Li, T. Liu, S. Xia, Y. Pan, Z. Zheng, X. Ding and Y. Peng, *J. Mater. Chem.*, 2011, **21**, 12213-12217.
31 L. Leibler, *Macromolecules*, 1980, **13**, 1602-1617.
32 P. Thorsten, *Smart Mater. Struct.*, 2010, **19**, 015006.
33 W. Wagermaier, K. Kratz, M. Heuchel and A. Lendlein, in *Shape-Memory Polymers*, ed. A. Lendlein, Springer Berlin Heidelberg, Berlin, Heidelberg, 2010, DOI: 10.1007/12_2009_25, pp. 97-145.
34 J. Diani, C. Frédy, P. Gilormini, Y. Merckel, G. Régnier and I. Rousseau, *Polym. Test.*, 2011, **30**, 335-341.
35 Q. Guan, S. J. Picken, S. S. Sheiko and T. J. Dingemans, *Macromolecules*, 2017, **50**, 3903-3910.
36 C. Liu, H. Qin and P. T. Mather, *J. Mater. Chem.*, 2007, **17**, 1543-1558.
37 R. A. Weiss, E. Izzo and S. Mandelbaum, *Macromolecules*, 2008, **41**, 2978-2980.

38 Q. Wang, Y. Bai, Y. Chen, J. Ju, F. Zheng and T. Wang, *J. Mater. Chem. A*, 2015, **3**, 352-359.
39 Q. Zhao, H. J. Qi and T. Xie, *Prog. Polym. Sci.*, 2015, **49**, 79-120.

Summary

The main objective of the research described in this thesis is to explore the design, synthesis and (thermo)mechanical properties of a new family thermoplastic high-performance elastomeric $(AB)_n$ multiblock copolymers. The backbone is based on bismaleimide-functionalized all-aromatic liquid crystalline (LC) or amorphous (AM) precursors coupled with dithiol terminated PDMS oligomers. Thiol-ene click chemistry was used to prepare high molecular weight multiblock copolymers in high yield. The chemistry, phase behavior, and (thermo)mechanical behaviour will be described in detail.

In ***Chapter 2***, the synthetic details of the bismaleimide end-functionalized oligomers are described. Both LC and AM reactive precursors were synthesized using a standard solution polycondensation procedure, with target molecular weights (M_n) of 1, 5 and 9 kg·mol^{-1}. All soluble samples showed unimodal molecular weight distributions and PDIs of ~2, which is consistent with step-growth polymerization. ^{1}H NMR shows that the maleimide end-groups remain intact during synthesis, enabling further functionalisation of these oligomers towards multiblock copolymers.

The temperature dependent properties and cure behavior of the LC- and AM-bismaleimide terminated oligomers are presented in ***Chapter 3***. The two oligomer series show different behaviour with respect to their crosslinking chemistry, phase behavior and (thermo)mechanical properties. The cured thermosets show good thermal stabilities with $T_d^{5\%}$ > 390 °C and DSC, POM and XRD results confirm the liquid crystalline and amorphous nature of the different oligomers. The uncured LC oligomers and reference polymer shows T_gs of 136 – 157 ˚C, whereas the T_gs of the AM series are in the 130 – 134 ˚C range. After cure, the T_gs of the oligomers increased to 140 – 190 ˚C, depending on the concentration of reactive end-groups. Rheology and gel fraction test shows that the two series of oligomers with M_n of 1 and 5 kg·mol^{-1} are highly crosslinked, whereas those with an M_n of 9 kg·mol^{-1} are only partly crosslinked on mostly chain extended. The cured AM oligomer films show good mechanical properties with high tensile strengths (> 90 MPa), elastic moduli (~2 GPa), elongation at break (~10%) and toughness (~8 MJ·m^{-3}).

In ***Chapter 4***, the synthesis and molecular weight characterization of the multiblock copolymers based on dithiol terminated PDMS and bismaleimide-functionalized oligomers (LC and AM) are described. All thiol-terminated PDMS

oligomers (M_n = 1, 5 and 10 kg·mol^{-1}) could be successfully copolymerized with either LC- or AM-oligomers (M_n = 5 kg·mol^{-1}), *via* thiol-ene click chemistry. ^{1}H NMR confirmed that the multiblock copolymers exhibited high molecular weights, in the range of 22 – 58 kg·mol^{-1}. The molecular composition, as calculated from ^{1}H NMR experiments, are consistent with the theoretical values.

The multiblock copolymers from Chapter 4 are characterized in terms of thermal stability, phase behavior, morphology and (thermo)mechanical properties, and are discussed in ***Chapter 5***. DSC and DMTA experiments shows that the multiblock copolymers with PDMS segments with M_n of 5K and 10K show two glass transitions, indicating (micro)phase separation, due to the incompatibility of the aromatic ester units and PDMS units. In tensile test, the AM5K-*b*-PDMS multiblock copolymers show superior mechanical properties over their LC5K-*b*-PDMS analogs. The AM5K-*b*-PDMS1K film shows outstanding tensile strength of ~125 MPa, elastic modulus of 3.4 GPa and elongation at break higher than 30%.

In ***Chapter 6***, the $(AB)_n$-multiblock copolymers based on all-aromatic polyester/PDMS as discussed in Chapter 4 and 5 were investigated as dual- and triple- shape memory polymers. The AM5K-b-PDMS1K film shows high R_f (100%) and R_r (>97%) in terms of dual- SME, while the LC5K-based analogue exhibits moderate shape memory performance with R_f of 97% and R_r > 80%. In triple- SME test, the AM5K-*b*-PDMS5K film shows high R_f (>95%) and high R_r (>96%), while the LC5K-based analogue exhibits slightly lower R_f of > 91% and R_r > 80%.

In conclusion, we have demonstrated that thermoplastic $(AB)_n$-multiblock copolymers can be prepared from all-aromatic oligomers and thiol-terminated PDMS oligomers via thiol-ene click chemistry. The best performing multiblock copolymer is AM5K-b-PDMS1K, which exhibits outstanding tensile strength (~125 MPa), elastic modulus (3.4 GPa) and elongation at break (>30%). These values surpass the mechanical test results of commercially available high-performance polymers such as PEKK, PPS and PEI.

Samenvatting

In dit proefschrift beschrijven we de synthese en (thermo)mechanische eigenschappen van een nieuwe familie thermoplastische hoogwaardige $(AB)_n$ multiblok copolymeren. De hoofdketen is gebaseerd op een aromatische vloeibaar kristallijne (LC) of amorfe (AM) precursor, welke gekoppeld is aan een dithiol PDMS oligomeer. We hebben *thiol-ene* click-chemie gebruikt om hoogmoleculair gewicht multiblok copolymeren te produceren in hoge opbrengst. De chemie, het fasegedrag en het (thermo)mechanisch gedrag van deze nieuwe polymeren zullen in deze thesis uitgebreid worden behandeld.

In ***Hoofdstuk 2***, worden de synthetisch details met betrekking tot de bismaleimide eind-gefunctionaliseerde oligomeren beschreven. Zowel de LC als AM reactieve precursors, met een (M_n) van 1, 5 en 9 $kg{\cdot}mol^{-1}$, zijn gesynthetiseerd middels een standaard, oplosmiddel-gebaseerde, polycondensatie methode. Alle oplosbare polymeren laten een unimodale molecuulgewichtdistributie (PDI ~2) zien, hetgeen consistent is met een condensatiepolymerisatie mechanisme. Met proton NMR kon worden aangetoond dat de maleimide eindgroepen intact blijven gedurende de syntheseprocedure. De maleimide eindgroepen maken het mogelijk om de oligomeren vervolgens om te zetten naar multiblok copolymeren.

De temperatuurafhankelijke eigenschappen en het cure-gedrag van de LC- en AM-maleimide getermineerde oligomeren worden besproken in ***Hoofdstuk 3***. De oligomeer series vertonen verschillend gedrag met betrekking tot cure, fasegedrag, en (thermo)mechanische eigenschappen. De thermoharders zijn thermisch zeer stabiel ($T_d^{5\%}$ > 390 °C) en DSC-, POM- en XRD-experimenten bevestigen het vloeibaar kristallijne (LC) en amorfe (AM) gedrag van de maleimide-getermineerde oligomeren. De reactieve LC oligomeren en het referentiepolymeer hebben een T_g tussen 136–157 ˚C, en de amorfe oligomeren hebben T_g waardes van 130–134 ˚C. Nadat de oligomeren thermisch gecrosslinkt zijn gaat de T_g omhoog naar 140–190 ˚C, afhankelijk van de concentratie reactieve eindgroepen. Rheologie en onderzoek naar de gelfractie bevestigen dat de 1 and 5 $kg{\cdot}mol^{-1}$ oligomeer series in hoge mate zijn gecrosslinkt. De 9 $kg{\cdot}mol^{-1}$ oligomeren daarentegen zijn slechts gedeeltelijk gecrosslinkt. Gecrosslinkte AM oligomeren gedragen zich redelijk in een trekproef. Filmpjes hebben een treksterkte van 90 MPa, een 2 GPa elasticiteitsmodulus, een breukrek van ~10% en een breuktaaiheid van ~8 $MJ{\cdot}m^{-3}$.

In ***Hoofdstuk 4*** wordt de synthese en de molecuulgewicht karakterisering besproken van de vloeibaar-kristallijne (LC) en amorfe (AM) blok copolymeren. Het bleek mogelijk om alle thiol-getermineerde PDMS oligomeren (M_n = 1, 5 and 10 kg·mol^{-1}) middels *thiol-ene* click chemie te copolymeriseren met zowel de LC- als de AM-oligomeren. Hoog moleculairgewicht polymeer kon worden bevestigd met ^{1}H NMR. De molecuulgewichtsverdeling is rond de 22 – 58 kg·mol^{-1}. De moleculaire compositie, zoals berekend uit de NMR-experimenten, komt overeen met de theoretisch compositie.

De thermische stabiliteit, het fasegedrag en de (thermo)mechanische eigenschappen van de nieuwe $(AB)_n$-multiblok copolymeren zal worden besproken in ***Hoofdstuk 5***. DSC- en DMTA-experimenten laten zien dat de multiblok copolymeren met de langere PDMS-segmenten (M_n van 5K and 10K) twee glastransitie overgangen hebben. De PDMS-segmenten zijn niet compatibel met de aromatische LC- of AM-segmenten waardoor er (micro)fase scheiding optreedt. Trekproeven bij 25 ˚C laten zien dat AM5K-*b*-PDMS multiblok copolymeren superieure mechanische eigenschappen hebben in vergelijking tot de LC5K-b-PDMS series. AM5K-*b*-PDMS1K filmpjes hebben een treksterkte van 125 MPa, een 3.4 GPa elasticiteitsmodulus, en een breukrek van ~30%.

In ***Hoofdstuk 6*** beschrijven we het dual- and triple-shape memory gedrag van de $(AB)_n$-multiblok copolymeren. In een dual-SME-experiment laat het thermoplastische AM5K-*b*-PDMS1K polymeer een hoge R_f waarde van 100% zien en een R_r waarde >97%. Het vloeibaar-kristallijne LC5K analoog daarentegen geeft waardes die lager zijn, te weten 97% (R_f) en 80% (R_r). In daaropvolgende triple-SME-experimenten laat het thermoplastische AM5K-*b*-PDMS5K polymeer R_f waardes zien van >95% en R_r waardes >96%. De LC5K analoog laat wederom lagere R_f en R_r waardes zien van 91% en 80%, respectievelijk.

Samenvattend kunnen we zeggen dat we er in zijn geslaagd om thermoplastische $(AB)_n$-multiblok copolymeren te synthetiseren gebaseerd op aromatisch oligomeren (LC en AM) en thiol-getermineerde PDMS oligomeren middels thiol-ene click chemie. Het multiblock copolymeer met de beste mechanisch eigenschappen is AM5K-*b*-PDMS1K. Dit thermoplastisch polymeer heeft een treksterkte van 125 MPa, een 3.4 GPa elasticiteitsmodulus, een breukrek van >30%. Deze waardes overstijgen die van commerciële PEKK, PPS en PEI polymeren.

Curriculum Vitae

Hongli Xu

Born on February 26, 1987 in Huangshan, China

Sept. 2005 – June 2009

Bachelor of Engineering in Polymer Materials and Engineering, Anhui University of Technology, Maanshan, China

Sept. 2009 – June 2012

Master of Science in Polymer Chemistry and Physics, University of Science and Technology of China, Hefei, China

Nov. 2012 – Present

PhD candidate in Novel Aerospace Materials group, Delft University of Technology, Delft, the Netherlands

Aug. 2017 – Present

Research assistant at Southern University of Science and Technology, Shenzhen, China

List of publications

2018

Synthesis and characterization of multi-block copolymers containing all-aromatic mesogenic segments. **H. Xu**, J. Bijleveld, T. J. Dingemans. Manuscript in preparation.

Semi-crystalline poly(decamethylene terephthalamide) thermosets based on side-group functionalized copolyamides: synthesis and characterization. **H. Xu**, J. Bijleveld. T. J. Dingemans. Manuscript in preparation

High voltage, solvent-free solid polymer electrolyte based on a star-comb PDLLA–PEG copolymer for lithium ion batteries. B. Wang, H. Lou, **H. Xu**, J. Zhao, Q. Wang, Q. Shi and Y. Deng. RSC Adv., 2018, 8, 6373.

Novel lignin-derived water soluble binder for micro silicon anode in lithium-ion batteries. C. Luo, L. Du, W. Wu, **H. Xu**, G. Zhang, C. Wang, Z. Lu, Y. Deng. Submitted to ACS Sustain. Chem. Eng..

2017

Synthesis and properties of siloxane-based multi-block copolymers with all-aromatic mesogenic UNITS, Poster presentation, Advanced Polymers via Macromolecular Engineering, 2017, Ghent, Belgium.

Synthesis and properties of siloxane-based multi-block copolymers with all-aromatic rigid units, oral presentation, Dutch Polymer Days, 2017, Lunteren, the Netherlands.

2016

Synthesis and properties of siloxane-based multi-block copolymers with all-aromatic mesogenic units, Poster presentation, Workshop on Functional liquid crystal materials, 2016, Eindhoven, the Netherlands.

Synthesis and properties of reactive precursors towards high temperature LC block copolymers, Poster presentation, Dutch Polymer Days, 2016, Lunteren, the Netherlands.

2015

Synthesis and properties of soluble all-aromatic liquid crystalline ester-based oligomers with reactive end-groups, Poster presentation, Dutch Polymer Days, 2015, Lunteren, the Netherlands.

Synthesis and properties of reactive precursors towards high temperature LC block copolymers, Poster presentation, European polymer congress, 2015, Dresden, Germany.

Zhu, C.; **H. Xu**; Geng, P.; Lu, Z. High Perform. Polym. 2015, 27, 217.

2014

Cross-linkable aromatic polyesters for composite and coating application, Poster presentation, Dutch Polymer Days, 2014, Lunteren, the Netherlands.

2013

H. Xu; Zhang, W.; Lu, Z.; Zhang, G. RSC Adv. 2013, 3, 3677.

Polybenzoxazine thermosets based on urushiol for composite applications, Oral presentation at SAMPE Benelux student meeting, 2013, Almere, the Netherlands.

2012

H. Xu; Lu, Z.; Zhang, G. RSC Adv. 2012, 2, 2768.

A preparation method for benzoxazine precursor and synthetic resin thereof. Patent application: CN102432560A.

Acknowledgements

This thesis and the work is approaching completion; however, I clearly understand that I would not have been able to do all this work without the supervision, help and support of many individuals involved directly or indirectly. I would like to take the opportunity to thank all who have contributed to this work.

First of all, I would like to sincerely thank my promotor and supervisor Prof. Theo Dingemans, for accepting me as a PhD candidate in his group and giving me the chance to work on an interesting research project. Besides the strong support, guidance and commitment to the project, your patience and enthusiasm was a strong encouragement for me. In addition, I learned a lot from you about scientific writing, presenting and collaborating with other people.

I owe special thanks to Prof. Sybrand van der Zwaag for his warm guidance, kindness and fatherly support during my stay in The Netherlands. Your special view points and insights into my research has always been very inspiring. Thanks for your continuous encouragement and valuable advice. I am also very grateful for the useful comments about my thesis. When I had difficulties either in my research or in daily life, I knew your door was always open.

My special thanks to Dr. Johan Bijleveld, who has been a very inspiring supervisor. You taught me so many skills in exploring science and gave me so many good suggestions about my research. You taught me how to extract as much information as possible from my data. I also appreciate the time you spent on editing my Thesis Chapters and correcting my scientific writing. When I was depressed, you tried your best to cheer me up. Johan, thanks for all of those suggestions, discussions, and support over the years.

I owe my gratitude to Prof. Stephen Picken for sharing his extensive knowledge on polymers. Through the helpful discussions, I have learned a lot in understanding the polymer system I worked on. I also thank Dr. Wallace Ambrose (Chapel Hill, NC), Dr. Wiel Evers (TNW, TU Delft) and Frans Oostrum for performing the TEM and SEM experiments. Without their help, measuring and analysing data would have been much harder. I warmly appreciate the help from Dr. Giuseppe Portale and Jingjin Dong (RUG) for their help in performing the 2D XRD experiments and discussions. I would like to thank Lijing for her day to day operations in the lab, helpful discussions and support for my work. I thank Dr. Stephen Eustace (TNW, TU

Delft) for the NMR measurements and also the helpful discussion of analysing data. I also thank Berthil and Johan for helping with the equipment in the laboratory and Aerospace hangar.

I enjoyed the time when I worked together with Wouter V., Zeljka, Ranjita, Jianwei, Qingbao, Jimmy and Chelsey, not only in science but also in everyday life. I warmly appreciate the help from Shanta in taking care of all the administrative work, which we mostly don't even know about. I thank my officemates, Michiel, Zeljka and Paul, who make our office a very pleasant place. I always feel so lucky to be a member of our the NovAM group. I also want to thank all former and present colleagues in Novam, Ricardo, Wei, Hao Chen, Qi, Xiaojun, Hao Yu, Haixing, Santiago, Mladen, Antonio, Nan, Wouter P., Arijana, Martino, Marianella, Mina, Jesus, Pim, Jibran, Nijesh, Hamideh, Paul, Hussein, Casper, Michael, Shuo, Vincenzo, Marlies, Sung-Hwan, Roserio, Amber, Zenan, Erik, Nora, Renee, Bart and the rest of the Novam colleagues for leaving me a memorable experience. I thank all my friends from the Delft fellowship for their companionship. The time we enjoyed together will benefit me for the rest of my life.

I would like to acknowledge Prof. Yonghong Deng and my colleagues at the Southern University of Science and Technology for their support during the final stages of finishing my thesis. I would also like to thank Prof. Guangzhao Zhang for his encouragement and advice on my studies and life in general.

Last but not least, I would like to express my love to my whole family who has always supported me in any case. I want to thank my parents for their selfless support. They raised me with their truly love and encouraged me to overcome all the challenges both in my research and daily life. Finally, I would like to thank my beloved wife, Xiaomei Lu, for her love and everything you have done for me. You have always been there for me, during great times and difficult moments. Life is fantastic and colourful with you and our daughter, Yunze.

Hongli Xu

Shenzhen, February 2018

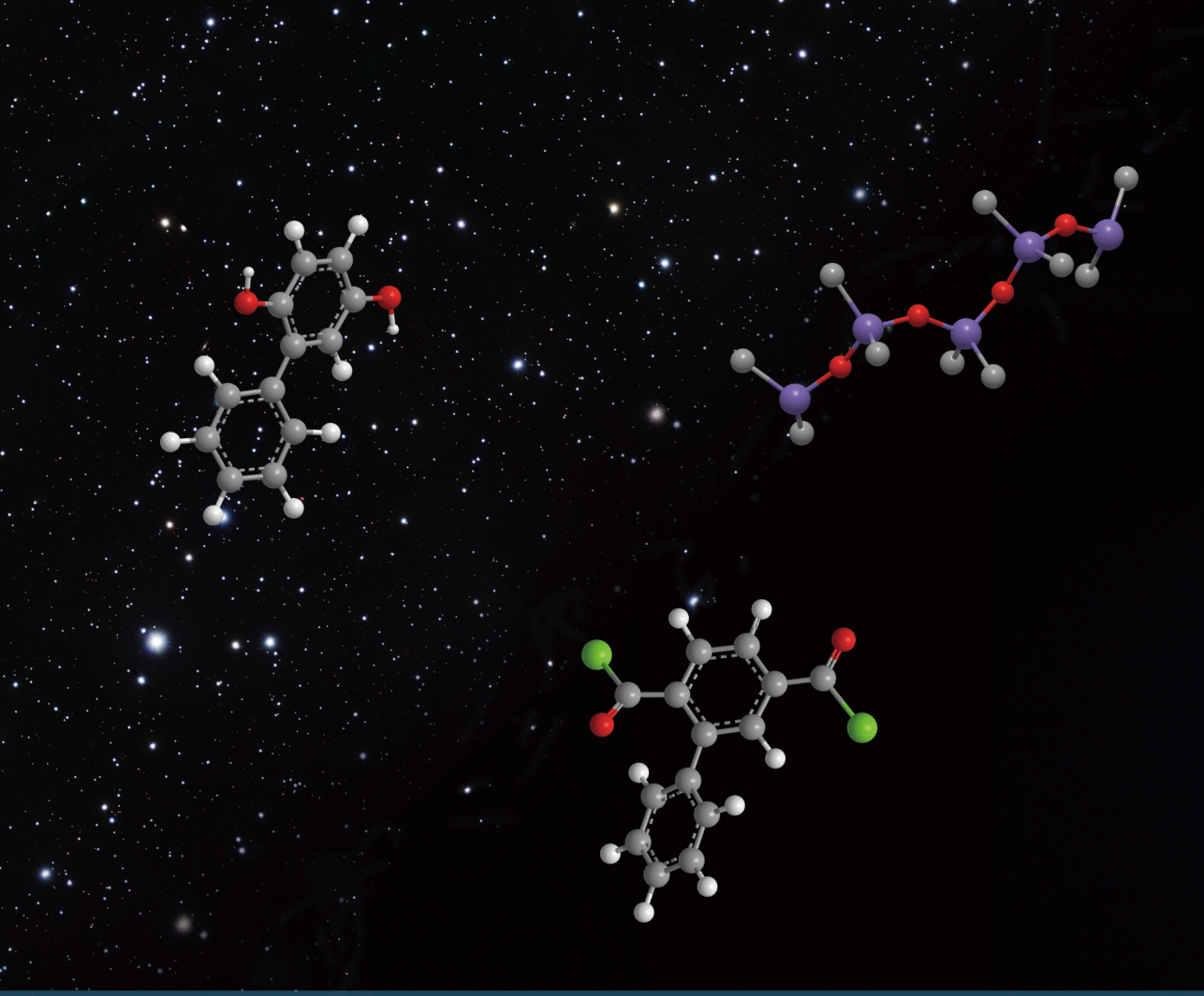

TU Delft

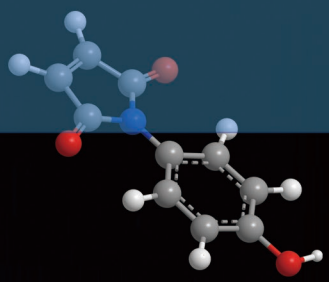

ISBN: 978-94-6186-908-1